NUREG/CR-1715
EGG-2061
Distribution Category: R3

FUEL ROD BEHAVIOR DURING TESTS PCM 8-1 RS, CHF SCOPING, AND PCM 8-1 RF

Roger L. Johnson[a]
Pamela L. Lassahn[a]
Zoel R. Martinson
Richard K. McCardell
Daniel T. Sparks
Philip E. MacDonald

Published November 1980

EG&G Idaho, Inc.
Idaho Falls, Idaho 83415

Prepared for the
U.S. Nuclear Regulatory Commission
Washington, D.C. 20555
Under DOE Contract No. DE-AC07-76IDO1570
FIN No. A6041

a. Stafco, Inc.

ABSTRACT

This report presents the results of the first three power-cooling-mismatch (PCM) tests—Tests 8-1 RS, CHF Scoping, and 8-1 RF—performed in the PCM Test series. The tests were performed with single, unirradiated, pressurized water reactor type fuel rods in the Power Burst Facility in May 1975 (8-1 RS), September 1975 (CHF Scoping), and December 1975 (8-1 RF). The tests were performed to scope the behavior of single fuel rods subjected to overpower or undercooling conditions sufficient to result in departure from nucleate boiling (DNB) and subsequent film boiling. Test results indicate that DNB can be induced by either increasing fuel rod power or reducing coolant mass flow. The power/flow conditions required to induce DNB were generally similar and repeatable. Fuel rod damage in the form of oxidation-induced embrittlement of the cladding was sufficient to cause failure of the 8-1 RS fuel rod, whereas the CHF Scoping and 8-1 RF rods remained intact. Fuel restructuring in the form of UO_2 grain growth and granular fracturing was observed. Instruments used to monitor the fuel rod behavior during testing were found to need improvement, particularly the cladding surface thermocouples, which exhibited significant fin-cooling effects.

SUMMARY

Power-Cooling-Mismatch (PCM) Tests 8-1 RS, CHF Scoping, and 8-1 RF were performed as part of the Thermal Fuels Behavior Program conducted by EG&G Idaho, Inc., for the U.S. Nuclear Regulatory Commission. The tests, conducted in the Power Burst Facility (PBF) at the Idaho National Engineering Laboratory, were the first tests performed in the PCM Test Series designed to scope the behavior of unirradiated pressurized water reactor (PWR) type fuel rods at power densities and flow conditions ranging from normal operation to beyond the occurrence of departure from nucleate boiling (DNB). Results from the PCM Test Series are intended to form an experimental data base that can be used to evaluate and further develop fuel rod behavior computer codes. These codes can be used to analyze hypothetical accident events in commercial light water reactors.

Common objectives of the three tests included determination of (a) the fuel-rod-power/coolant-flow conditions required for the onset of DNB, (b) the thermal and mechanical response of fuel rods subjected to film boiling conditions, (c) the permanent fuel rod damage resulting from varying durations of film boiling and stresses induced during quenching and posttest handling, and (d) the response and behavior of instrumentation on the fuel rod and in the coolant. The tests also provided data useful in evaluating and improving (a) analytical models used to predict the behavior of fuel rods under PCM conditions, (b) experimental methods used to conduct PCM tests, and (c) postirradiation examination methods and analyses. Generally, results from these three scoping tests provided a foundation for planning, performance, and analysis of subsequent PCM tests.

The experimental hardware for each test was contained within the in-pile tube of the PBF and comprised a single, unirradiated PWR-type fuel rod enclosed in a circular flow shroud. Nominal PWR conditions of 14.3 to 15.2 MPa coolant pressure and about 600 K coolant inlet temperature were maintained. Each of the tests was initiated by performance of a heat-balance power calibration and concluded with several DNB cycles. Following the power calibration, Test 8-1 RF also included a preconditioning phase to crack and restructure the fuel, and a cladding aging phase to drive off adsorbed gases from the cladding surface.

Departure from nucleate boiling was induced during the tests by two methods: (a) incremental increases in test rod power while maintaining the coolant mass flow rate constant (Tests 8-1 RS and CHF Scoping) and (b) incremental decreases in the coolant mass flow rate while maintaining the test rod power constant (Test 8-1 RF). Departure from nucleate boiling, which was induced several times during each test, first occurred at lower than expected peak fuel rod powers during the first cycle of Tests 8-1 RS and CHF Scoping. This premature occurrence of DNB was attributed to the presence of adsorbed gases on the cladding surfaces and was effectively eliminated by the cladding aging phase performed in Test 8-1 RF. Within nominal variations, excluding the premature DNB occurrences, the fuel-rod-peak-power/coolant-mass-flow conditions at the onset of DNB were generally similar and repeatable.

Sustained film boiling was allowed to develop several times during Tests 8-1 RS and CHF Scoping, but only during the final cycle of Test 8-1 RF. The total durations of film boiling were about 660 s for Test 8-1 RS, 40 s for Test CHF Scoping, and 65 s for Test 8-1 RF. Cladding peak temperatures determined from postirradiation measurement of the extent of oxidation and BUILD5 computer code analysis indicated cladding surface temperatures reached about 2020 K during Test 8-1 RS, 1610 K during Test CHF Scoping, and 1590 K during Test 8-1 RF. These temperatures were 550 to 850 K greater than those measured during the tests using cladding surface thermocouple assemblies because of significant fin-cooling effects. Film boiling was terminated during the tests by rapid reactor power decreases, in some instances by manual insertion of control rods and in other instances by reactor scram. As indicated by the cladding surface thermocouples, rewet occurred within a few seconds following the power decrease in all cases.

Permanent fuel rod cladding damage, primarily in the form of collapse, waisting (cladding collapse into pellet interfaces), and oxidation, occurred within the film boiling region of each test rod. The Test 8-1 RS fuel rod exhibited significantly more damage than the other two test

rods. Loss of cladding integrity, probably in the form of a cladding crack, was detected about 60 s after Test 8-1 RS reactor shutdown; complete fracture of the rod occurred in two places during posttest handling due to the highly embrittled condition of the cladding. Neither the CHF Scoping nor the 8-1 RF test rods failed during or following testing. The CHF Scoping rod had a permanent bend, and the 8-1 RF rod showed evidence of localized cladding collapse into voids created by chipped fuel pellets. Evaluations of the likelihood of cladding failure from embrittlement based on three postirradiation methods agreed with the experimental findings, in that sufficient embrittlement of the 8-1 RS rod occurred to expect failure, whereas insufficient embrittlement of the CHF Scoping and 8-1 RF rods occurred to expect failure.

The high temperatures associated with film boiling resulted in fuel restructuring within the film boiling zone of the 8-1 RS and CHF Scoping fuel rods. Restructuring was characterized by equiaxed grain growth in the central area of the fuel column. Fuel shattering (granular fracture) was also detected in localized regions near the center of some fuel pellets in the 8-1 RS rod. Fuel restructuring was insignificant in the 8-1 RF rod.

The results of these three scoping PCM tests indicate that single, unirradiated fuel rods in a nominal PWR environment can be operated in film boiling with cladding temperatures exceeding 1250 K for times on the order of tens of seconds without failure; however, film boiling durations for times on the order of several hundred seconds can result in cladding degradation to an extent sufficient to result in failure. The cladding maintains some ductility at high temperatures and generally fails upon cooldown due to thermal stresses on the embrittled cladding.

CONTENTS

Note: All of the appendices to this report are presented on microfiche attached to the inside of the back cover.

FIGURES

TABLES

FUEL ROD BEHAVIOR DURING TESTS PCM 8-1 RS, CHF SCOPING, AND PCM 8-1 RF

1. INTRODUCTION

Procedures for licensing and operation of commercial nuclear power plants require detailed investigations of the phenomena associated with postulated reactor accidents. The result of many hypothesized accident scenarios is an imbalance between the heat generation rate of the nuclear core and the heat removal rate of the coolant. Two extreme cases have commonly been designated the loss-of-coolant accident (LOCA), in which all or part of the core coolant is rapidly lost, and the reactivity initiated accident (RIA), in which a sudden power increase is initiated within the nuclear core. Between these two extremes lie a wide range of off-normal power-cooling conditions, commonly referred to as power-cooling-mismatch (PCM) accidents. There are many credible single and coincident events that may initiate PCM accidents. For example, overpower events could result from malpositioned or unplanned withdrawal of control rods, xenon instability, improper loading and operation of a fuel assembly (enrichment error), decrease in the soluble poison concentration within the coolant, increased reactor coolant flow rate, or a decrease in the coolant inlet temperature by startup of a cooler or an inactive flow loop. Similarly, undercooling may result from equipment malfunctions, flow blockages, or secondary system malfunctions that result in decreased heat removal from the primary coolant system. If departure from nucleate boiling (DNB) occurs during a PCM event, the potential for fuel rod damage and release of radioactivity is enhanced.

The Power-Cooling-Mismatch Test Series is being conducted by the Thermal Fuels Behavior Program of EG&G Idaho, Inc., as part of the U.S. Nuclear Regulatory Commission's (NRC) Fuel Behavior Program.[1] These tests are being performed to characterize the behavior of unirradiated, pressurized water reactor (PWR) type fuel rods at power densities and flow conditions ranging from normal operating conditions to beyond the occurrence of DNB. The test series is directed toward providing an experimental data base to satisfy a major objective of the NRC Fuel Behavior Program—the development and assessment of analytical models for fuel rod behavior during normal and off-normal operating conditions.

During a PCM event, five categories of possible post-DNB fuel rod behavior have been identified, as shown in Table 1. The physical processes that determine the particular category of expected post-DNB fuel rod behavior during a PCM event are zirconium phase change, the degree of zirconium-water and zirconium-fuel reaction (both of which influence cladding ductility), and fuel melting. The principal variables that control these processes are cladding temperature, the time at temperature, and rod power. The PCM test program was designed as a parametric evaluation of fuel rod behavior response during film boiling, with cladding temperature, time in stable film boiling, and rod power as the primary variables, as shown in Table 2.

Results of the first three tests performed in the PCM Test Series, PCM 8-1 RS, CHF Scoping, and PCM 8-1 RF, are described in this report. These tests were conducted for the purpose of scoping the behavior of fuel rods subjected to overpower or undercooling conditions sufficient to result in DNB and subsequent film boiling. The experiments were performed in the Power Burst Facility (PBF), located at the Idaho National Engineering Laboratory, on the following dates: PCM 8-1 RS — May 1975; CHF Scoping — September 1975; and PCM 8-1 RF — December 1975.

The test assembly for each of the three tests comprised a single PWR-type fuel rod enclosed in a circular flow shroud. Initial coolant pressure, temperature, and mass flux were typical of nominal PWR operating conditions. Test PCM 8-1 RS included a power calibration and four DNB cycles, Test CHF Scoping included a power calibration and seven DNB cycles, and Test PCM 8-1 RF included a power calibration, fuel preconditioning, cladding surface aging, and

Table 1. Categories of post-DNB fuel rod behavior during a PCM event

Category	Stabilized Cladding Temperature Range (K)	Stabilized Zircaloy Cladding Phase	Zirconium/ Water Reaction	Cladding Ductility	Potential Fuel Rod Failure Modes
1	<920	Low temperature alpha	None	Normal	None for unirradiated fuel rods.
2	920 to 1105	High temperature alpha	None	High	Large deformations to rupture.[a]
3	1105 to 1250[b]	Alpha + beta transition	Minimal	Low	Small deformations to rupture.[a]
4	1250 to 1650	Low temperature beta	Severe	High to low[c]	Cladding oxidation and oxygen embrittlement. Fuel melting if powers are relatively high.
5	>1650	High temperature beta	Severe	Low	Severe cladding oxidation and oxygen embrittlement. Possible cladding and fuel melting.

a. Cladding ballooning is unlikely and only possible after the internal rod pressure exceeds the system pressure.

b. This temperature range is intended to bound the cladding ductility minimum that occurs during the alpha + beta phase transition.

c. The cladding ductility is initially high in beta zirconium, but will decrease rapidly as the zircaloy is embrittled by oxidation and oxygen absorption.

Table 2. PCM test program description

Test Parameters	PCM 8-1 RS	CHF Scoping	PCM 8-1 RF	PCM-1	PCM-2A	PCM-2	PCM-3	PCM-4	PCM-5	PCM-7
Number of test rods	1	1	1	1	1	4[a]	4[a]	4[a]	9	9
Temperature stabilization category[b]	4	—	4	5	2	2	3	4	4	4
Total film boiling time (s)	660	40	65	900	210	117	45	160	665	1710
Maximum linear peak power (kW/m)	80	64	61	78	58	51	54	68	64	58
Number of DNB cycles	4	7	6	1	9	8	5	4	1	3
References—Test Results Reports	—	—	—	2	3	4	5	6	7	c

a. Four test rods situated in a square array with individual flow shrouds.

b. Categories are from Table 1. Values shown are original target temperatures; values actually attained may be found in the individual Test Results Reports.

c. Test results repo t not yet published.

DNB cycles. The DNB cycles for Tests 8-1 RS and CHF Scoping were achieved by incrementally increasing the test rod power level while maintaining coolant flow constant. The DNB cycles for Test 8-1 RF were achieved by incrementally reducing the coolant flow while maintaining the test rod power constant.

Section 2 of this report briefly describes the test rods, test assemblies, instrumentation, and test sequences for each of the three tests. Sections 3, 4, and 5 present the test results and analyses for each of the tests. Each section includes an overview, discussions of DNB and film boiling behavior, descriptions of the posttest condition of the test rods, and cladding and fuel behavior discussions. The primary results of the three tests are discussed and compared in Section 6, and relevant conclusions are presented in Section 7. The appendices contain supporting information, including pretest fuel rod characterization data, experiment designs and instrumentation, power calibration methods and results, postirradiation examination results, and experimental data plots. All of the appendices to this report are presented on microfiche attached to the inside of the back cover.

2. DESCRIPTION AND CONDUCT OF EXPERIMENTS

The Power Burst Facility consists of an open tank reactor vessel, a driver core region with an active fuel length of 0.914 m, and a central flux trap region containing an in-pile tube, with a loop coolant system capable of providing an environment of nominal PWR system conditions. The reentrant in-pile tube, which encloses the test space, has inlet and outlet connections for loop coolant flow located at its upper end above the driver core.

The PBF reactor is a facility capable of simulating, through steady state or transient operation, the environment necessary to evaluate various responses of nuclear fuel rods under postulated accident conditions. Tests 8-1 RS, CHF Scoping, and 8-1 RF were designed to scope the behavior of unirradiated PWR-type fuel rods under power-cooling-mismatch conditions. Similar fuel rods, coolant temperature and pressure conditions, and experiment configurations were used in each of the tests; fuel rod power or coolant flow rate, or both, were varied during the tests.

This section generally describes the experiment configurations and conduct of the tests. Detailed information on fuel rod characteristics, test train designs and instrumentation, and test rod power determinations is provided in Appendices A, B, and C, respectively.

2.1 Experiment Configurations

Each test assembly contained a single unirradiated fuel rod enclosed in an open-ended flow shroud. Instrumentation was installed to monitor coolant conditions and fuel rod behavior.

2.1.1 Fuel Rods. The fuel rods used in Tests 8-1 RS (Rod UTA-0004), CHF Scoping (Rod UTA-0005), and 8-1 RF (Rod UTA-0006) were of nominal PWR design, except that the length was only about 1 m, compared with about 4 m for commercial PWR rods, and the fuel was 20% enriched. Figure 1 shows the instrumented fuel rod and associated coolant flow shroud used in Test 8-1 RF; similar shroud geometries and instrumentation were used in the other two tests. Table 3 summarizes the fuel rod design details and the type and location of fuel rod instrumentation for each of the three tests.

2.1.2 Test Assembly. The test assembly hardware was designed to (a) symmetrically position individual test fuel rods in the in-pile tube (IPT), (b) provide appropriate flow path and distribution geometry, (c) provide locations for mounting instruments, and (d) allow changeout of fuel rods and flow shrouds as required between tests. Fuel rods were fixed at the top and free to expand downward against an axial elongation transducer (Table 3). The test assembly was centered in the IPT within the IPT flow tube. Coolant flow entered the IPT near the top and passed down the annulus outside of the flow tube. The coolant then reversed to the upward direction and entered the bottom of the test assembly. Most of the coolant bypassed along the outside of the fuel rod shroud, while the remainder entered the shroud and passed along the surface of the fuel rod. All coolant recombined above the flow shroud and exited the IPT.

Flow shroud dimensions were varied for each of the three tests to obtain the desired annular flow area for each fuel rod. Characteristics of the flow shrouds are given in Table 4.

Conditions external to the fuel rod during each of the tests were monitored by instruments mounted within or in the vicinity of the flow shroud. Transducer locations for Test 8-1 RF are shown in Figure 1; transducers were similarly located for the other two tests. Table 5 lists the instruments used for each of the three tests.

2.2 Conduct of Experiments

Nuclear operation during each of the three tests consisted of several distinct phases. A brief discussion of the operating history for each test is presented in this section; further details are presented in Appendices C and E.

2.2.1 Test PCM 8-1 RS Conduct. Test 8-1 RS consisted of two primary phases: (a) a power calibration phase and (b) a DNB test phase. The fuel rod power and coolant conditions during these phases are given in Table 6.

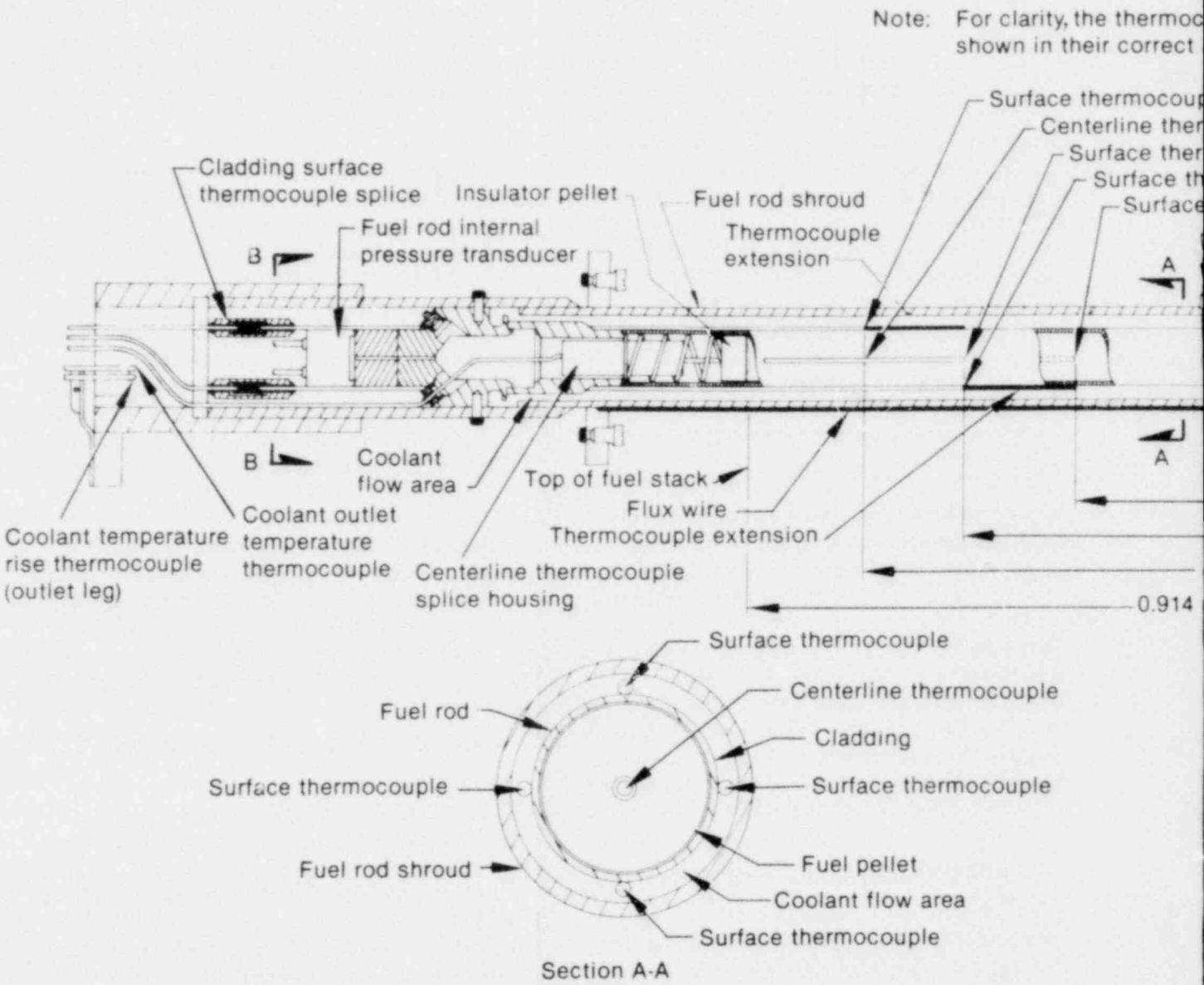

Figure 1. Test 8-1 RF fuel rod and instrum

ouples are not
azimuthal positions.

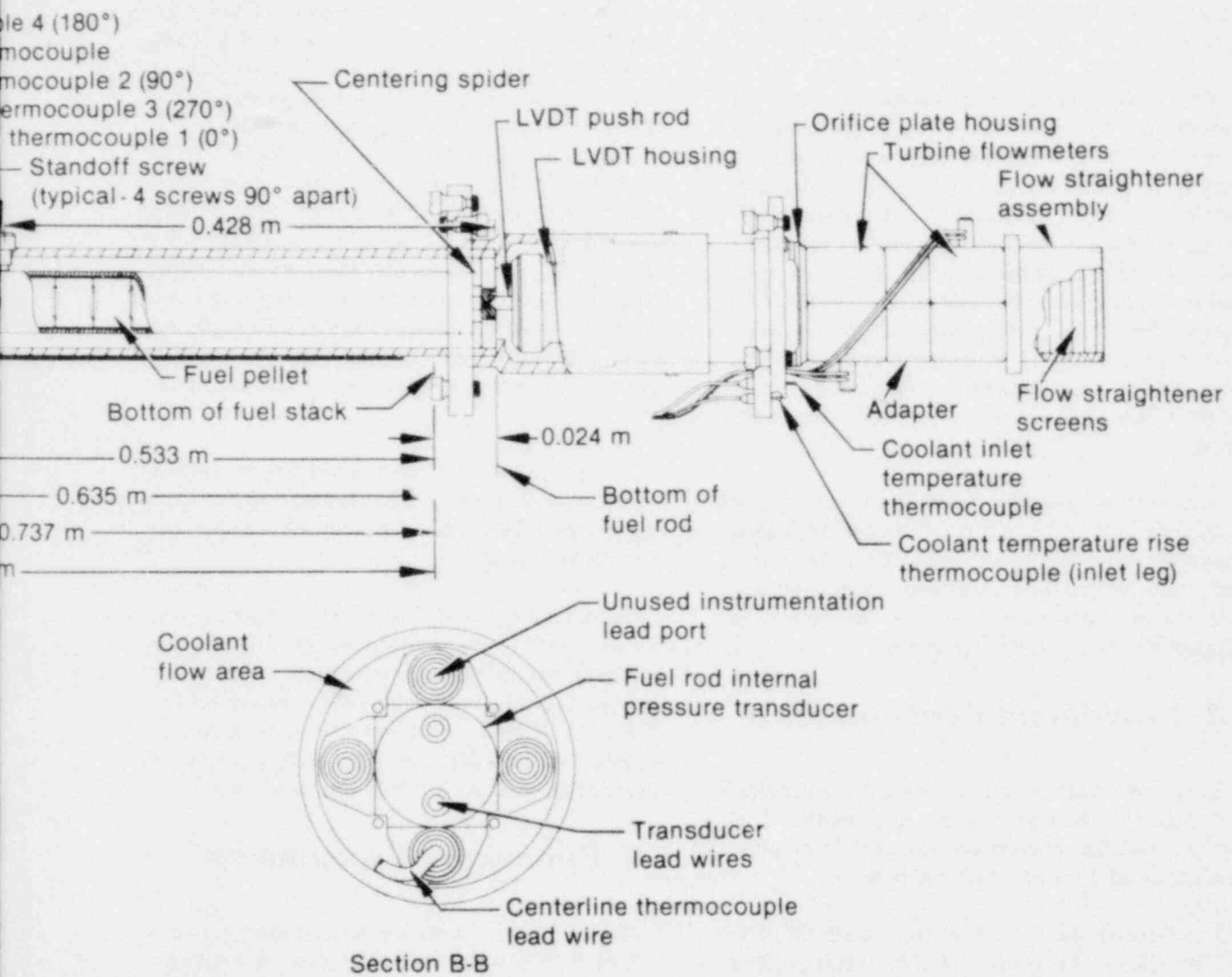

Section B-B

ntation shown installed in flow shroud.

Table 3. Fuel rod design characteristics and associated instrumentation (Tests 8-1 RS, CHF Scoping, and 8-1 RF)

Rod (Test)	Overall Rod Length (m)	Rod Outside Diameter (mm)	Cladding Wall Thickness[a] (mm)	Fuel Column Length (m)	Fuel Pellet Density[b] (% theoretical)	Diametral Gap (mm)	Fuel Rod Internal Pressure[c] (MPa)	Fuel Centerline[d,e] Thermocouple (m)	Cladding Surface Thermocouples	Axial Elongation Transducer	Internal Pressure Transducer
UTA-0004 (8-1 RS)	1.01	10.7	0.61	0.915	93	0.2	3.79	0.737	0°, 0.635 m 90°, 0.686 m 180°, 0.737 m 270°, 0.787 m	Below bottom end plug	Located in upper plenum
UTA-0005 (CHF Scoping)	1.01	10.7	0.61	0.915	93	0.2	3.79	0.679	0°, 0.483 m 90°, 0.533 m 180°, 0.635 m 270°, 0.667 m	Below bottom end plug	Located in upper plenum
UTA-0006 (8-1 RF)	1.01	10.7	0.61	0.915	93	0.2	3.82	0.737	0°, 0.533 m 90°, 0.635 m 270°, 0.635 m 180°, 0.737 m	Below bottom end plug	Located in upper plenum

a. Zircaloy-4 cladding.

b. Fuel pellets were 15.5 mm long, 9.3 mm in diameter, 20% enriched, and had dished ends.

c. All rods were pressurized with helium. The pressure measurements were made at room temperature.

d. Instrumentation locations measured from bottom of fuel stack.

e. W5%Re/W26%Re, tantalum-sheathed thermocouples.

f. W5%Re/W26%Re, zircaloy-sheathed thermocouples used for Rods UTA-0004 and UTA-0005; Pt/Pt-10% Rh, titanium-sheathed (Type S) thermocouples used for Rod UTA-0006.

g. Linear variable differential transformer (LVDT).

h. Diaphragm type, 0 to 20.7 MPa.

Table 4. Flow shroud characteristics (Tests 8-1 RS, CHF Scoping, and 8-1 RF)

	Test		
	8-1 RS	CHF Scoping	8-1 RF
Shroud Inner Diameter (mm)	17.9	19.2	19.4
Annular Flow Area about Fuel Rod (mm^2)	161	199	204

2.2.1.1 Power Calibration—The objective of the power calibration phase was to determine the fuel rod power generation over the expected operating range relative to the PBF core power as measured by ionization chambers. This information allowed effective performance of subsequent DNB cycles and posttest data analyses.

The power calibration was performed under subcooled conditions by measuring coolant flow and coolant temperature rise across the shrouded fuel rod at 11 different fuel rod peak powers in the range of 16 to 68 kW/m. Data were recorded for about 10 min at each of the 11 power levels. The fuel rod axial power profile was determined by fitting a Fourier sine series to the activation data obtained from scanning a cobalt flux wire attached to the outside of the fuel rod shroud. A linear regression analysis of the coolant temperature and flow data was performed to relate fuel rod peak power to ion chamber current (core power).

Fuel rod power was also determined by posttest radiochemical analysis of three fuel pellets from the test rod. The power levels determined from the radiochemical analysis were about 7% lower than those obtained from the thermal heat balance measurements, a difference that is within the experimental uncertainties of the two methods. The heat balance measurements were used for all power determinations cited in this report for Test 8-1 RS. The heat balance and radiochemical methods are described and compared in Appendix C.

2.2.1.2 Departure from Nucleate Boiling Testing—Following the power calibration, four separate DNB cycles were induced by incremental increases in fuel rod power (see Table 6). During each cycle, the rod power was held constant for at least 10 min before an additional increase was initiated. Coolant flow, inlet temperature, and pressure were maintained approximately constant throughout each DNB cycle. Indicated cladding surface temperatures were not allowed to exceed about 810 K for the first two cycles and about 1090 K for the final two cycles. Departure from nucleate boiling occurred several times during each of the cycles, occurring first at about 56 kW/m during Cycle 1. Most of the DNB occurrences were short and self-terminating. Cycles 1 and 3 were terminated by manually decreasing the reactor power, whereas Cycles 2 and 4 were terminated by reactor scrams when the indicated cladding surface temperatures reached the 810 and 1090 K setpoints, respectively.

2.2.2 Test CHF Scoping Conduct. Test CHF Scoping consisted of two primary phases: (a) a power calibration phase and (b) a DNB test phase. The rod power and coolant conditions during these phases are shown in Table 7.

2.2.2.1 Power Calibration—The objectives, methods, and results of the power calibration for Test CHF Scoping were similar to those for Test 8-1 RS (see Subsection 2.2.1.1). The power levels determined from the posttest radiochemical analysis of fuel pellets from the Test CHF Scoping rod were about 6% higher than those obtained from the thermal heat balance measurements, a difference within experimental uncertainties. Results from the heat balance measurements were used for all Test CHF Scoping power determinations cited in this report. Results of both the heat

Table 5. Test assembly instrumentation (Tests 8-1 RS, CHF Scoping, and 8-1 RF)

Parameter	Test		
	8-1 RS	CHF Scoping	8-1 RF
Coolant inlet flow rate to fuel rod	One turbine flowmeter on lower shroud extension	Two turbine flowmeters in series on lower shroud extension	Two turbine flowmeters in series on lower shroud extension
Coolant outlet flow rate from fuel rod	None	Turbine flowmeter at shroud outlet	None
Coolant temperature rise across test shroud	Two pairs Chromel-Alumel (Type K) thermocouples and two platinum resistance thermometers	Two pairs Chromel-Alumel (Type K) thermocouples and two platinum resistance thermometers	Two pairs copper-constantan (Type T) thermocouples and and two platinum resistance thermocouples
Fuel rod coolant inlet temperature	Chromel-Alumel (Type K) thermocouple at shroud inlet	Chromel-Alumel (Type K) thermocouple at shroud inlet	Two Chromel-Alumel (Type K) thermocouples at shroud inlet
Fuel rod coolant outlet temperature	None	None	One Chromel-Alumel (Type K) thermocouple at shroud exit
Coolant system pressure	One (0 to 20.7 MPa) strain gauge pressure transducer at shroud outlet	One (0 to 20.7 MPa) strain gauge pressure transducer at shroud outlet	One (0 to 34.5 MPa) eddy current diaphragm pressure transducer at shroud outlet
Large overpressure in in-pile tube	One (0 to 69 MPa) diaphragm strain-post-type transducer at shroud outlet	One (0 to 69 MPa) diaphragm strain-post-type transducer at shroud outlet	One (0 to 69 MPa) diaphragm strain-post-type transducer at shroud outlet
Integrated relative neutron flux	Cobalt flux wire outside shroud	0.51% cobalt-aluminum flux wire outside shroud	Cobalt flux wire outside shroud
Relative instantaneous neutron flux	One cobalt self-powered neutron detector outside shroud	None	Five, 0.1-m-long, cobalt self-powered neutron detectors outside shroud

balance and radiochemical analyses are described and compared in Appendix C.

2.2.2.2 Departure from Nucleate Boiling Testing—Seven separate DNB cycles were induced during Test CHF Scoping by incremental increases in fuel rod power (see Table 7). The rod power was held constant for at least 10 min at each power level before an additional increase was initiated. Coolant flow, inlet temperature, and pressure were maintained approximately constant during each cycle. Automatic reactor shutdown occurred if indicated cladding surface temperatures exceeded about 810 K during the first six cycles and 920 K during the seventh cycle. Departure from nucleate boiling occurred once during each of the seven cycles, followed by reactor shutdown. Cycles 1 and 2 were terminated by manually decreasing the reactor power, whereas Cycles 3 through 7 were terminated by a reactor scram when indicated cladding surface temperatures exceeded the setpoint values.

2.2.3 Test PCM 8-1 RF Conduct. Test 8-1 RF consisted of four primary phases: (a) a power calibration, (b) a preconditioning phase, (c) a fuel rod aging phase, and (d) a DNB test phase. The rod power and coolant conditions during these phases are shown in Table 8.

Table 6. Fuel rod power and coolant conditions during Test 8-1 RS

	Test Rod Peak Power[a,b] (kW/m)	Coolant Mass Flux[c] (kg/s·m^2)	Inlet Temperature[c] (K)	Coolant Pressure[c] (MPa)
Power Calibration Phase (~2 h operation)	16.4	2280	583	14.8
	24.9			
	31.2			
	38.1			
	44.6			
	46.6			
	51.8			
	58.4			
	64.6			
	67.9			
	45.6			
DNB Phase (~5 h operation)				
Cycle 1	41.2	1370	600	14.3
	44.9			
	48.2			
	52.2			
	56.1			
	59.0			
	62.3			
Cycle 2	56.1	1490	601	14.3
	58.7			
	62.0			
	65.3			
	67.9			
	71.5			
Cycle 3	59.7	1470	600	14.3
	62.7			
	65.9			
	68.9			
	72.5			
	75.8			
Cycle 4	58.7	1450	601	14.3
	62.0			
	65.9			
	68.9			
	72.5			
	75.8			
	79.7			

a. Test rod peak power is based on a measured axial peak-to-average ratio of 1.345.

b. Power held constant for about 10 min at each power level.

c. Nominal values during power level variations.

Table 7. Fuel rod power and coolant conditions during Test CHF Scoping

	Test Rod Peak Power[a,b] (kW/m)	Coolant Mass Flux[c] (kg/s·m^2)	Inlet Temperature[c] (K)	Coolant Pressure[c] (MPa)
Power Calibration Phase (~2 h operation)	27.6 34.8 39.7 48.5 54.8 60.7 63.6 55.4 48.9	2370	585	15.2
DNB Phase (~8 h operation)				
Cycle 1	50.5	1280	602	15.2
Cycle 2	43.3 47.2 50.2 53.8 61.3	1440	601	15.2
Cycle 3	41.3 50.5 53.8 57.4 61.0 63.3	1420	602	15.2
Cycle 4	50.5 58.7 60.7	1390	601	15.2
Cycle 5	50.2 53.9 57.4	1380	601	15.2
Cycle 6	50.2 53.8 57.4 60.4	1400	600	15.2
Cycle 7	50.5 54.1 57.1 60.0	1400	601	15.2

a. Test rod peak power is based on a measured axial peak-to-average ratio of 1.346.

b. Power held constant for about 10 min at each power level.

c. Nominal values during power level variations.

Table 8. Fuel rod power and coolant conditions during Test 8-1 RF

	Test Rod Peak Power[a,b] (kW/m)	Coolant Mass Flux[c] (kg/s·m^2)	Inlet Temperature[d] (K)	Coolant Pressure[d] (MPa)
Power Calibration Phase (~9 h operation)	17.1 33.8 48.9 60.0 67.2 50.8 17.7 49.5 33.5	2720	580	15.2
Preconditioning Phase (~7 h operation)	16.4 32.8	1360 2790	555	15.2
Fuel Rod Aging Phase (~1 h operation)	32.8 52.5	1900	600	15.2
DNB Phase (~2 h operation)				
Cycle 1	50.8	1900 to 500 (incremental)	600	15.2
Cycle 2	56.7	1900 to 460 (incremental)	602	15.2
Cycle 3	59.4	1900 to 610 (incremental)	599	15.2
Cycle 4	60.7	1900 to 600 (incremental)	600	15.2
Cycle 5	61.0	1900 to 570 (incremental)	600	15.2
Cycle 6	60.7	1900 to 510 (incremental)	600	15.2

a. Test rod peak power is based on a measured peak-to-average ratio of 1.34.

b. Power held constant at indicated power levels for periods in the range of 10 min to 4 h.

c. Nominal values during various phases of operation. Coolant mass flux incrementally decreased over range shown during DNB cycles.

d. Nominal values during various phases.

2.2.3.1 Power Calibration—The objectives, methods, and results of the power calibration for Test 8-1 RF were similar to those for Test 8-1 RS (see Subsection 2.2.1.1). The power levels determined from the posttest radiochemical analysis of the fuel pellets from the Test 8-1 RF rod were about 7% higher than those obtained from the thermal heat balance measurements, a difference within experimental uncertainties. Results from the heat balance measurements were used for all Test 8-1 RF power determinations cited in this report. Results of both the heat balance and radiochemical analysis are described and compared in Appendix C.

2.2.3.2 Preconditioning—The test fuel rod was preconditioned for about 7 h to crack and restructure the fuel, thus more nearly simulating the conditions existing in power reactor fuel rods after a period of operation. Data were also obtained during the preconditioning phase to estimate the fuel pellet-to-cladding gap heat transfer coefficient (gap conductance) as a function of test rod power density.

2.2.3.3 Aging—To age the fuel rod cladding surface under nucleate boiling conditions, the test rod was operated at a power level of about 33 kW/m for 10 min and 53 kW/m for about 1 h before DNB testing. This aging procedure removes adsorbed gases from the cladding surface and reduces the possibility of premature DNB.[3,8]

2.2.3.4 Departure from Nucleate Boiling Testing—Following aging, six separate DNB cycles were induced by incremental coolant flow reductions (see Table 8). Fuel rod peak powers, coolant inlet temperature, and coolant pressure were held constant during each cycle. Coolant flow was reduced in a series of steps until DNB occurred; each step had about 95% of the flow for the previous step. Flow was held constant for at least 60 s after each step. Indicated fuel rod cladding surface temperatures were not allowed to reach high post-DNB values except during the final cycle. A scram occurred if the indicated cladding surface temperatures exceeded about 700 K during the first five cycles. For the sixth and final cycle, the scram setpoint was increased to about 1920 K. Departure from nucleate boiling did not occur during Cycle 1, but was indicated during Cycles 2 through 6. All DNB cycles were terminated by manually decreasing the reactor power.

3. RESULTS AND ANALYSES - TEST PCM 8-1 RS

The primary objective of Test PCM 8-1 RS was to achieve departure from nucleate boiling on a single fuel rod operating at a peak linear power generation rate of approximatey 65 kW/m. Of particular interest were

1. The fuel rod power at which DNB would occur
2. Any change in test rod power required to achieve DNB or any change in axial location of DNB due to repeated cycling in and out of DNB
3. The thermal and mechanical response of the test rod during film boiling
4. Fuel rod damage due to film boiling operation
5. The adequacy of the test instrumentation.

The following sections present and evaluate the results of Test PCM 8-1 RS in accordance with these objectives.

3.1 Summary of Results

This section provides a brief overview of the Test 8-1 RS results and an evaluation of the fuel rod behavior during post-DNB operation. Detailed results are presented in subsequent sections.

Numerous occurrences of DNB were indicated during performance of the four DNB cycles. Most of these occurrences were self-terminating and did not result in stable, high temperature film boiling. Departure from nucleate boiling was first detected at a fuel rod peak power of 56.1 kW/m during Cycle 1; during subsequent cycles, DNB first occurred in the range of 63.9 to 65.9 kW/m. The comparatively low rod power at the onset of DNB during Cycle 1 was probably caused by gas entrapment on the fuel rod surface. Film boiling was established during Cycles 3 and 4, and the fuel rod was exposed to film boiling conditions for a cumulative time of about 660 s during the test (total time that the cladding surface thermocouples indicated temperatures in excess of the rewet temperature of 670 K[9]).

Loss of cladding integrity occurred in-pile shortly after completion of the test. Postirradiation examination of the fuel rod showed significant damage in the form of cladding collapse, waisting (cladding collapse at pellet interfaces), and oxidation. The cladding was highly embrittled because of nearly complete oxidation in some locations; complete fracture of the rod occurred in two locations during posttest handling. Cladding temperature estimates based on the measured extent of oxidation indicated that cladding peak temperatures exceeded 2000 K — about 850 K greater than determined from cladding surface thermocouple measurements. Fin-cooling effects associated with the thermocouple sheaths are believed to be the major cause of the atypically low temperatures measured by the thermocouples. Thermal restructuring of the UO_2 fuel occurred in the form of grain growth and intergrannular shattering in the central region of the fuel column.

3.2 Film Boiling

Departure from nucleate boiling occurred several times during each of the four DNB cycles of Test 8-1 RS, with sustained film boiling occurring during Cycles 3 and 4. This section discusses the onset of DNB, film boiling propagation, and film boiling termination.

3.2.1 Onset of DNB. As described in Subsection 2.2.1.2, each DNB cycle was performed by incrementally increasing the test rod power while maintaining coolant flow, inlet temperature, and pressure approximately constant (see Table 6). The occurrence of DNB was detected by monitoring changes in the cladding surface temperatures, fuel rod axial growth, and fuel centerline temperature. These parameters, as well as fuel rod power and coolant flow during each of the four cycles, are illustrated in Figures 2 through 9.

The occurrence of DNB was first indicated during Cycle 1 at a test rod peak power of 56.1 kW/m. Three subsequent occurrences of DNB were detected during Cycle 1 at test rod peak powers in the range of 59.0 to 62.3 kW/m. Departure from nucleate boiling was sustained for about 12 to 45 s and was self-terminating in all instances. During Cycles 2, 3, and 4, DNB was first detected at test rod peak powers of 65.3, 63.9, and

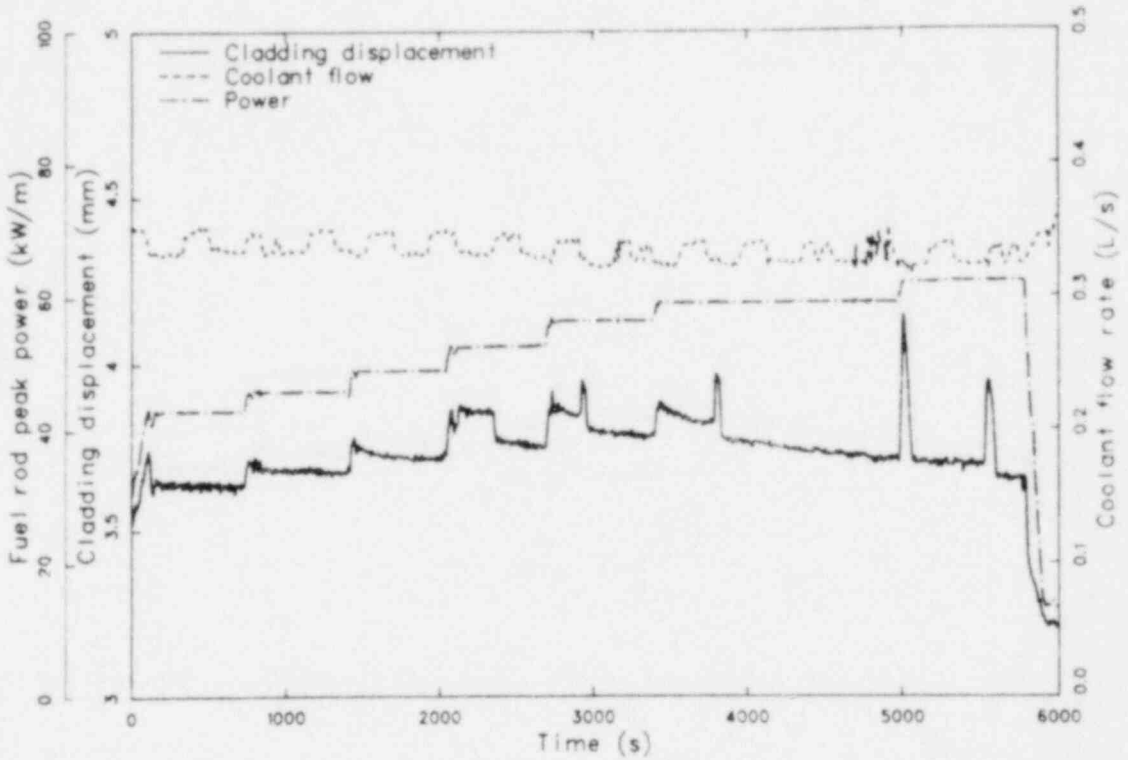

Figure 2. Fuel rod peak power, cladding displacement, and coolant flow rate versus t me during Test 8-1 RS (DNB Cycle 1).

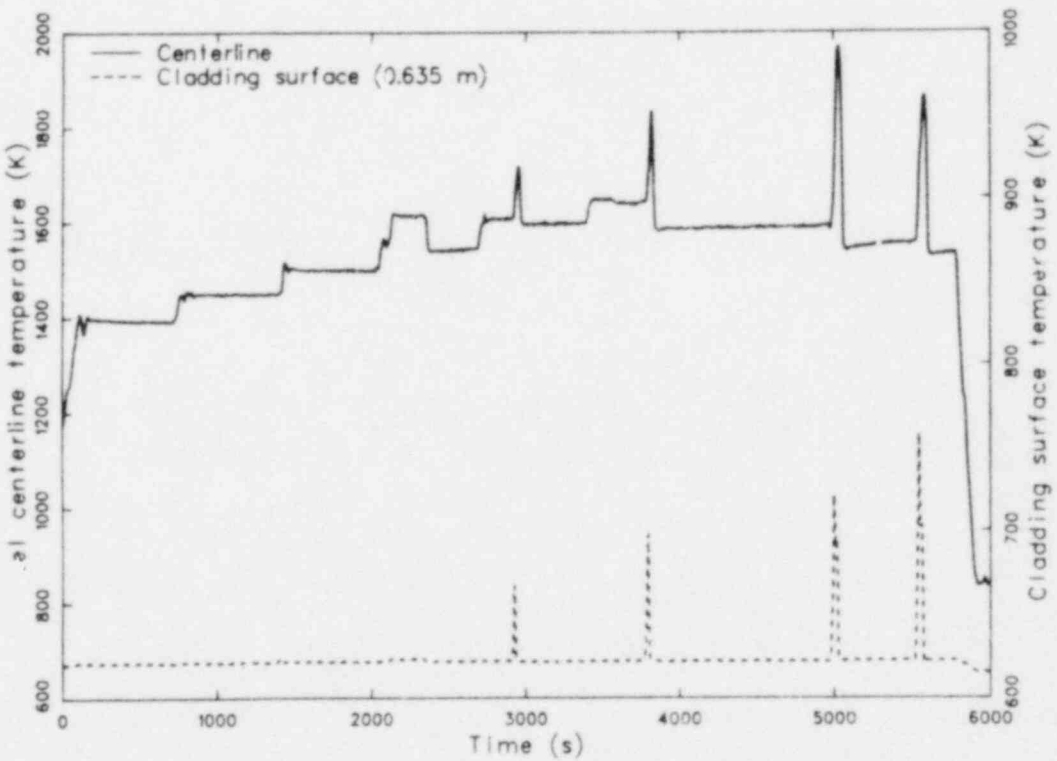

Figure 3. Fuel centerline temperature and cladding surface temperature versus time during Test 8-1 RS (DNB Cycle 1).

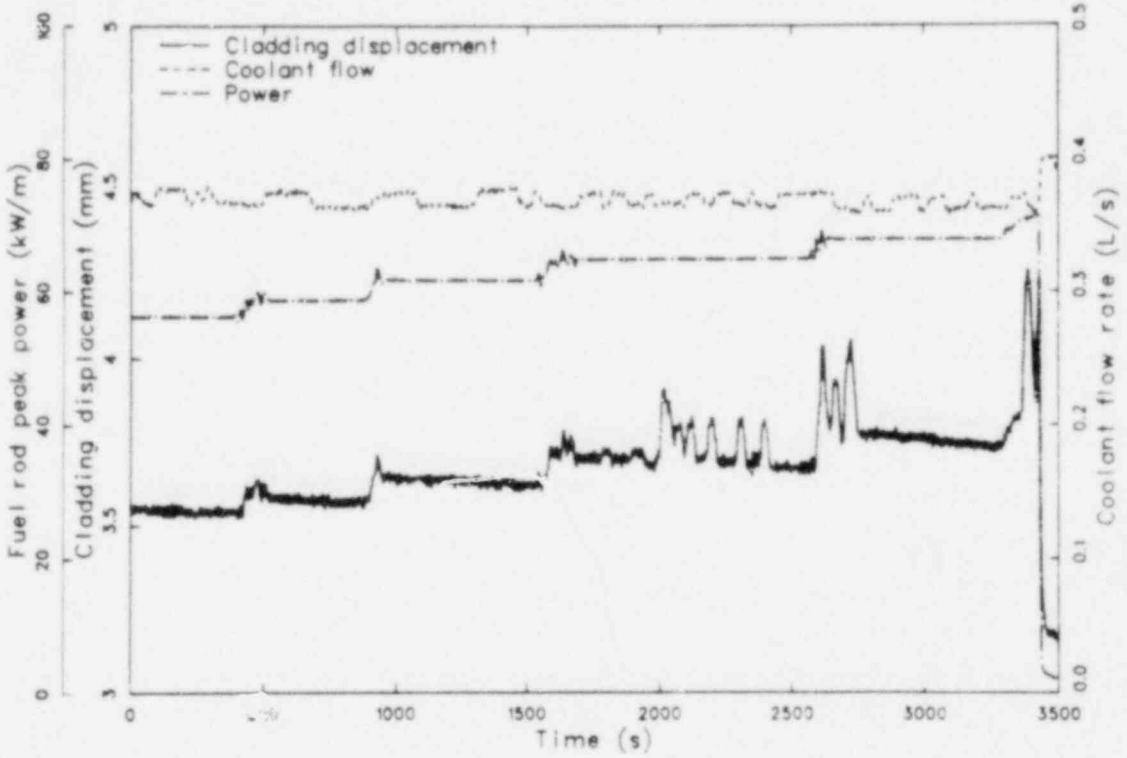

Figure 4. Fuel rod peak power, cladding displacement, and coolant flow rate versus time during Test 8-1 RS (DNB Cycle 2).

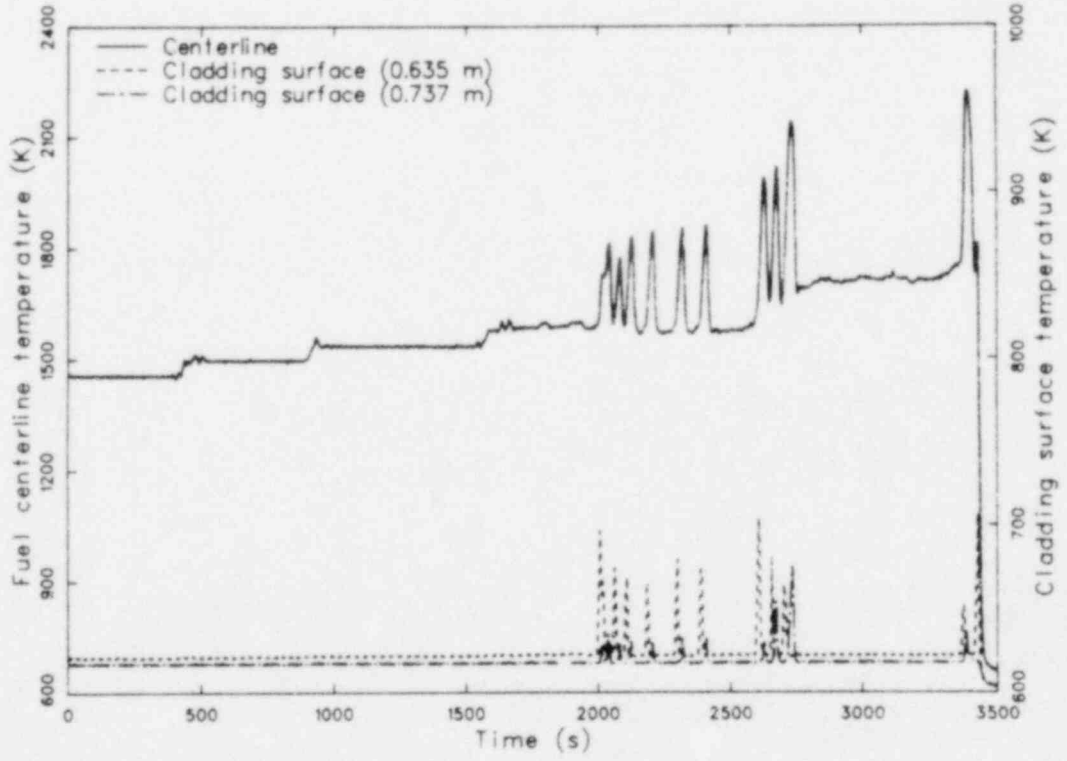

Figure 5. Fuel centerline temperature and cladding surface temperature versus time during Test 8-1 RS (DNB Cycle 2).

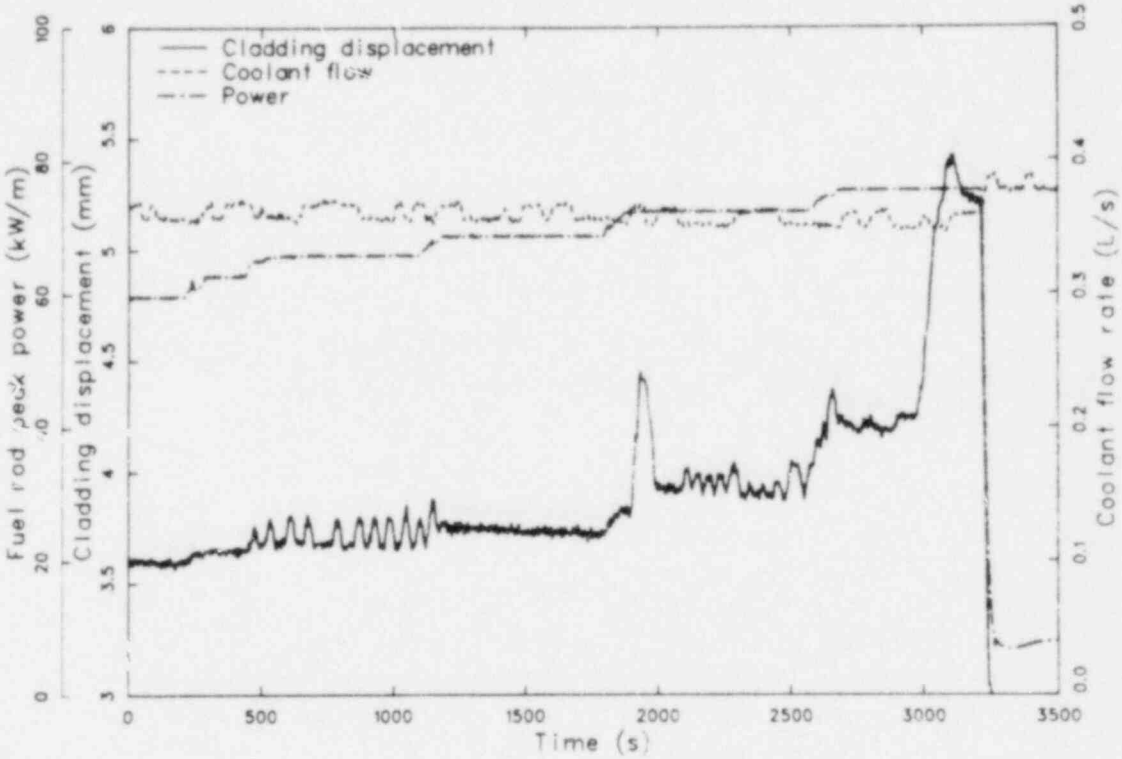

Figure 6. Fuel rod peak power, cladding displacement, and coolant flow rate versus time during Test 8-1 RS (DNB Cycle 3).

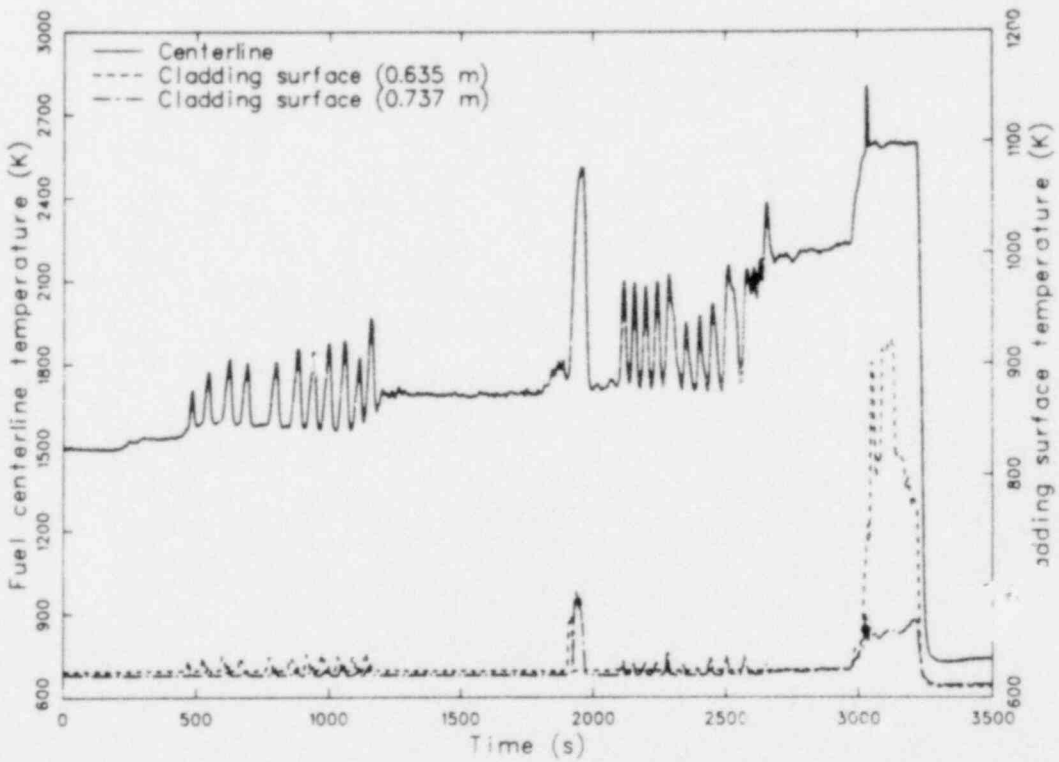

Figure 7. Fuel centerline temperature and cladding surface temperature versus time during Test 8-1 RS (DNB Cycle 3).

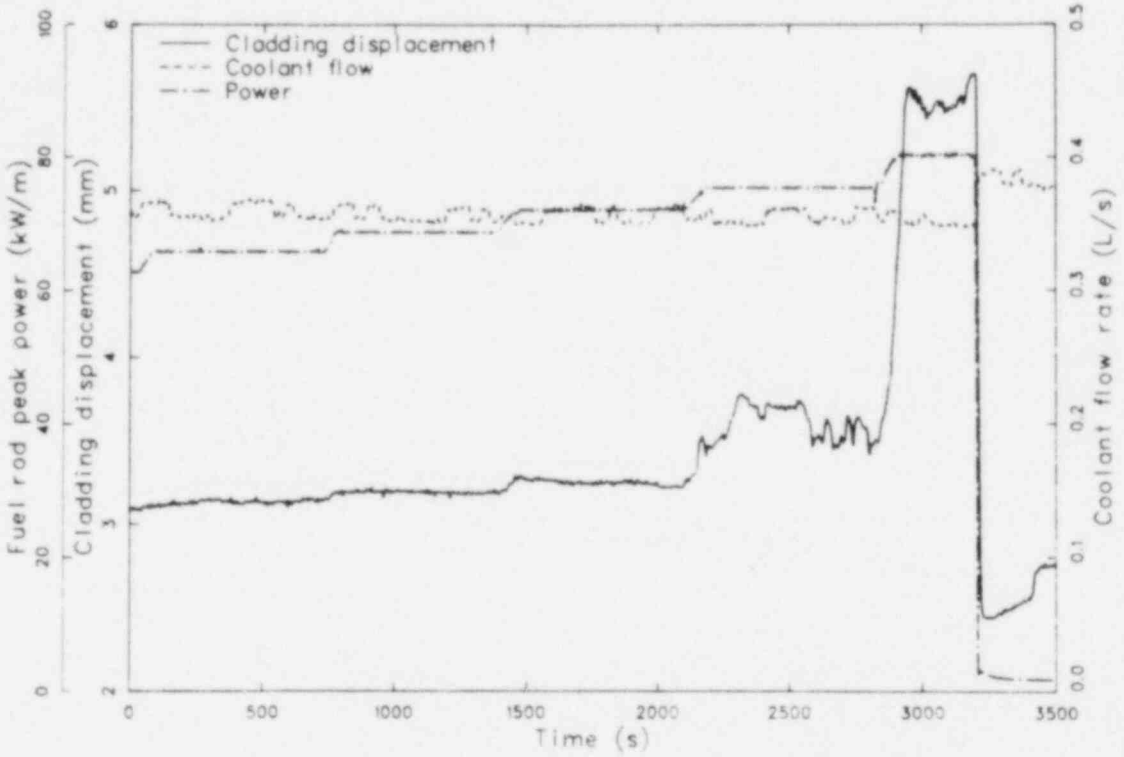

Figure 8. Fuel rod peak power, cladding displacement, and coolant flow rate versus time during Test 8-1 RS (DNB Cycle 4).

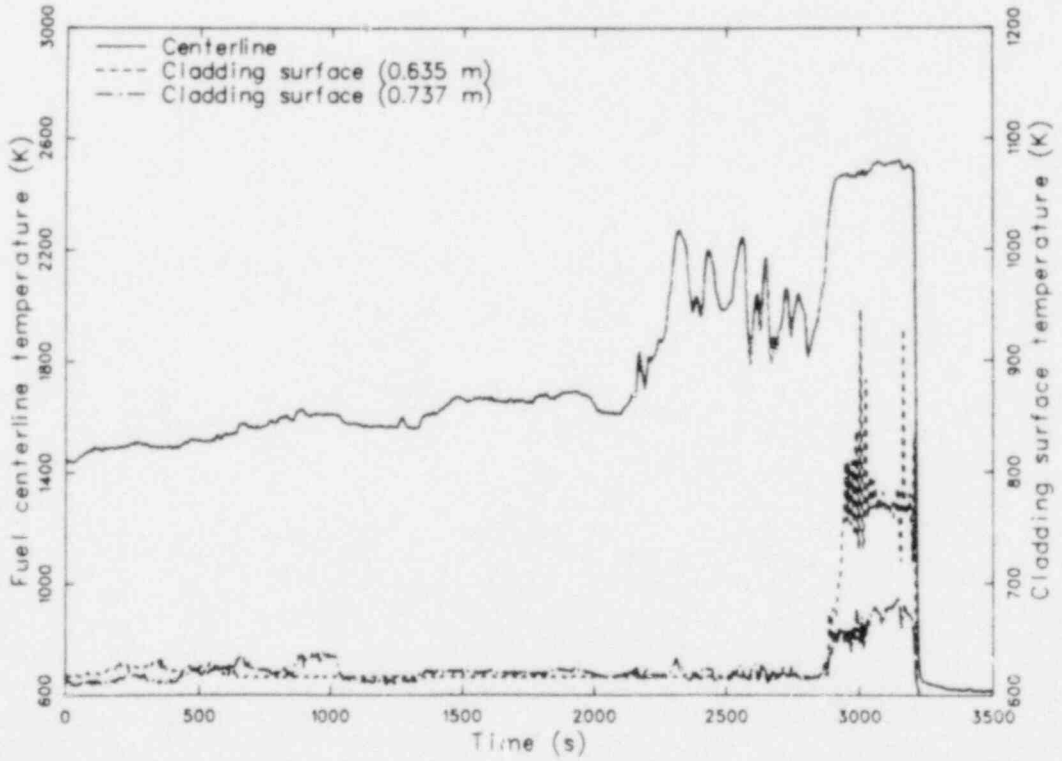

Figure 9. Fuel centerline temperature and cladding surface temperature versus time during Test 8-1 RS (DNB Cycle 4).

65.9 kW/m, respectively. Several self-terminating DNB occurrences were detected during each of these cycles before shutdown.

Calculations were performed to predict the fuel rod peak power at the onset of DNB for each of the four DNB cycles using the Westinghouse Electric Corporation correlation, W-3.[10] For the first cycle, the Babcock and Wilcox Company correlation, B&W-2,[11] was also used. Calculated and measured fuel rod peak powers at the onset of DNB are compared in Table 9.

The W-3 correlation closely predicted the measured rod peak power required to produce DNB. The comparatively low measured power at the onset of DNB for Cycle 1 was probably caused by gas entrapment on the fuel rod surface.[3,8]

3.2.2 Propagation of Film Boiling. Pretest thermal-hydraulic calculations indicated that film boiling would first occur from 0.64 to 0.74 m above the bottom of the fuel stack. Cladding surface thermocouples were therefore positioned at 0.635, 0.686, 0.737, and 0.787 m above the bottom of the fuel stack. Once initiated, film boiling would be expected to slowly progress down the surface of the fuel rod. The thermocouple histories during each DNB cycle should provide information on the axial progression of film boiling.

Examination of the thermocouple data plots, however, does not provide any obvious trends regarding axial film boiling propagation. With slight variations, each of the four thermocouples indicated the occurrence of DNB and subsequent film boiling at approximately the same time during each DNB cycle. Thus, it would appear that film boiling developed nearly simultaneously over the axial region of the thermocouples. This may have been due, in part, to the relatively close axial proximity of the thermocouples, which were located 0.051 m apart and covered an axial length from the top to bottom thermocouple of only 0.152 m.

3.2.3 Termination of Film Boiling. As shown in Figures 2 through 9, numerous cladding temperature fluctuations indicative of film boiling occurred during each of the four DNB cycles. The self-termination of these cladding temperature fluctuations may have been caused by (a) thermocouple fin-cooling effects or (b) variations in coolant flow, or both. The raised thermocouple sheaths act as cooling fins and may have contributed to intermittent wetting and film boiling in the vicinity of the sheaths. Variations in the inlet coolant flow rate were about ±7% and may also have contributed to the observed oscillatory behavior. Figure 10 presents a composite plot of the measured cladding surface temperature, inlet coolant flow, cladding axial length change, and fuel centerline temperature for the six temperature fluctuations observed at 65.3 kW/m rod peak power during Cycle 2. Although the data in Figure 10 do not show a correlation between film boiling and coolant flow rate variations, the cladding surface temperature is clearly related to changes in axial fuel rod length and fuel centerline temperature. This correlation indicates that the cladding surface temperature oscillations were indicative of actual fuel rod temperature increases during film boiling and not just local fluctuations at the thermocouple locations.

Departure from nucleate boiling Cycles 1 and 3 were terminated by manually decreasing the reactor power. No film boiling was apparent when Cycle 1 was terminated. Film boiling had occurred for about 200 s before termination of Cycle 3 (see Figure 6). Cladding surface thermocouples indicated that rewet occurred within a few seconds after the power decrease was initiated. A rapid recovery was also indicated by the fuel rod elongation measurement.

Cycles 2 and 4 were terminated by reactor scrams while film boiling was in progress. Again, the cladding surface thermocouples indicated rewet within a few seconds and the fuel rod elongation measurement showed a rapid recovery (see Figures 4, 5, 8, and 9).

3.3 Posttest Condition of Fuel Rod

The posttest condition of the Test 8-1 RS fuel rod is shown in Figure 11. Two complete breaks are shown; the first, at 0.59 m, was discovered when the fuel rod was removed from the flow shroud, and the second, at 0.51 m, occurred during posttest handling. The effects of film boiling were clearly discernible in the form of cladding collapse, waisting, heavy surface oxidation, and spalling of the surface oxide. Cladding collapse and extensive cladding oxidation extended from 0.454 to 0.877 m above the bottom of the fuel stack. Permanent fuel rod bowing was insignificant.

Table 9. Comparison of measured and calculated fuel rod peak powers at the onset of DNB during Test 8-1 RS

DNB Cycle[a]	Coolant Mass Flux ($kg/s \cdot m^2$)[b]	Inlet Temperature (K)	Fuel Rod Peak Power at Onset of DNB (kW/m)		
			Measured	Calculated (W-3)	Calculated (B&W-2)
1	1340	600	56.1	58.7	71.5
2	1480	601	65.3	59.7	c
3	1500	600	63.9	60.0	c
4	1480	601	65.9	59.0	c

a. Coolant system pressure constant at 14.3 MPa.

b. Multiply coolant flow rate (L/s) in Figures 2, 4, 6, and 8 by 4081 to get mass flow in $kg/s \cdot m^2$.

c. Not calculated.

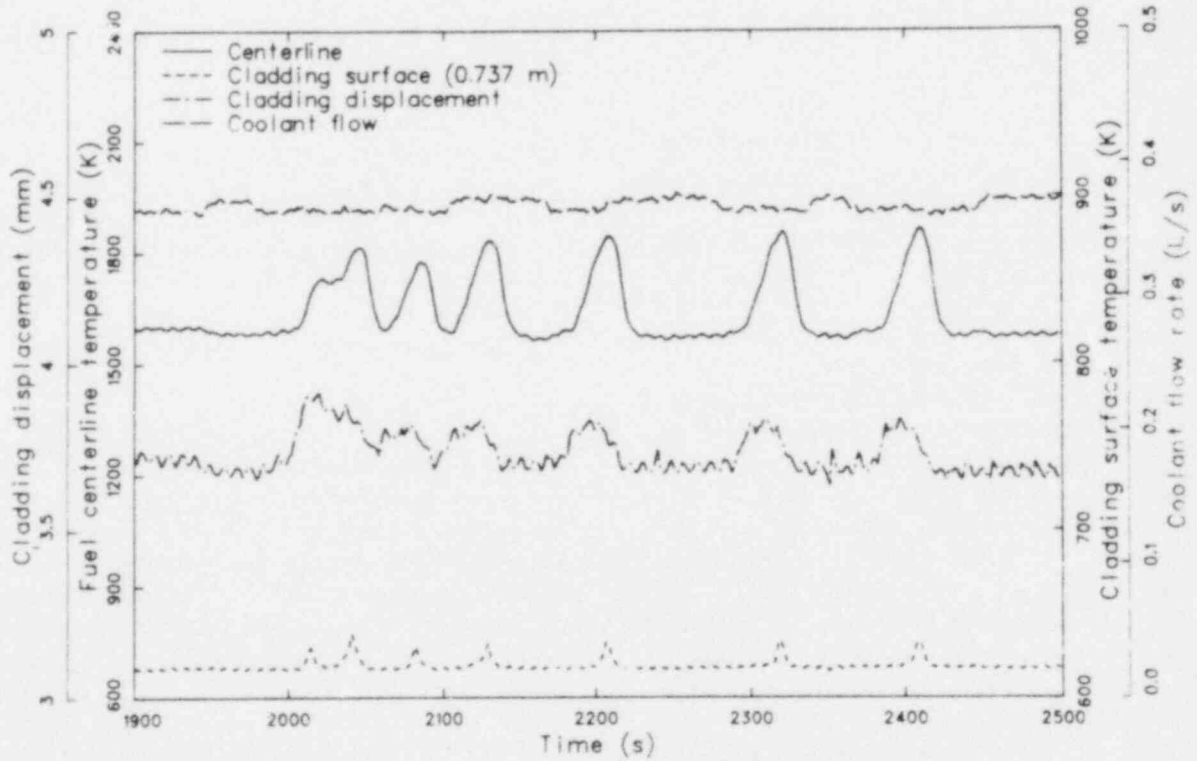

Figure 10. Measured fuel centerline temperature, cladding axial length change, inlet coolant flow rate, and cladding surface temperature versus time during Test 8-1 RS (DNB Cycle 2).

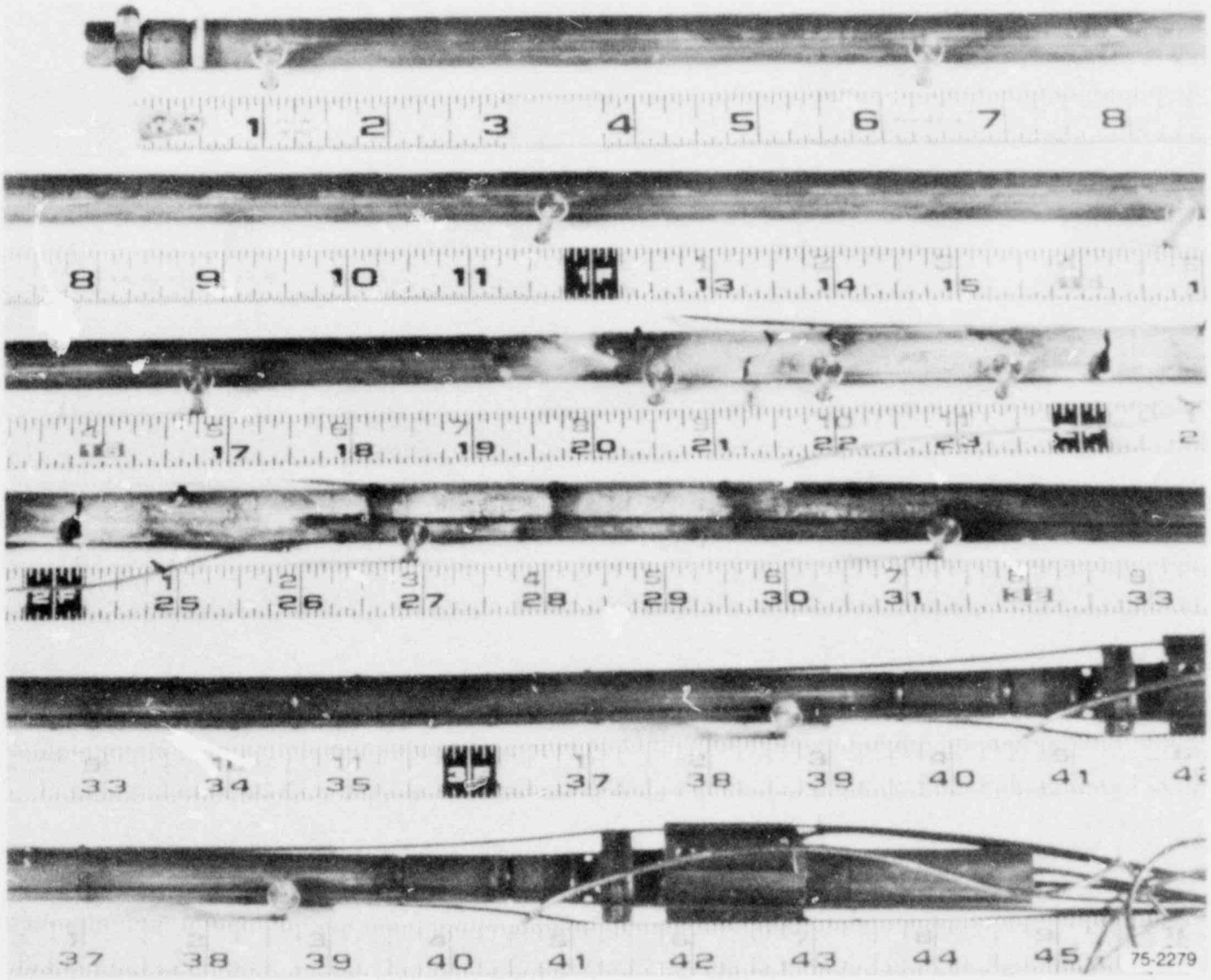

Figure 11. Posttest photograph of Test 8-1 RS fuel rod.

3.4 Cladding Behavior

Cladding temperatures during the film boiling periods of Test 8-1 RS increased to values sufficient to cause significant cladding damage. This section presents estimates of the maximum cladding temperatures attained and discusses cladding deformation, microstructure, and embrittlement.

3.4.1 Cladding Temperature Estimates. The response of selected cladding surface thermocouples during the four DNB cycles of Test 8-1 RS were shown in Figures 2 through 9. These measurements were known to be atypically low because of the fin-cooling effects associated with the surface-mounted thermocouples. Fin-cooling effects cause (a) atypical cooling of the cladding material in the immediate vicinity of the thermocouple sheath assembly and (b) cooling of the sheath-enclosed junction. Therefore, the thermocouple-measured cladding temperatures are often several hundred kelvin lower than the cladding temperatures at unperturbed locations. Alternate methods based on postirradiation analyses were therefore used to estimate the maximum cladding temperatures attained during film boiling at various locations on the fuel rod.

Cladding surface temperatures were estimated using three techniques: (a) metallographic examination of cladding microstructures (see Subsection 3.4.3), (b) isothermal reaction rate correlations that relate the sum of the external surface ZrO_2 layer thickness and the adjacent oxygen-stabilized alpha layer with the time in film boiling and the effective isothermal temperature of exposure, and (c) BUILD5 computer code calculations to determine cladding peak temperatures using linearized cladding thermocouple time-temperature response histories as input. Descriptions of each technique and detailed results are provided in Reference 12.

Figure 12 shows the peak temperatures at various axial locations estimated from the isothermal reaction rate correlations and the BUILD5 code; thermocouple measurements are also shown for comparison. The BUILD5-calculated temperatures are the best-estimate values of the cladding peak temperatures attained during the test. The thermocouple-indicated temperatures are consistently low because of fin-cooling effects. As shown, the best-estimate peak temperatures from the BUILD5 code at locations unperturbed by thermocouple sheaths are as much as 850 K greater than those determined from thermocouple locations at nearby axial locations. As expected, the cladding peak temperatures occurred in the lower part of the film boiling zone. The location of the peak temperature determined from the postirradiation analyses (0.581 m) was, in fact, below the location of the lowest thermocouple (0.635 m).

3.4.2 Cladding Deformation and Failure. Cladding geometry changes in the form of fuel rod elongation and cladding collapse in the film boiling zone occurred during Test 8-1 RS; loss of cladding integrity was indicated immediately following the test, and gross cladding failure occurred during posttest handling.

As cladding temperatures increased following the onset of DNB, fuel rod elongations occurred, as shown in Figures 2 through 9. The maximum measured elongation, which occurred near the end of Cycle 4, was 2.3 mm (0.25% of active fuel length). Most of the indicated elongation probably occurred within the film boiling zone of the test rod.

Radial cladding deformation in the form of cladding collapse and waisting occurred within the film boiling zone of the test rod. Both cladding collapse and waisting result from high cladding temperatures combined with high differential pressures across the cladding (system pressure external to the fuel rod greater than the internal fuel rod pressure). The high cladding temperatures experienced during Test 8-1 RS film boiling should have been sufficient to cause cladding collapse within a few seconds after these temperatures were attained. The fragile condition of the fuel rod following the test prevented detailed measurement of the diametral reduction.

Following termination of DNB Cycle 4 by a reactor scram, the internal fuel rod pressure decreased to about 6.9 MPa and then slowly increased, indicating that the fuel rod had developed a leak to the coolant. The slow leak continued for about 150 s and then the internal pressure suddenly increased to the system pressure of 14.3 MPa in about 10 s. Shortly thereafter, fission products were detected in the loop and various radiation alarms were activated. The loss of cladding integrity was believed to have been in the form of one or more small cladding cracks, the exact location(s) of which was not determined during postirradiation examination.

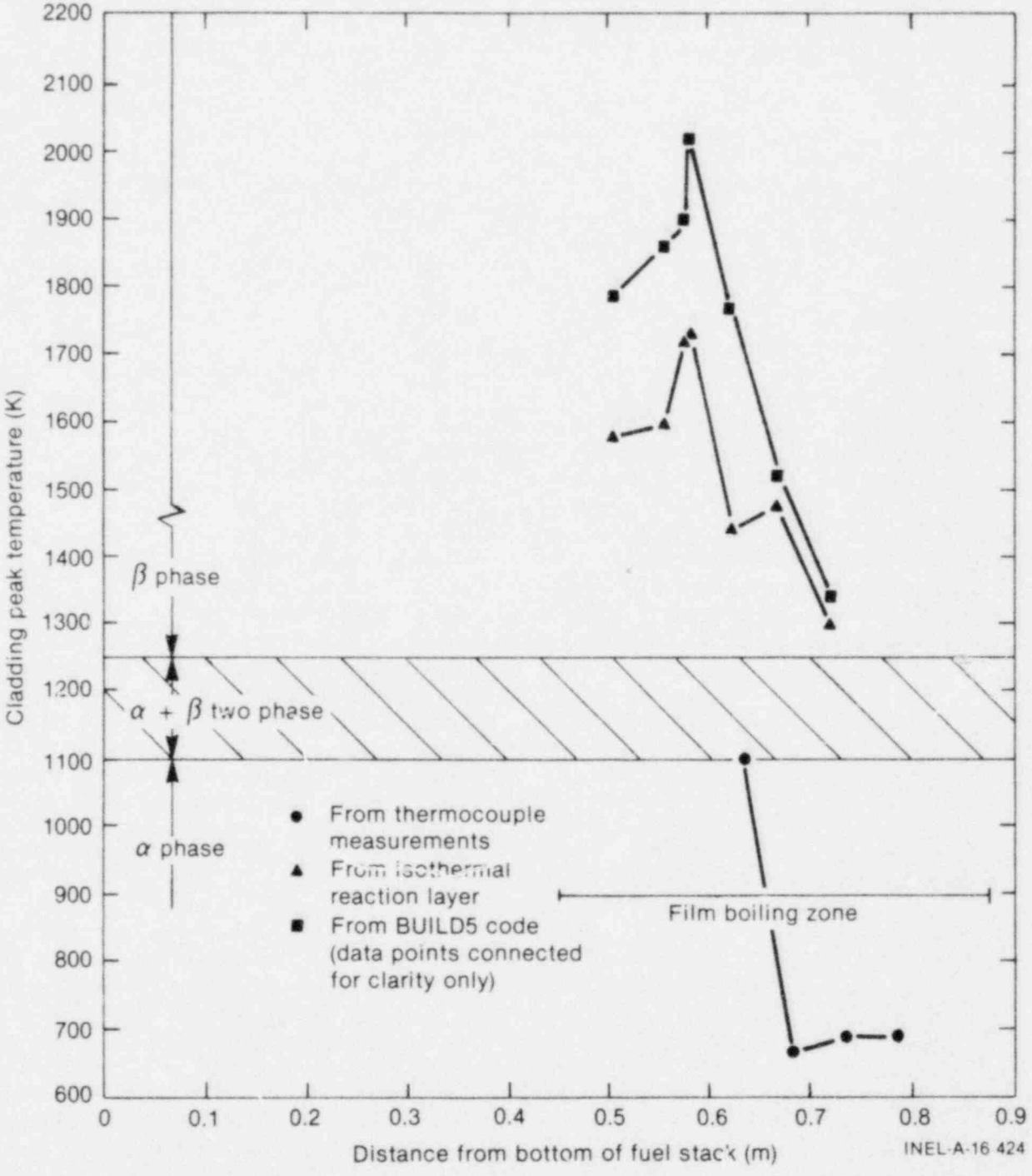

Figure 12. Cladding peak temperatures during Test 8-1 RS.

During removal of the fuel rod from the flow shroud, it was discovered that the rod was in two pieces, with the separation at about 0.59 m from the bottom of the fuel stack. This break was believed to have occurred dur[illegible] the removal process. As the lower portion of the rod was lowered onto a table, the broken end of the rod touched the table first and broke from the weight of the rod at a location about 0.51 m from the bottom of the fuel stack. Both fractures occurred through the main portion of a fuel pellet, rather than at a pellet-to-pellet interface. The fractures appeared to be brittle, with no evidence of ductile tearing. Because of the brittleness of the rod, great care was taken in preparing the rod for metallurgical examination.

3.4.3 Cladding Microstructure. Film boiling temperatures induce phase transformations that modify the microstructures of both the cladding and fuel, resulting in changes in the mechanical properties and overall behavior of fuel rods. Additional microstructural changes arise from oxidation of the cladding. Metallographic examination of cladding microstructures provided an indication, from phase changes, of the temperature range achieved during the test. Examination of cladding samples from the Test 8-1 RS fuel rod showed the following microstructures[12] (the film boiling zone was 0.454 to 0.877 m above the bottom of the fuel stack):

1. Samples at 0.175, 0.429, and 0.441 to 0.460 m contained stress-relieved zircaloy, which occurs when the temperature is <920 K.

2. Samples at 0.505, 0.556, 0.575, 0.581, 0.622, 0.644 to 0.663, and 0.670 m contained prior beta zircaloy, which occurs when the temperature exceeds 1250 K.

3. A sample at 0.721 m contained microstructures ranging from recrystallized alpha zircaloy on one side of the sample to prior beta zircaloy on the other, representing a temperature range of ~920 to above 1250 K.

4. Samples at 0.733 and 0.775 m contained recrystallized alpha zircaloy, which occurs when the temperature is in the range of 920 to 1105 K.

Figure 13 shows the cladding microstructure from a longitudinal section taken from the film boiling zone at 0.556 m. The sample illustrates the prior beta microstructure typical of cladding that exceeded 1600 K (from reaction layer kinetics, Figure 12).

Figure 14 shows the cladding microstructure from a longitudinal section taken from the film boiling zone at 0.581 m. This section illustrates a small thickness of remaining prior beta zircaloy, most of the cladding having been oxidized. A crack that completely penetrates the cladding is also shown.

Figure 15 shows a composite, transverse section illustrating cladding microstructures and estimated temperatures near the 0.635-m thermocouple location. It is apparent that the cladding was cooler beneath the thermocouple than to either side. The prior beta structure vanishes in the weld between the cladding and the thermocouple sheath, with the sheath showing no evidence of having been at a temperature greater than about 1050 K, which is in good agreement with the maximum temperature indicated by this thermocouple.

3.4.4 Cladding Embrittlement. As discussed previously, the Test 8-1 RS fuel rod attained cladding temperatures well above the beta transformation temperature ($T > 1250$ K) during film boiling. Temperatures of this magnitude induce oxidation at both the outer and inner cladding surfaces. A zircaloy-water (steam) reaction, in which oxygen diffusion into the cladding becomes significant, occurs at the outer surface and causes the formation of an oxygen-stabilized alpha-zircaloy layer beneath the ZrO_2 layer. When the cladding is in intimate contact with the fuel, a cladding-fuel reaction occurs at the inner surface, forming uranium-zircaloy and oxygen-stabilized alpha-zircaloy reaction layers. Each of the cladding samples shown in Figures 13 and 14 exhibits these inner and outer surface reaction layers. The simultaneous development of such oxidation layers on the outer and inner cladding surfaces results in cladding embrittlement, which increases the likelihood of cladding failure.

Cladding oxidation, embrittlement, and failure criteria are treated in detail in Reference 12. The failure potential for the Test 8-1 RS fuel rod has

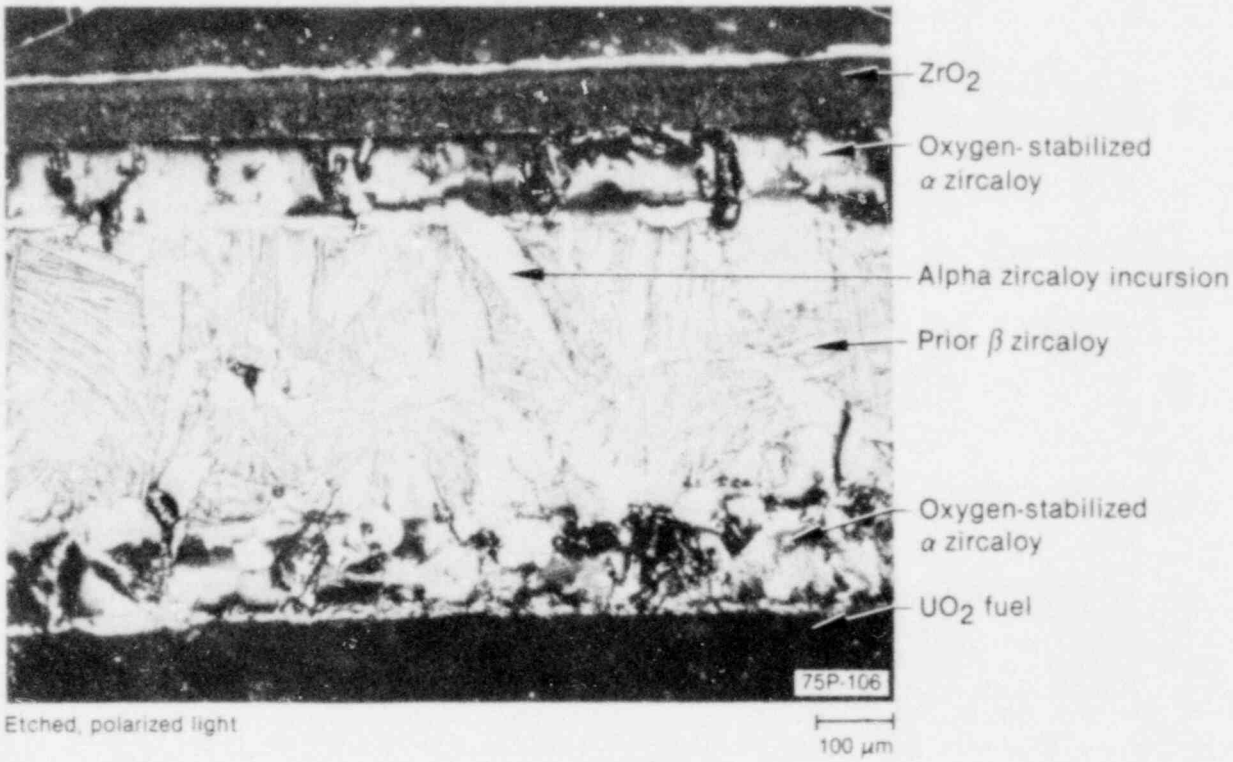

Figure 13. Longitudinal section of fuel rod at 0.556 m from bottom of fuel stack showing cladding microstructure (Test 8-1 RS).

been evaluated by three methods: (a) criteria based on oxygen concentration in the beta phase,[13] (b) the fractional thickness of remaining beta phase criterion,[14] and (c) the equivalent cladding reacted method.[14] The results of these evaluations are summarized in Table 10. As shown, each of the three criteria predicts embrittlement well in excess of that required to cause fuel rod failure.

3.5 Fuel Behavior

Increased fuel temperatures during film boiling resulted in thermal restructuring of the UO_2 fuel in the film boiling region of the Test 8-1 RS fuel rod. Restructuring was characterized by grain growth toward the center of the fuel column and shattering of the fuel along grain boundaries. Grain sizes near the center of the fuel were generally in the range of 8 to 40 μm, with one sample showing grains the order of 155 μm. Near the edge of the fuel pellets, grain sizes were only slightly larger than the prefabricated grain size of about 3.4 μm.

Figure 16 shows a composite photomicrograph across the fuel rod at a location 0.622 m above the bottom of the fuel stack. The section illustrates the radial microstructure typical of the high temperature film boiling zone. Figure 17 shows a higher magnification of the fuel structure near the center at the same axial location as Figure 16.

Fuel shattering occurred in localized regions, particularly near the center of the fuel. The intergranular form of this localized grain fracturing is illustrated in Figure 17 and is also shown in Figure 18, which is a transverse section taken from an axial location 0.721 m above the bottom of the fuel stack. Examinations performed to determine if the fuel melted were inconclusive. Further details are provided in Appendix D.

The Test 8-1 RS fuel rod was instrumented with a tungsten-rhenium, tantalum-sheathed thermocouple to measure fuel centerline temperature at an axial location 0.737 m above the bottom of the fuel stack. The maximum measured fuel temperature of about 2550 K occurred during DNB Cycle 4, well below the UO_2 melting temperature of 3100 K.

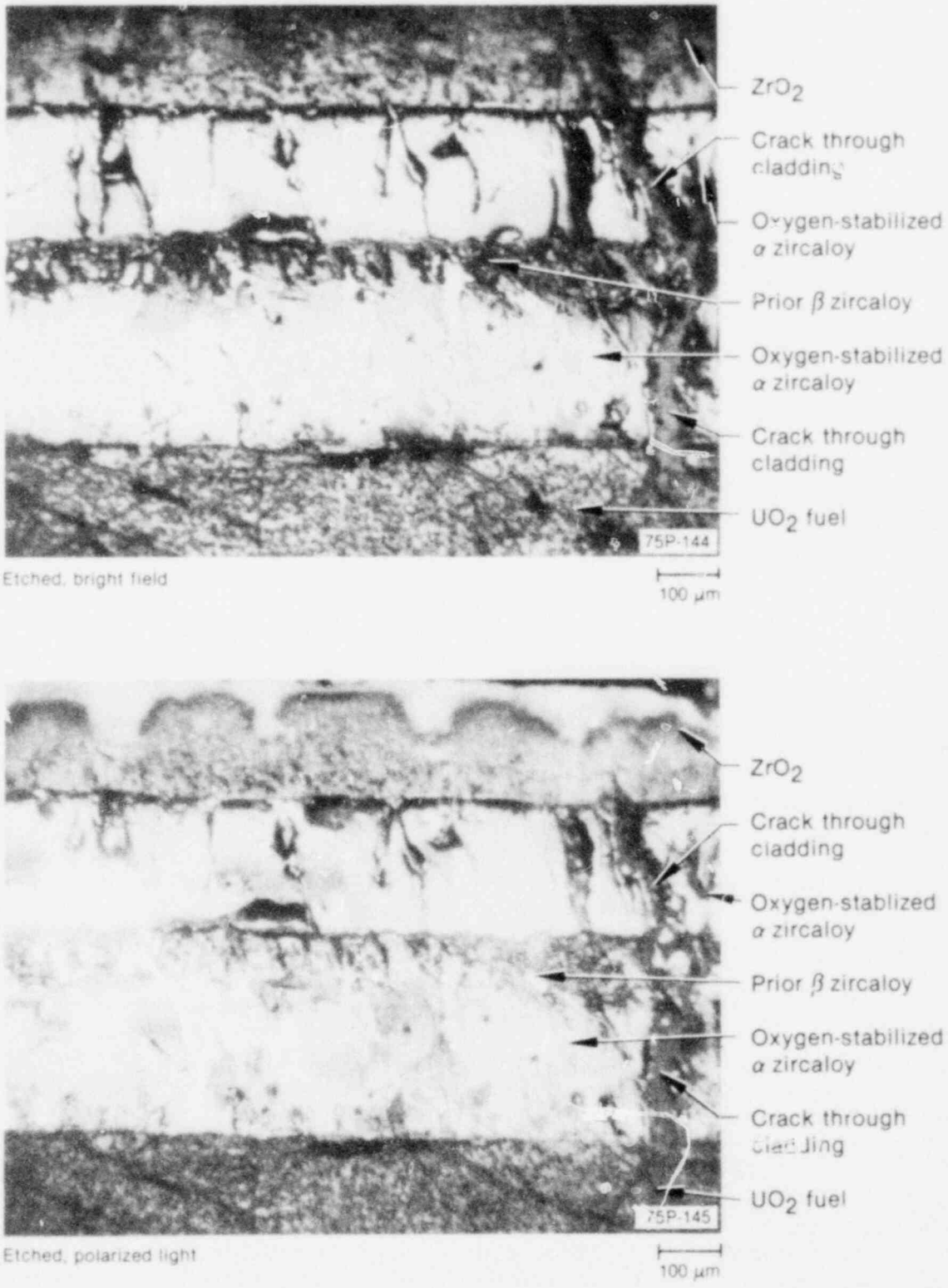

Figure 14. Longitudinal section of fuel rod at 0.581 m from bottom of fuel stack showing cladding microstructure (Test 8-1 RS).

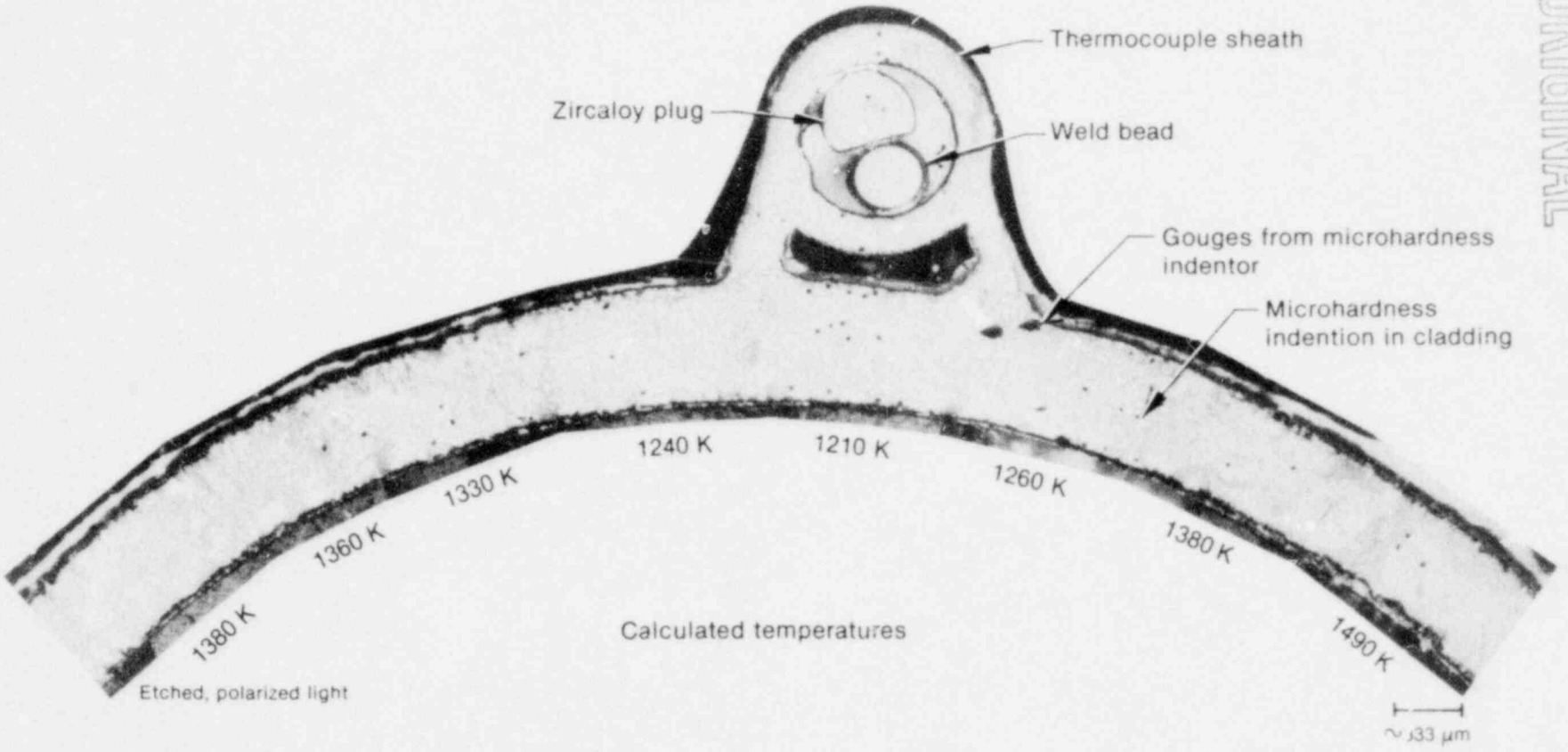

Figure 15. Composite transverse section of fuel rod showing microstructure in cladding near 0.635-m thermocouple (0.622-m location) (Test 8-1 RS).

Table 10. Cladding embrittlement evaluation, Test 8-1 RS fuel rod

Maximum Cladding Temperature and Location[a]	Time in Film Boiling[b] (s)	Pawel's Criteria[c] Critical Oxidation Time (corrected) (s)	Pawel's Criteria[c] Failure Predicted	Scatena's Remaining Beta Phase Criterion[d] F_w	Scatena's Remaining Beta Phase Criterion[d] Failure Predicted	Scatena's ECR Criterion[e] Equivalent Cladding Reacted (mole %)	Scatena's ECR Criterion[e] Failure Predicted
1740 K—0.581 m	362	20	Yes	0.03	Yes	27	Yes

a. Temperatures determined from isothermal correlations based on reaction layer thicknesses (Reference 12); locations are distance from bottom of fuel stack.

b. Film boiling time is at maximum cladding temperature location as determined in Reference 12.

c. Cladding failure predicted when time in film boiling exceeds critical oxidation time. Correction factor applied to critical oxidation times to account for difference in cladding wall thickness of PBF test rods compared with out-of-pile tubes.

d. Cladding failure predicted when fractional thickness of remaining beta-phase zircaloy (F_w) is <0.5.

e. Cladding failure predicted when equivalent cladding reacted exceeds 17 mole %.

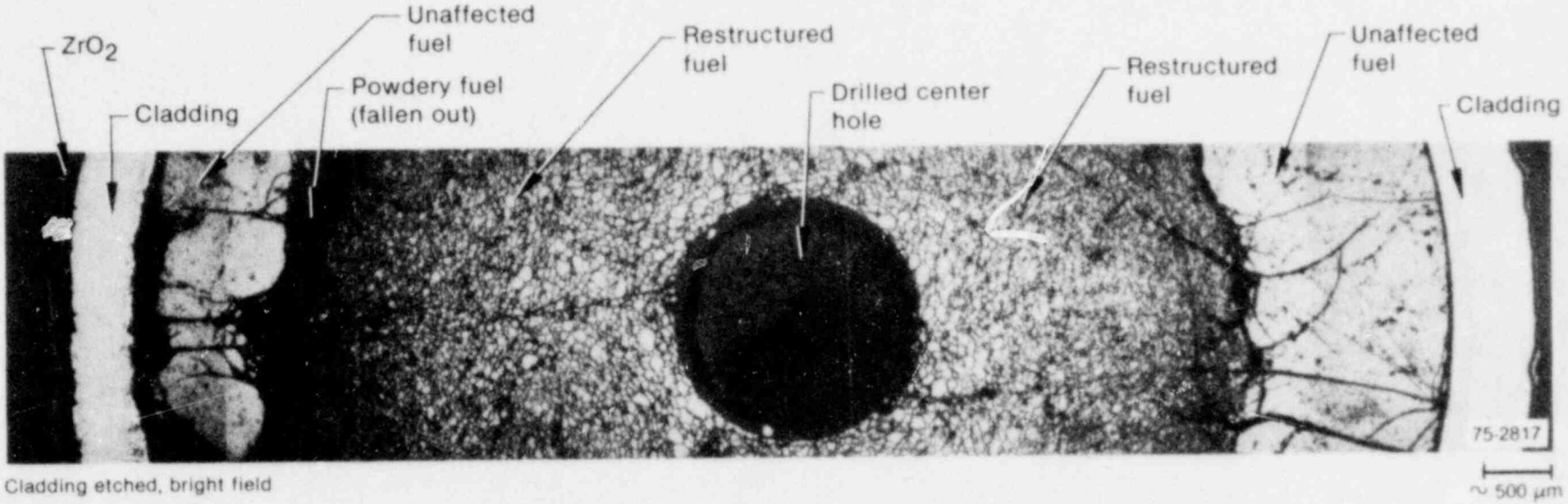

Figure 16. Composite photomicrograph ... oss fuel rod at about 0.622 m from bottom of fuel stack showing fuel restructuring and cladding oxidat... Test 8-1 RS).

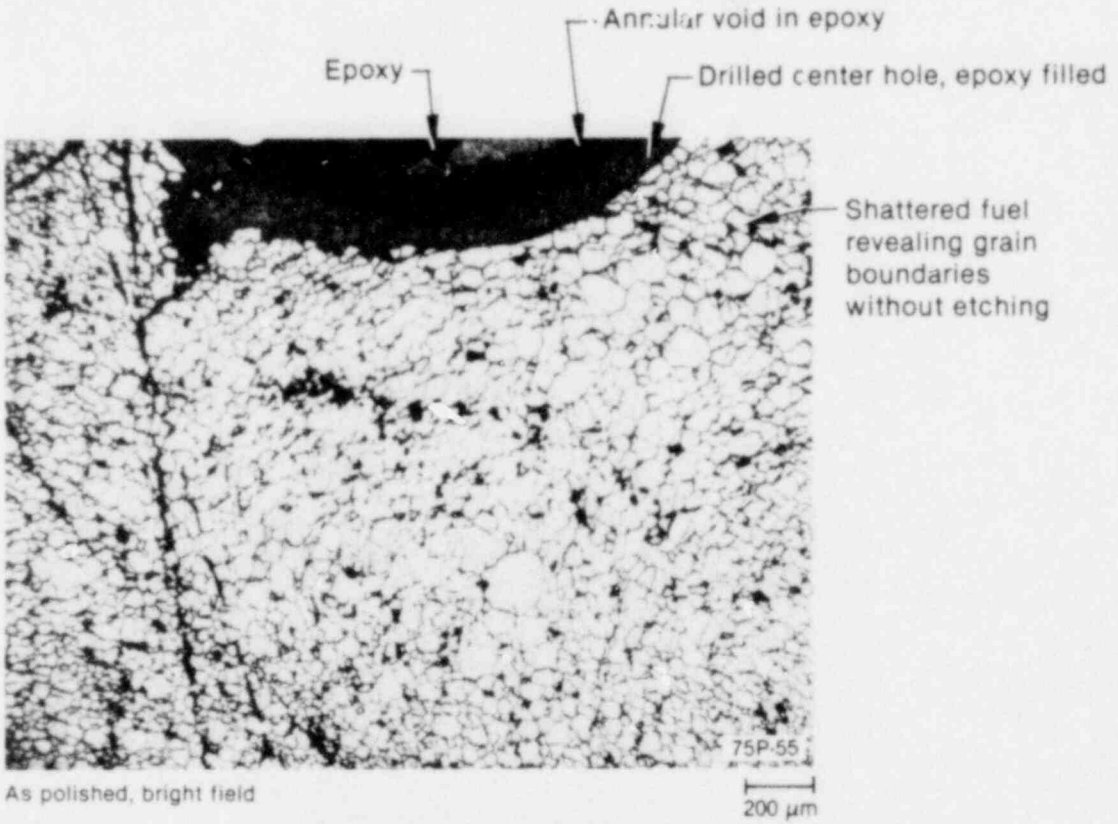

Figure 17. Transverse section of fuel rod showing fuel structure near center hole of fuel pellet, 0.622 m from bottom of fuel stack (Test 8-1 RS).

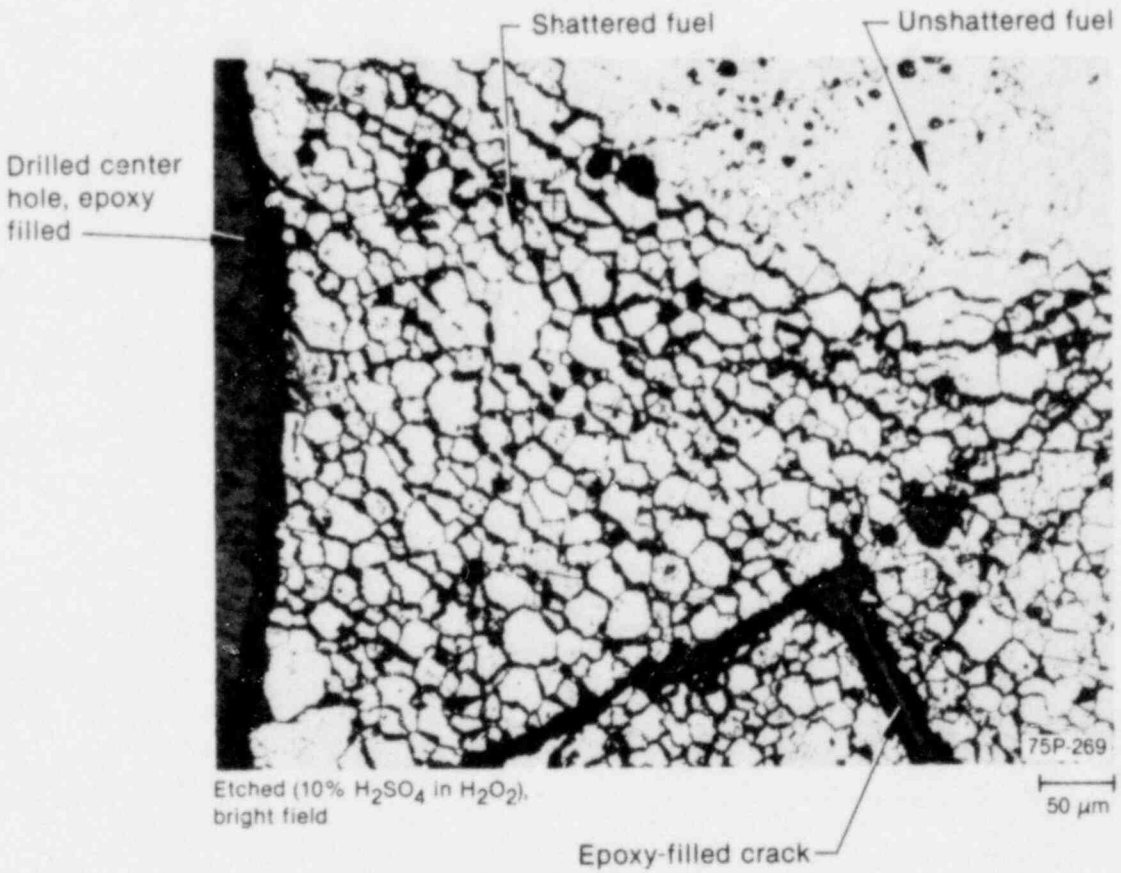

Figure 18. Transverse section of fuel rod showing fuel structure near center hole of fuel pellet, 0.721 m from bottom of fuel stack (Test 8-1 RS).

4. RESULTS AND ANALYSES - TEST CHF SCOPING

The primary objective of the CHF Scoping test was to evaluate the effect of short-term operation on the reproducibility of the onset of DNB. Specific areas of interest were

1. The power at which DNB occurred on the test rod
2. Any shift in the test rod power to achieve DNB and any shift in the axial location of DNB occurring from repeated cycling in and out of DNB
3. The test conditions at which detectable axial cladding deformation began
4. The response and behavior of the test instruments.

The following sections present and evaluate the results of Test CHF Scoping in accordance with these objectives.

4.1 Summary of Results

Post-DNB test results and fuel rod behavior are briefly summarized in this section. Detailed results are presented in subsequent sections.

During Cycles 2 through 7, DNB occurred in a narrow range of rod peak powers from 60.0 to 63.3 kW/m. Departure from nucleate boiling was first detected at 50.5 kW/m during Cycle 1; this relatively low rod peak power was believed to have been a result of gas entrapment on the fuel rod surface. Cladding surface thermocouple data indicated that film boiling was initiated on the upper part of the fuel rod and spread down the surface of the rod. The rod was exposed to film boiling conditions for a cumulative time of about 40 s during the test (total time that the cladding surface thermocouples indicated temperatures in excess of the rewet temperature of 670 K[9]).

Postirradiation examination of the fuel rod showed damage in the form of cladding collapse, waisting (cladding collapse at pellet interfaces), oxidation, and bowing. The cladding remained intact during and following the test. Cladding temperature estimates based on the measured extent of oxidation indicated that cladding peak temperatures exceeded 1600 K, about 550 K greater than determined from cladding surface thermocouple measurements. The thermocouple measurements were atypically low because of fin-cooling effects. Evaluation of the extent of cladding embrittlement in accordance with several documented methods indicated that insufficient embrittlement occurred to result in failure. Thermal restructuring of the fuel occurred in the form of UO_2 grain growth in the central region of the fuel column.

4.2 Film Boiling

Departure from nucleate boiling occurred once during each of the seven DNB cycles in Test CHF Scoping. Film boiling was established during four of the seven cycles. This section discusses the onset of DNB, film boiling propagation, and film boiling termination.

4.2.1 Onset of DNB. Each DNB cycle was performed by incrementally increasing the test rod power while maintaining coolant flow, inlet temperature, and pressure approximately constant (see Subsection 2.2.2.2 and Table 7). Increases in the cladding surface temperatures and fuel rod axial elongation were used to detect DNB. Figures 19 through 32 show the changes in these parameters, as well as in fuel rod power and coolant flow rate during the latter part of each of the seven cycles. Table 11 summarizes the test rod peak power levels at the onset of DNB for each of the seven cycles.

As shown in Table 11, DNB occurred in a narrow range of rod peak powers from 58.4 to 63.3 kW/m, with the exception of Cycle 1. The relatively low power, 50.5 kW/m, at which the onset of DNB occurred during Cycle 1 was probably caused by gas entrapment on the fuel rod surface.[3,8]

Calculations to predict the fuel rod power at the onset of DNB were performed using the W-3[10] and B&W-2[11] correlations. Coolant conditions assumed for the calculations were 1360 kg/s·m^2 flow, 600 K inlet temperature, and 14.5 MPa pressure. Calculated rod peak powers at the onset of DNB were 64.9 kW/m using the W-3 correlation and 78.4 kW/m using the B&W-2 correlation. Although the coolant conditions assumed for

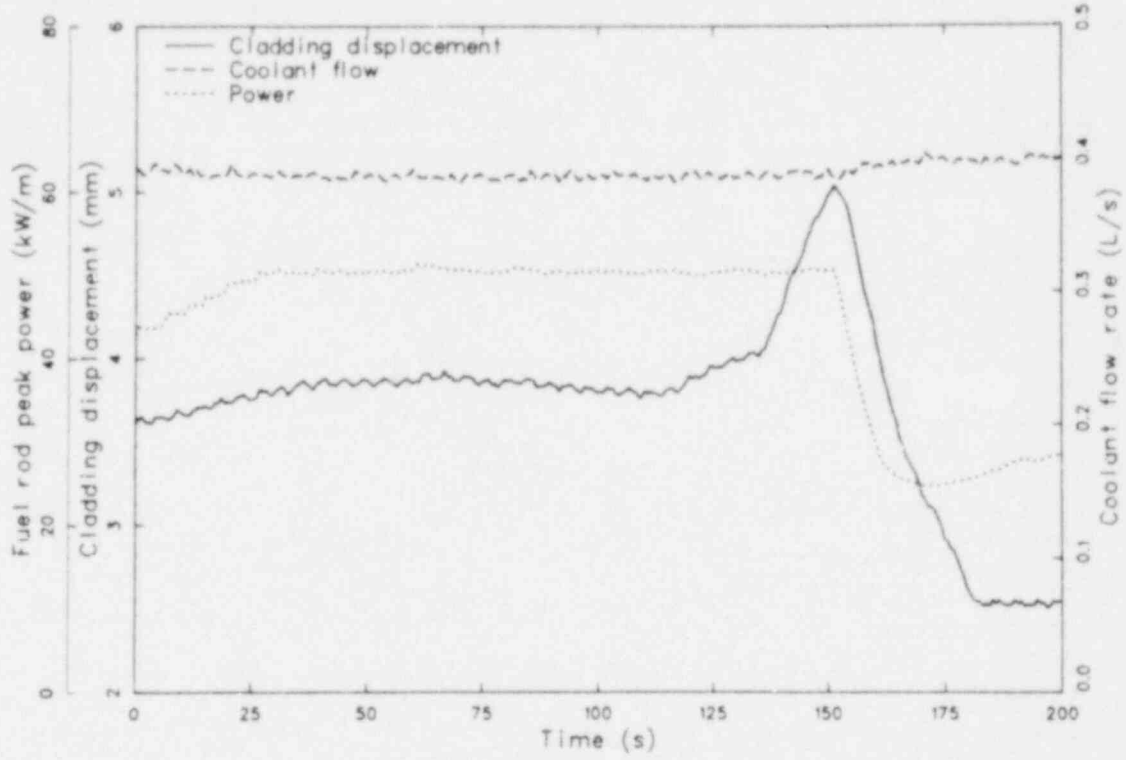

Figure 19. Fuel rod peak power, cladding displacement, and coolant flow rate versus time during Test CHF Scoping (DNB Cycle 1).

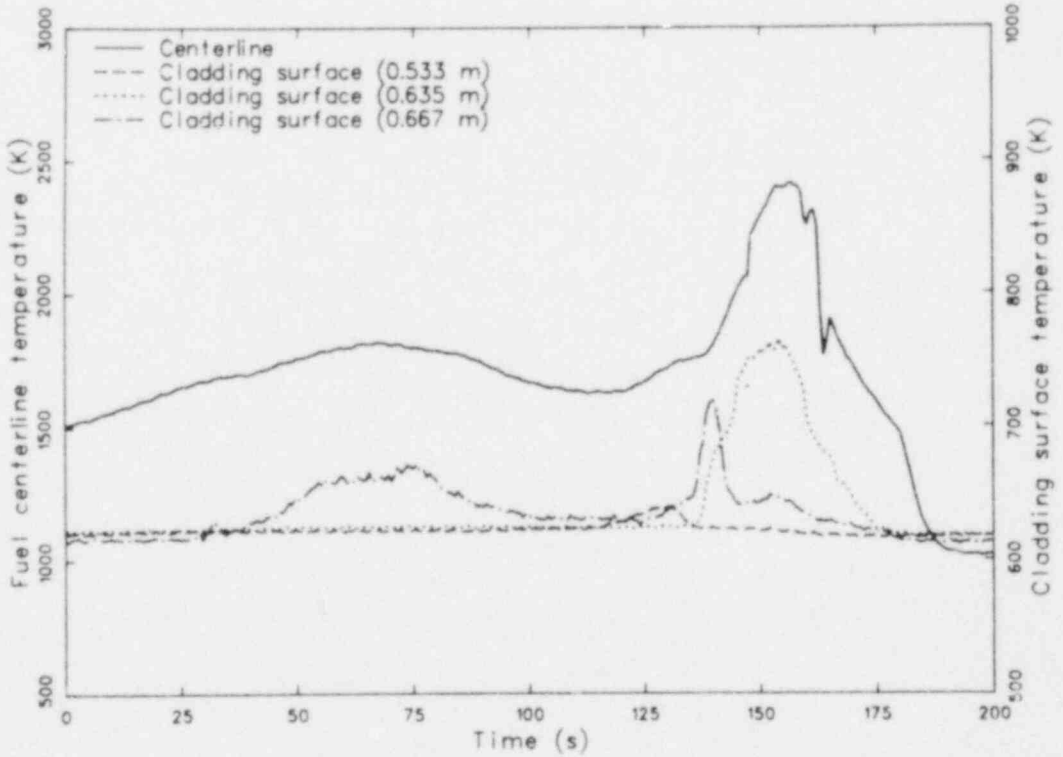

Figure 20. Fuel centerline temperature and cladding surface temperature versus time during Test CHF Scoping (DNB Cycle 1).

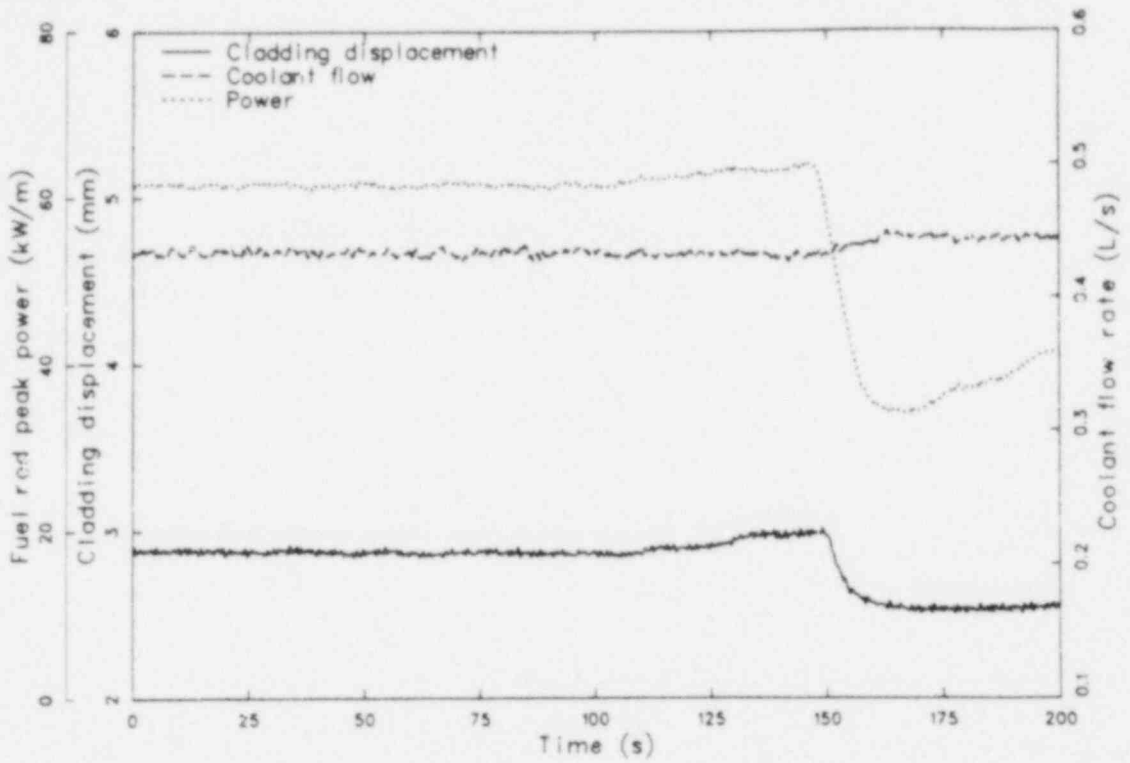

Figure 21. Fuel rod peak power, cladding displacement, and coolant flow rate versus time during Test CHF Scoping (DNB Cycle 2).

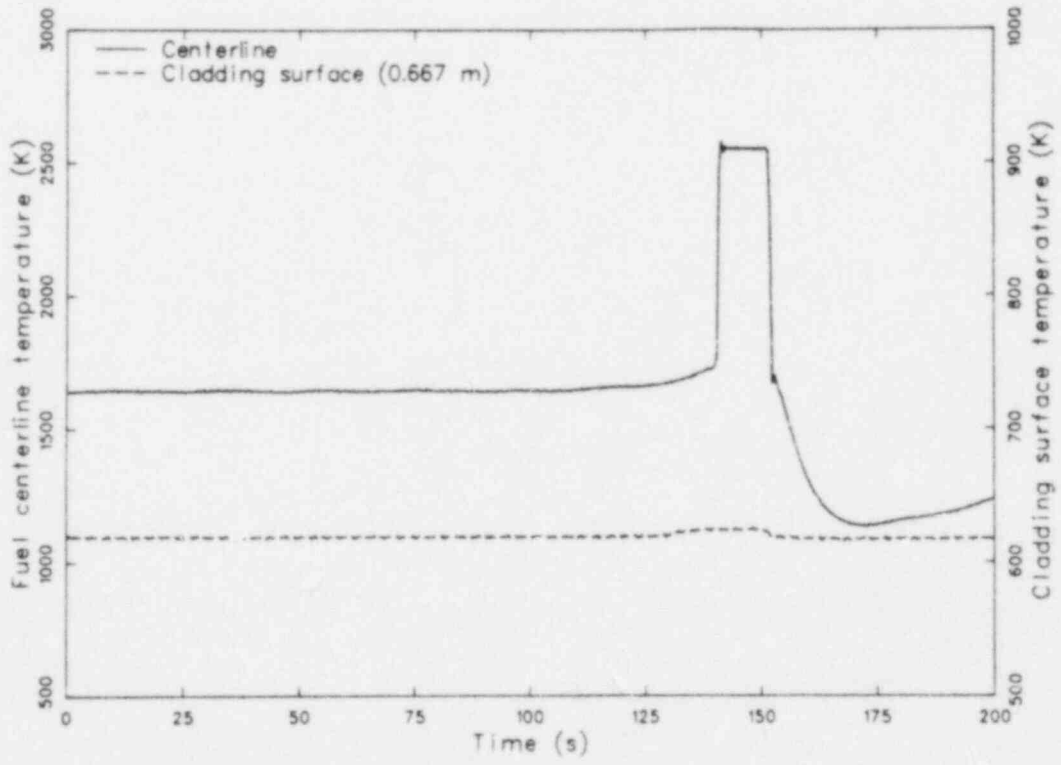

Figure 22. Fuel centerline temperature and cladding surface temperature versus time during Test CHF Scoping (DNB Cycle 2).

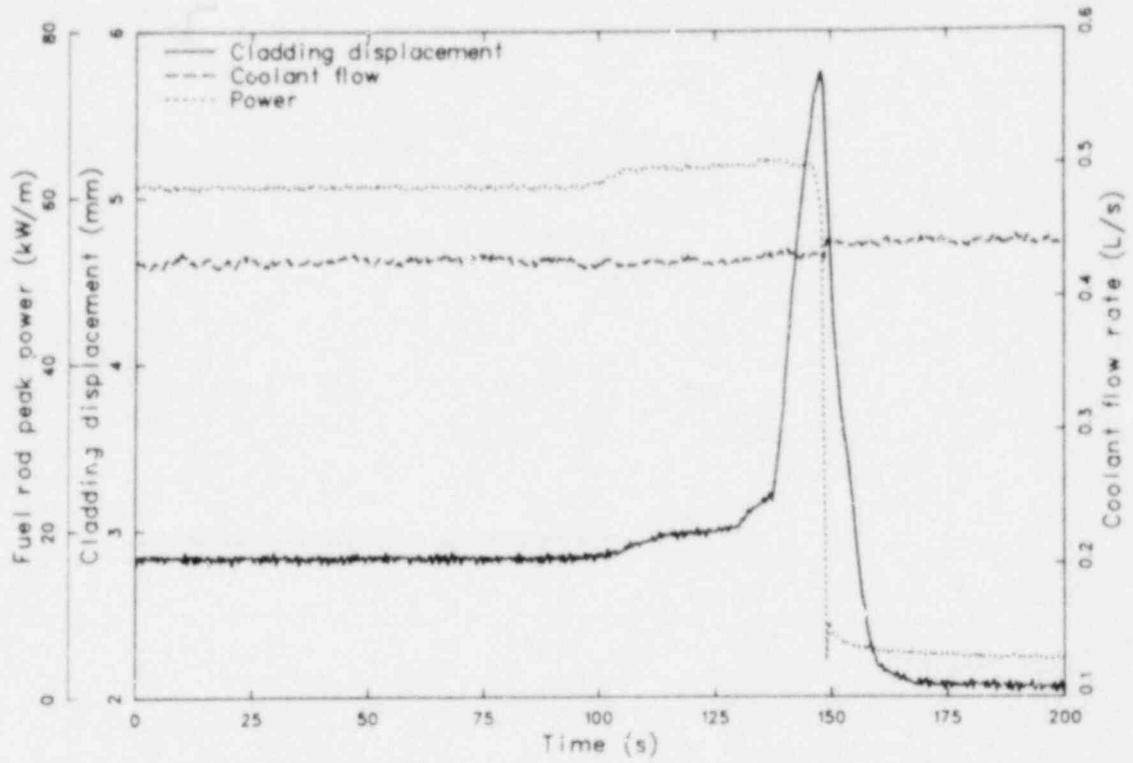

Figure 23. Fuel rod peak power, cladding displacement, and coolant flow rate versus time during Test CHF Scoping (DNB Cycle 3).

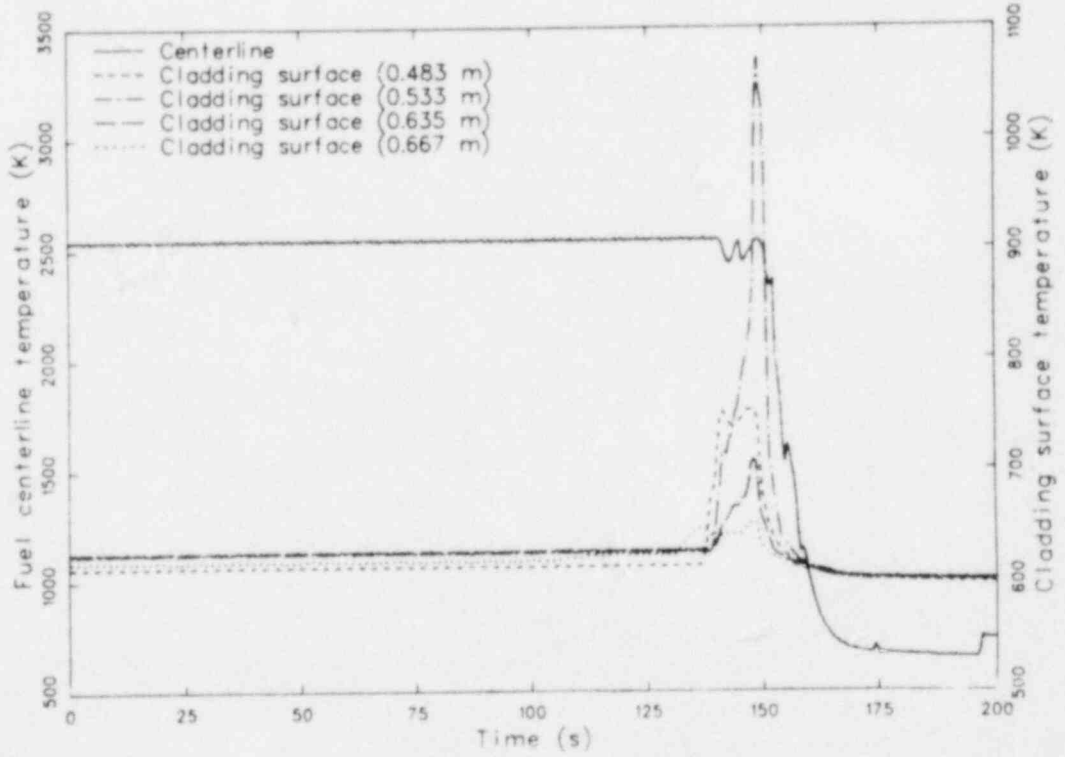

Figure 24. Fuel centerline temperature and cladding surface temperature versus time during Test CHF Scoping (DNB Cycle 3).

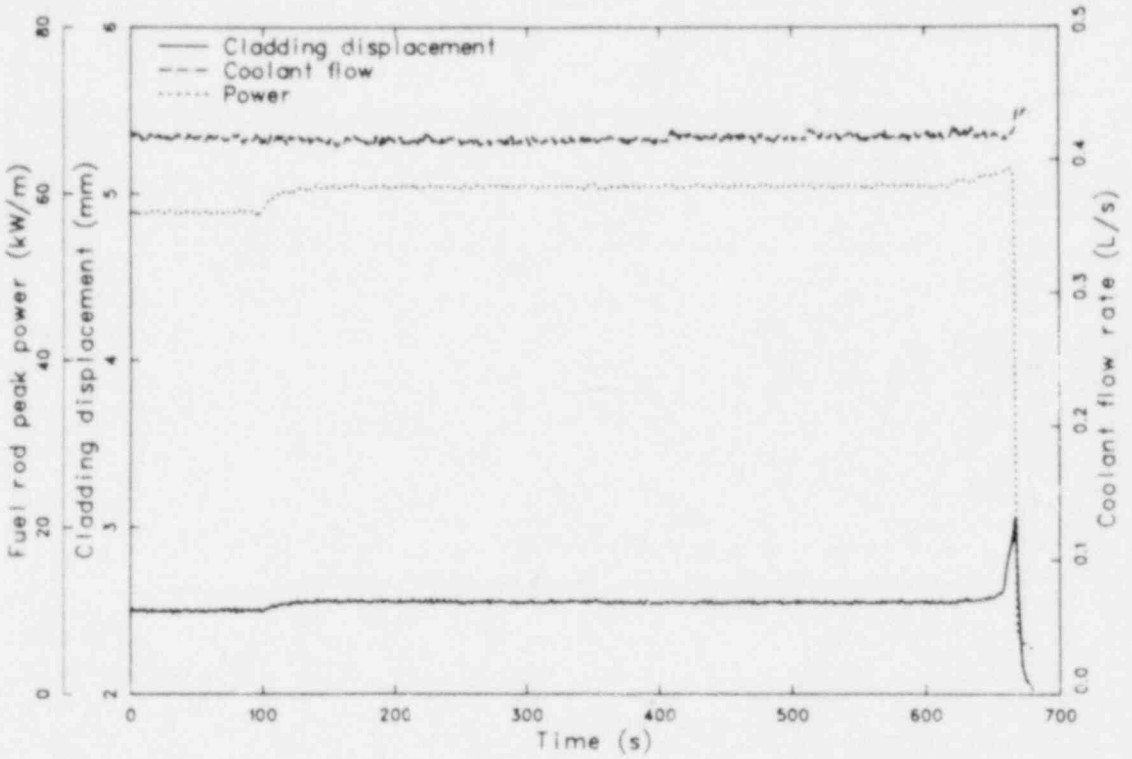

Figure 25. Fuel rod peak power, cladding displacement, and coolant flow rate versus time during Test CHF Scoping (DNB Cycle 4).

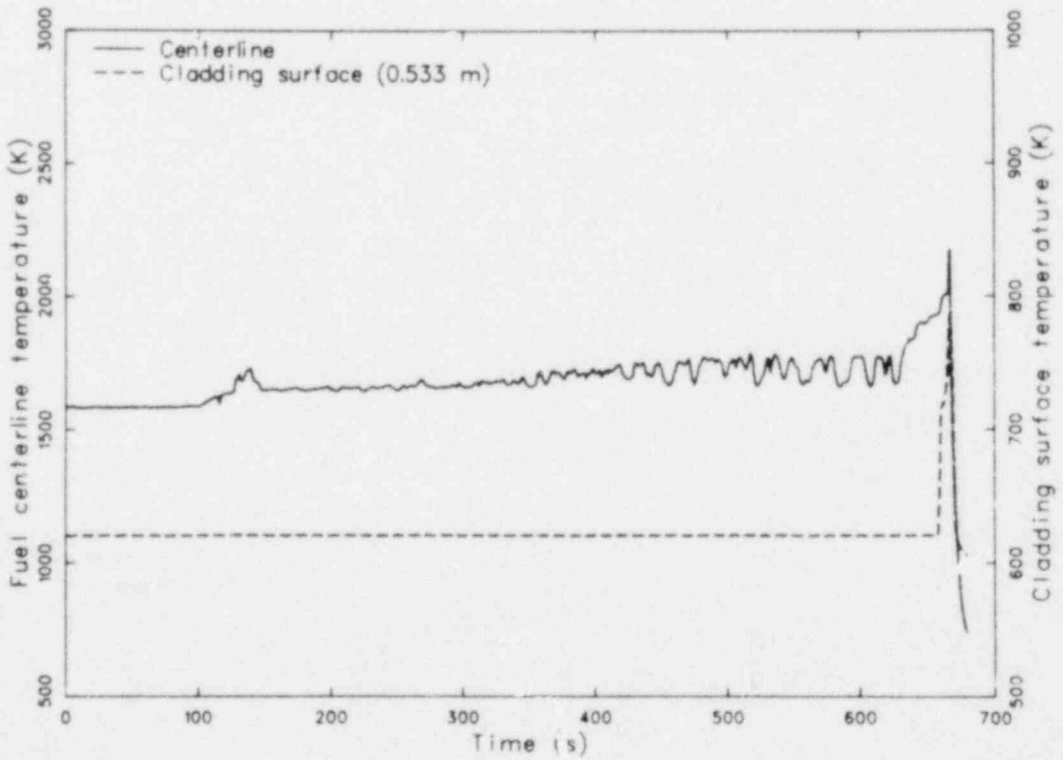

Figure 26. Fuel centerline temperature and cladding surface temperature versus time during Test CHF Scoping (DNB Cycle 4).

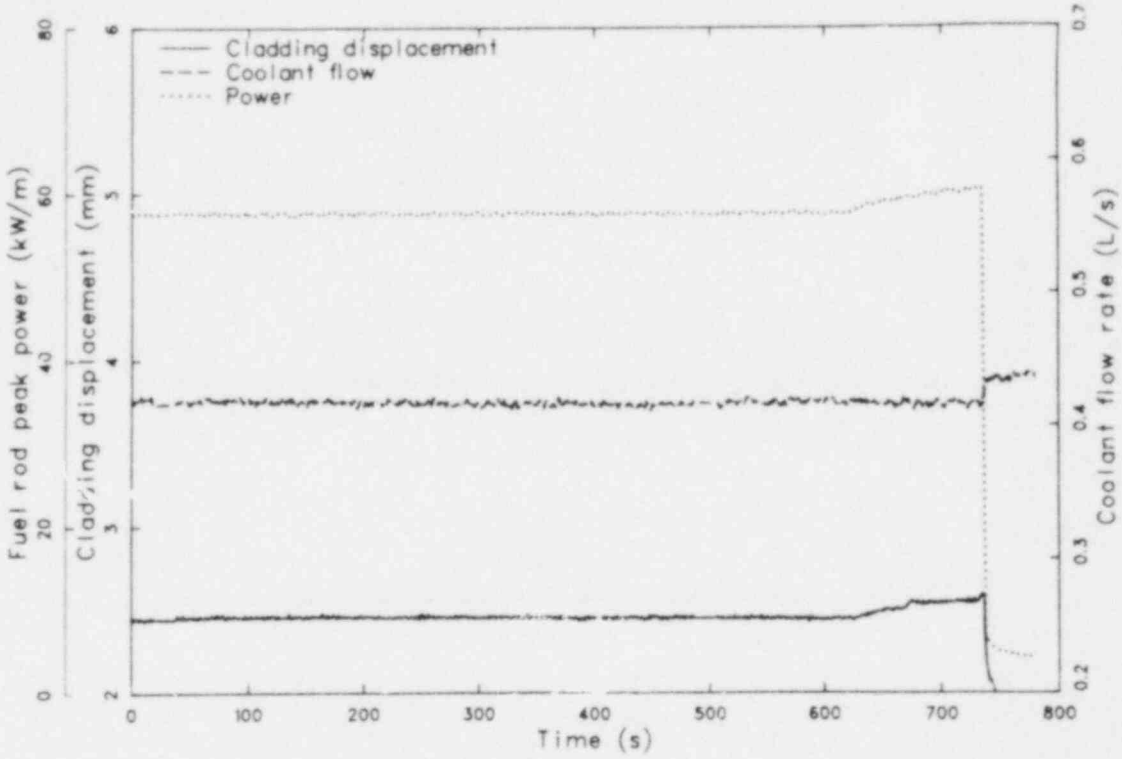

Figure 27. Fuel rod peak power, cladding displacement, and coolant flow rate versus time during Test CHF Scoping (DNB Cycle 5).

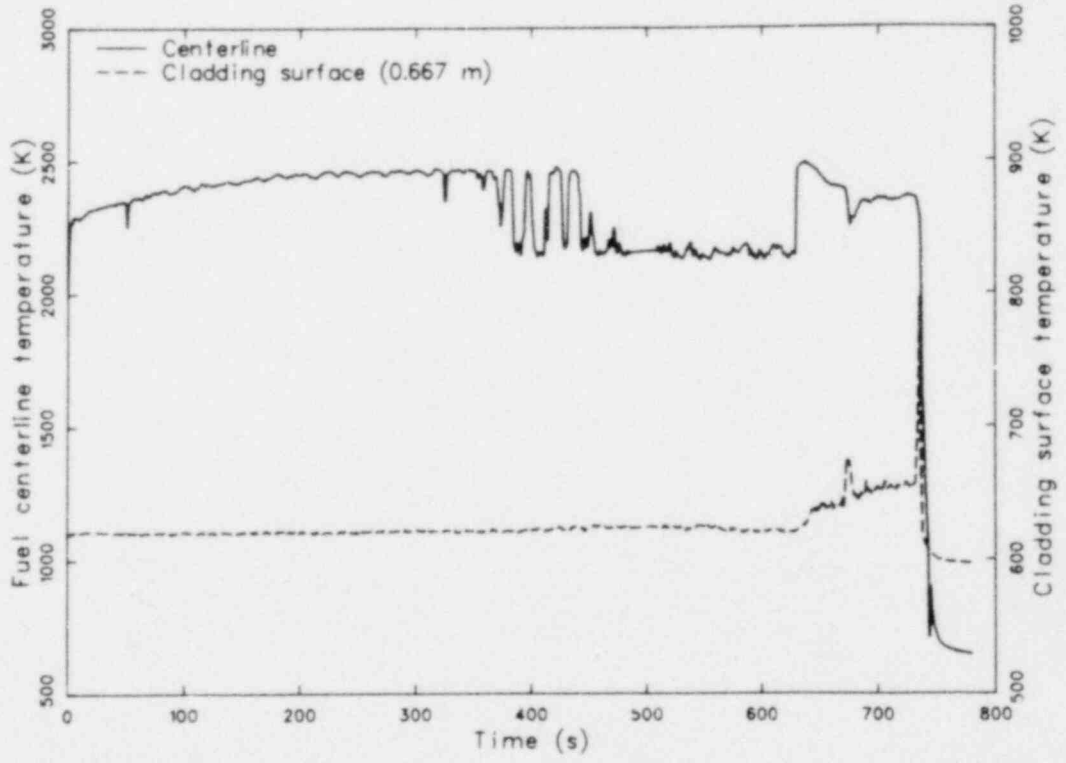

Figure 28. Fuel centerline temperature and cladding surface temperature versus time during Test CHF Scoping (DNB Cycle 5).

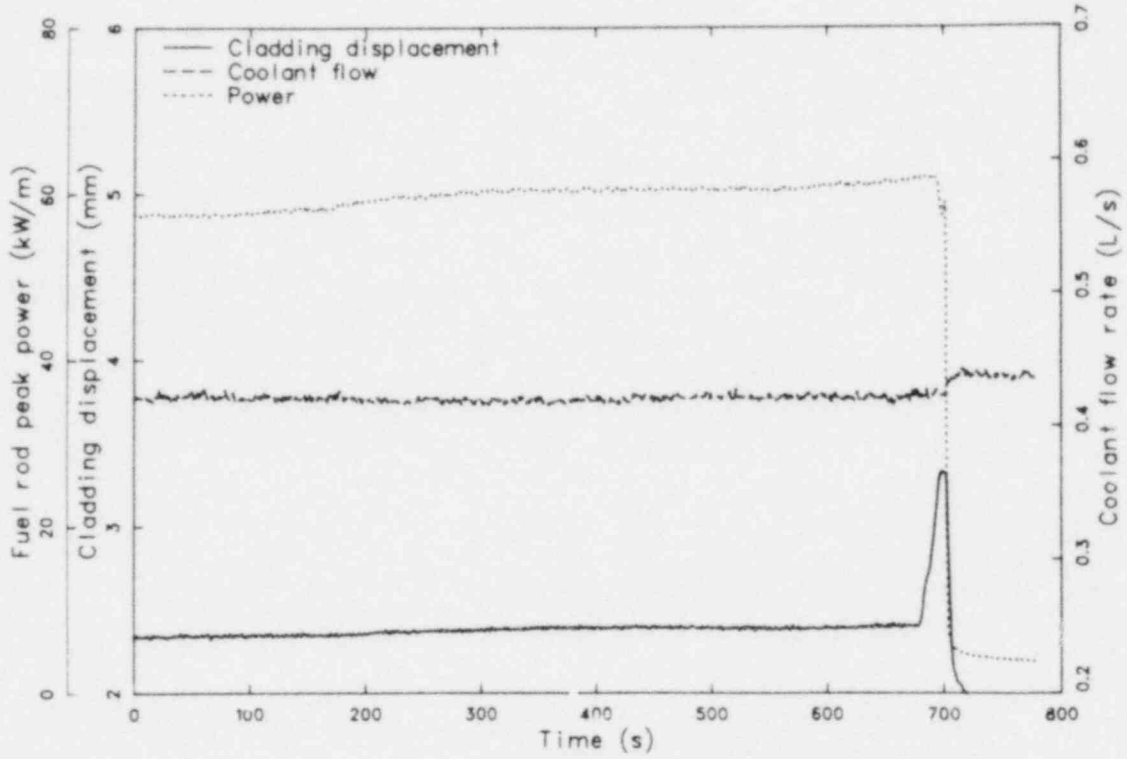

Figure 29. Fuel rod peak power, cladding displacement, and coolant flow rate versus time during Test CHF Scoping (DNB Cycle 6).

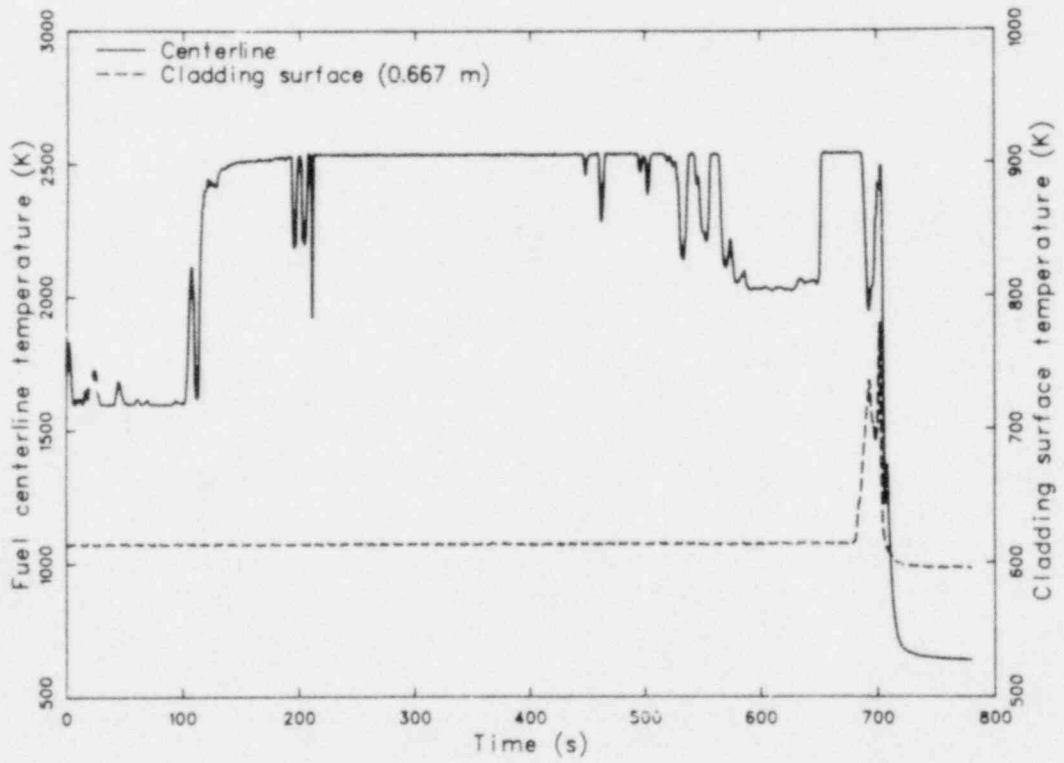

Figure 30. Fuel centerline temperature and cladding surface temperature versus time during Test CHF Scoping (DNB Cycle 6).

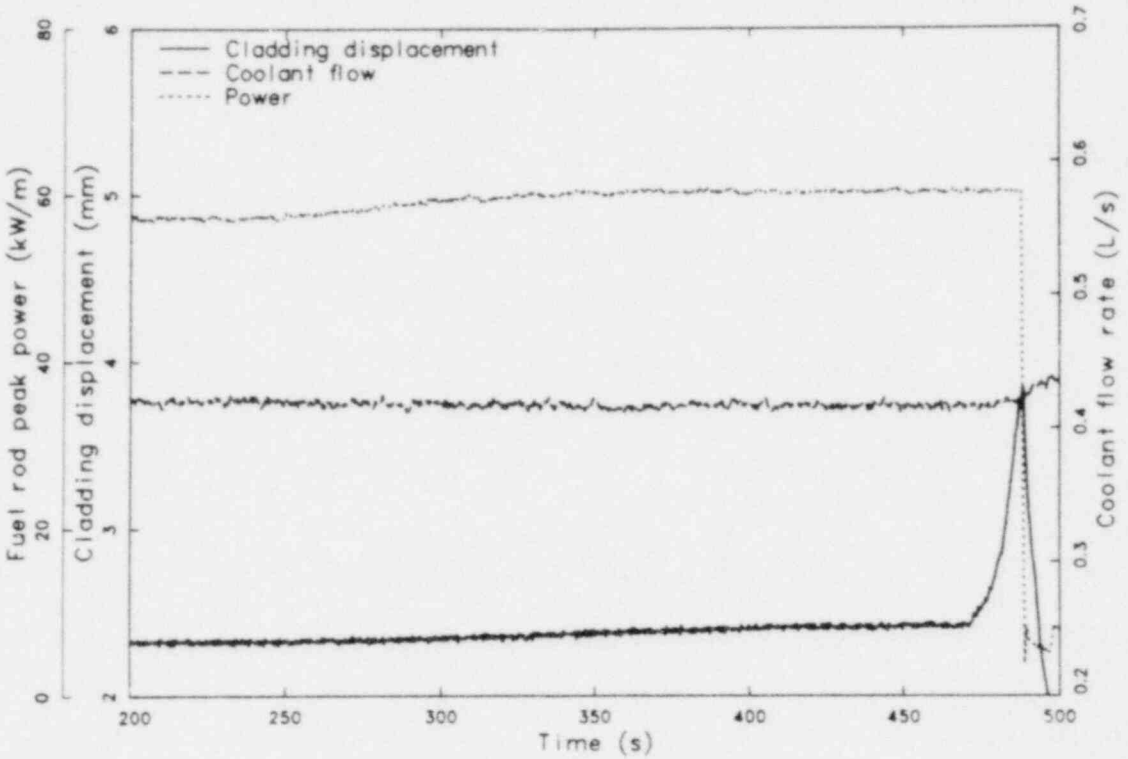

Figure 31. Fuel rod peak power, cladding displacement, and coolant flow rate versus time during Test CHF Scoping (DNB Cycle 7).

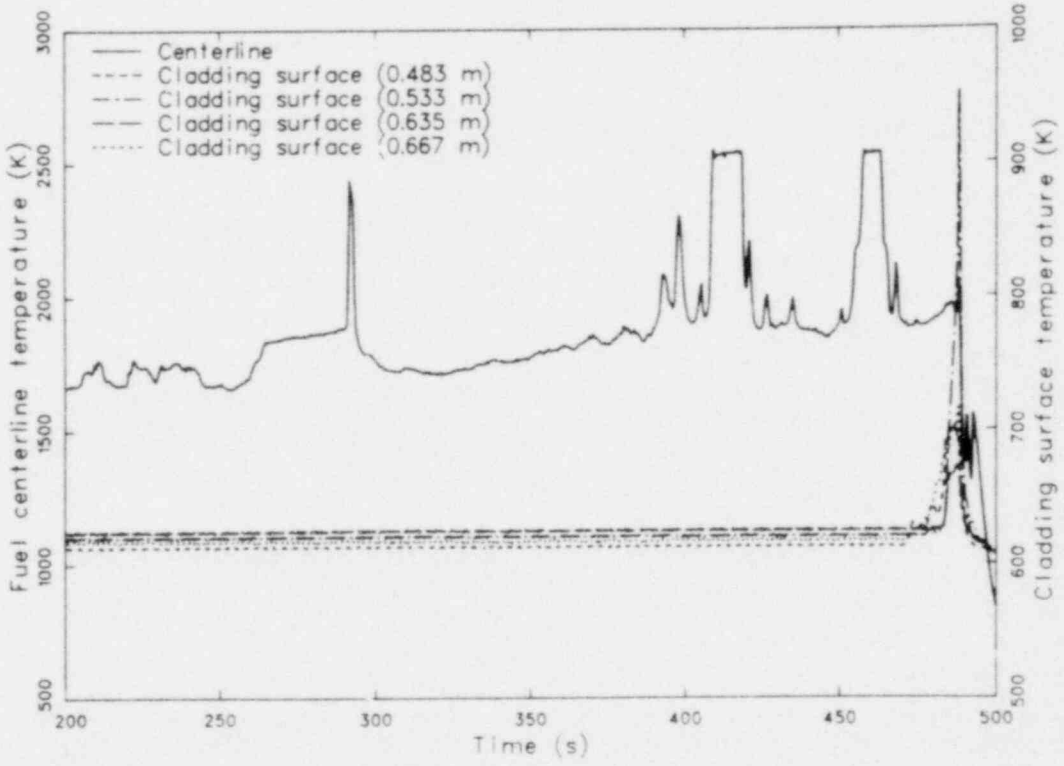

Figure 32. Fuel centerline temperature and cladding surface temperature versus time during Test CHF Scoping (DNB Cycle 7).

Table 11. Onset of DNB—Test CHF Scoping

DNB Cycle	Rod Peak Power at DNB (kW/m)	Inlet Flow ($kg/s \cdot m^2$)[a]	Inlet Temperature (K)	Coolant Pressure (MPa)
1	50.5	1260	602	15.2
2	63.0	1430	601	15.2
3	63.3	1430	602	15.2
4	62.3	1380	601	15.2
5	58.4	1380	601	15.2
6	61.7	1400	600	15.2
7	60.0	1380	601	15.2

a. Multiply coolant flow rate (L/s) in Figures 19, 21, 23, 25, 27, 29, and 31 by 3318 to get mass flow in $kg/s \cdot m^2$.

the calculations were slightly different than those for the DNB cycles, the effects should be insignificant. Both correlations predicted higher rod peak powers at the onset of DNB than were measured; however, the W-3 correlation more closely predicted the measured behavior.

4.2.2 Propagation of Film Boiling. Pretest calculations predicted that film boiling would first occur about 0.68 m above the bottom of the fuel stack. Once initiated, film boiling would be expected to slowly progress down the surface of the fuel rod. Such propagation is generally indicated by the cladding surface thermocouple measurements shown in Figures 20 and 24. During Cycle 1 (Figure 20), DNB was first indicated by the thermocouple mounted at the 0.667-m location; 85 s later, DNB was indicated at the 0.533-m location; and 20 s later, DNB was indicated at the 0.635-m location. The lowest thermocouple (0.483 m) did not indicate the occurrence of DNB. The onset of DNB at the 0.533-m location before the 0.635-m location could indicate an independent occurrence of film boiling unrelated to that spreading downward from above. However, the spread of film boiling could have initially passed by the 0.635-m location by spreading down the opposite side of the fuel rod. Also, the temperature excursion at 0.533 m was of low magnitude and short duration, more indicative of transition boiling than film boiling.

During Cycle 3 (Figure 24), DNB again occurred first at the 0.667-m location, followed by the 0.483-m location about 15 s later, and the 0.533- and 0.635-m locations after another 5 s. As during Cycle 1, these data may indicate independent occurrences of film boiling or may indicate a spreading of film boiling that bypassed intermediate thermocouple locations by passing down uninstrumented sides of the fuel rod.

4.2.3 Termination of Film Boiling. Cycles 1 and 2 were terminated by manually decreasing the reactor power, whereas Cycles 3 through 7 were terminated by reactor scram. During Cycle 3, a manual power decrease was initiated, followed by a reactor scram when the 810-K setpoint was exceeded by the 0.533-m thermocouple. Shutdown occurred while film boiling or transition boiling was in progress on the rod. Following shutdown, cladding surface thermocouples indicated rewet within a few seconds. Cooldown also resulted in rapid recovery of fuel rod elongation.

4.3 Posttest Condition of Fuel Rod

The posttest condition of the Test CHF Scoping fuel rod is shown in Figure 33. The fuel rod cladding remained intact, with no indication of failure as a result of the high temperature operation and

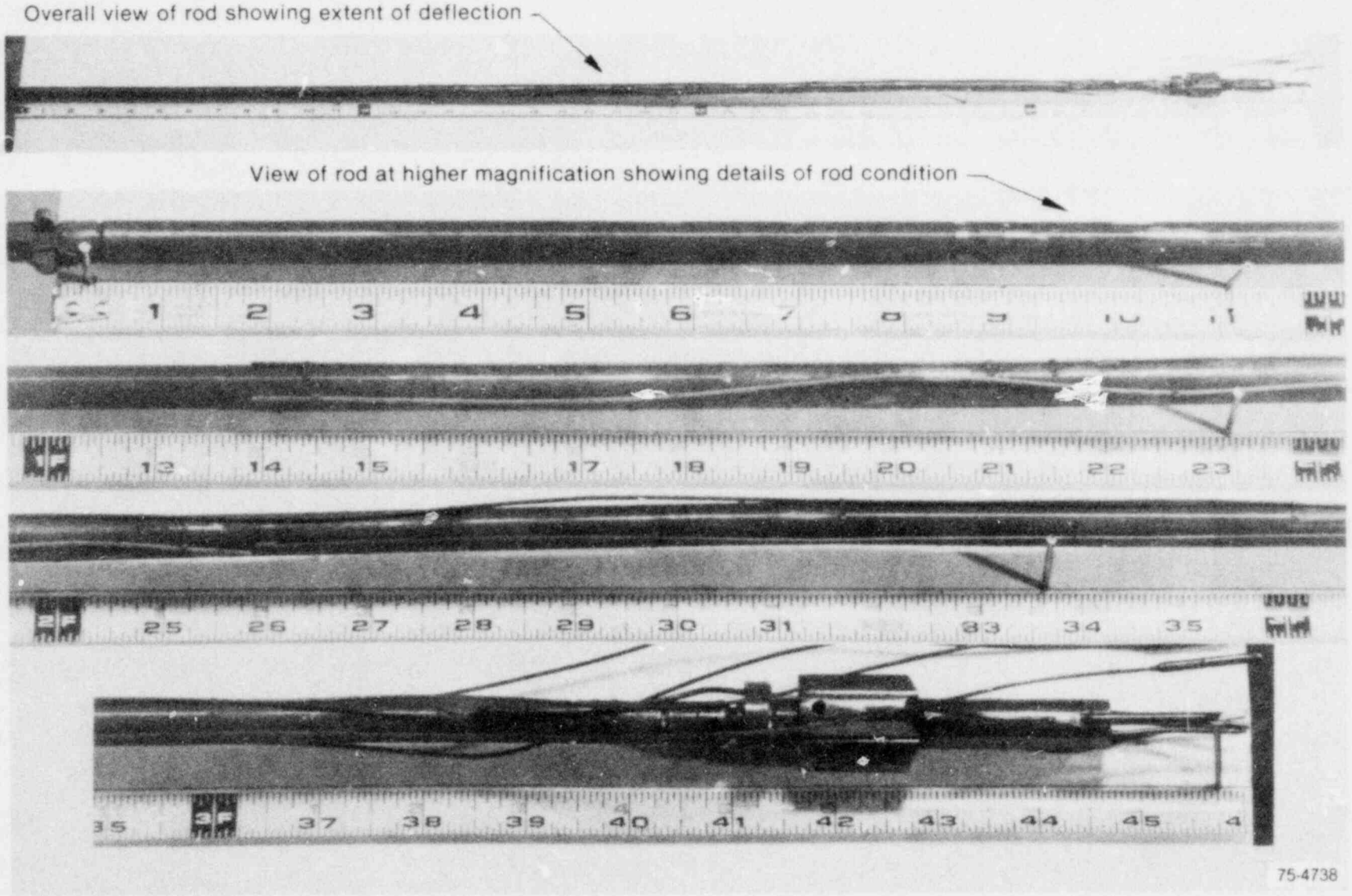

Figure 33. Posttest photograph of Test CHF Scoping fuel rod (90-degree orientation).

stresses induced during quenching and posttest handling. The effects of film boiling were discernible in the form of cladding collapse, waisting, heavy surface oxidation, and spalling of the surface oxide. The rod also exhibited a bend at about 0.77 m above the bottom of the fuel stack; the deflection was about 0.025 m.

4.4 Cladding Behavior

Cladding temperatures attained during Test CHF Scoping were sufficient to cause permanent cladding damage. This section presents estimates of the maximum cladding temperatures attained and discusses cladding deformation, microstructure, and embrittlement.

4.4.1 Cladding Temperature Estimates. As discussed in Subsection 3.4.1, cladding surface temperature measurements made with thermocouples are known to be atypically low because of fin-cooling effects. Maximum cladding surface temperatures attained during Test CHF Scoping were therefore estimated using three postirradiation analysis methods: (a) metallographic examination of cladding microstructures (see Subsection 4.4.3), (b) isothermal reaction rate correlations, and (c) BUILD5 computer code calculations. Descriptions of each technique and detailed results are presented in Reference 12.

Figure 34 shows the cladding peak temperatures at various axial locations estimated from the isothermal reaction rate correlations and the BUILD5 code; thermocouple measurements are also shown for comparison. The BUILD5-calculated temperatures are the best-estimate values of the cladding peak temperatures attained during the test. The thermocouple-indicated temperatures are consistently low because of fin-cooling effects. Note that the best-estimate peak temperatures from the BUILD5 code at locations unperturbed by thermocouple sheaths are as much as 550 K greater than those determined from thermocouples at nearby axial locations. As expected, the cladding peak temperatures occurred in the lower part of the film boiling zone.

4.4.2 Cladding Deformation. Cladding geometry changes in the form of fuel rod elongation, cladding collapse in the film boiling zone, and bowing occurred during Test CHF Scoping.

Cladding temperature increases following the onset of DNB resulted in fuel rod elongations (see, for example, Figures 19 and 23). The maximum measured elongation, which occurred near the end of Cycle 3, was 2.9 mm (0.29% of active fuel length). Most of the elongation probably occurred within the film boiling zone of the test rod.

R[illegible] cladding deformation in the form of cladding collapse and waisting occurred within the film boiling zone of the test rod. These deformations result from high cladding temperatures combined with high differential pressures across the cladding (system pressure greater than fuel rod internal pressure). Cladding collapse likely occurred during the initial film boiling cycle. The extent of cladding collapse is illustrated in Figure 35, which shows postirradiation outside diameter measurements versus axial location. Cladding collapse occurred over the range of 0.381 to 0.838 m above the bottom of the fuel stack, which is considered to be the film boiling zone. The maximum diametral reduction was 0.13 mm at 0.580 m from the bottom of the fuel stack, which corresponds to a 71% closure of the fuel-cladding cold gap.

Bowing in the form of a permanent bend about 0.77 m above the bottom of the fuel stack was found during postirradiation examination. The maximum deflection of the bend was about 0.025 m.

4.4.3 Cladding Microstructure. Cladding microstructure changes were induced by the high temperatures and subsequent oxidation. These microstructure changes provide an indication of the maximum temperatures attained during the test. Examination of cladding samples showed the following microstructures (film boiling zone was 0.381 to 0.838 m above the bottom of the fuel stack):

1. Samples at 0.171 and 0.189 to 0.208 m contained stress-relieved zircaloy, which occurs when the temperature is <920 K.

2. Samples at 0.449, 0.478 to 0.497, and 0.713 m ranged from recrystallized alpha to prior beta zircaloy, indicating temperatures of ~920 to above 1250 K.

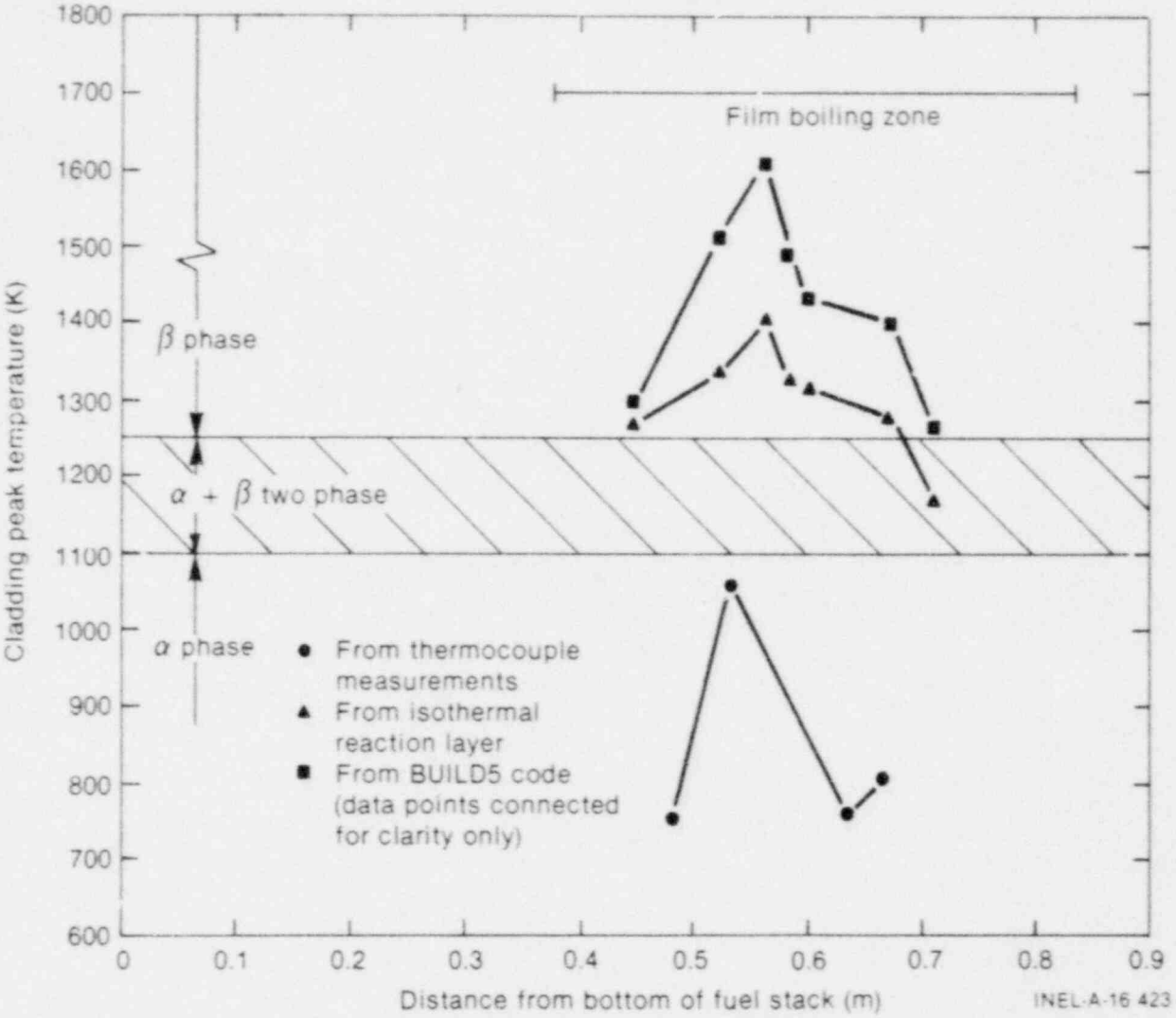

Figure 34. Cladding peak temperatures during Test CHF Scoping.

3. Samples at 0.525, 0.605, and 0.675 m contained alpha + beta to prior beta zircaloy, which occur for temperatures of 1105 to above 1250 K.

4. Samples at 0.567 and 0.586 to 0.605 m contained prior beta zircaloy, which occurs for temperatures greater than 1250 K.

Figure 36 shows a composite transverse section illustrating cladding microstructures and estimated temperatures near the 0.533-m thermocouple location. The cladding temperatures near the thermocouple are similar to those observed in Test 8-1 RS (Figure 15), in that the cladding is cooler beneath the thermocouple than it is to either side.

4.4.4 Cladding Embrittlement. As previously noted, a portion of the Test CHF Scoping fuel rod cladding attained temperatures above the beta transformation temperature (T > 1250 K) during film boiling. Such temperatures induce oxidation at both the inner and outer cladding surfaces. The simultaneous development of these oxidation layers results in cladding embrittlement, which increases the likelihood of cladding failure.

The failure potential of the Test CHF Scoping rod has been evaluated by the same three methods used for the Test 8-1 RS rod: (a) criteria based on oxygen concentration in the beta phase,[13] (b) the fractional thickness of remaining beta phase criterion,[14] and (c) the equivalent cladding

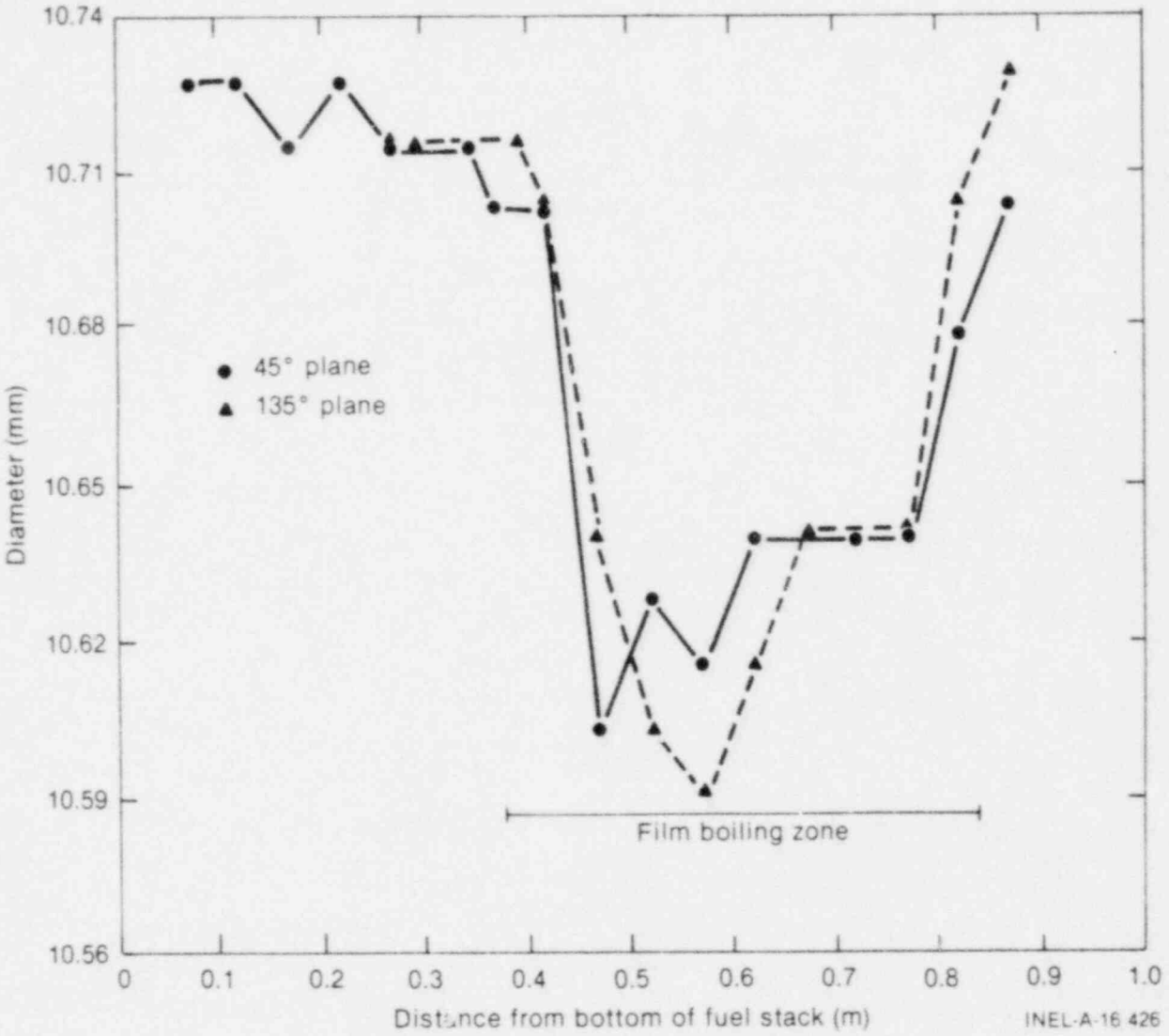

Figure 35. Diametral measurements of Test CHF Scoping fuel rod.

reacted method.[14] The results of these calculations are summarized in Table 12. None of the three criteria predict sufficient embrittlement to cause fuel rod failure, which is in agreement with the experimental findings, since the fuel rod remained intact during and after the test.

4.5 Fuel Behavior

Postirradiation examination of fuel samples from the film boiling zone of the test rod showed UO_2 grain growth near the center of the fuel pellets. Grain sizes near the center of the fuel column were in the range of about 5 to 23 μm. Near the edge of the fuel pellets, grain sizes were nominally the same as the prefabricated grain size of about 3 μm. No evidence of fuel shattering in the form of intergrannular fracturing was detected. Further, no fuel melting was detected.

The Test CHF Scoping fuel rod was instrumented with a tungsten-rhenium, tantalum-sheathed thermocouple to measure fuel centerline temperature at a location 0.679 m above the bottom of the fuel stack. The device indicated a maximum temperature of 2420 K during Cycle 1, and failed during Cycle 2.

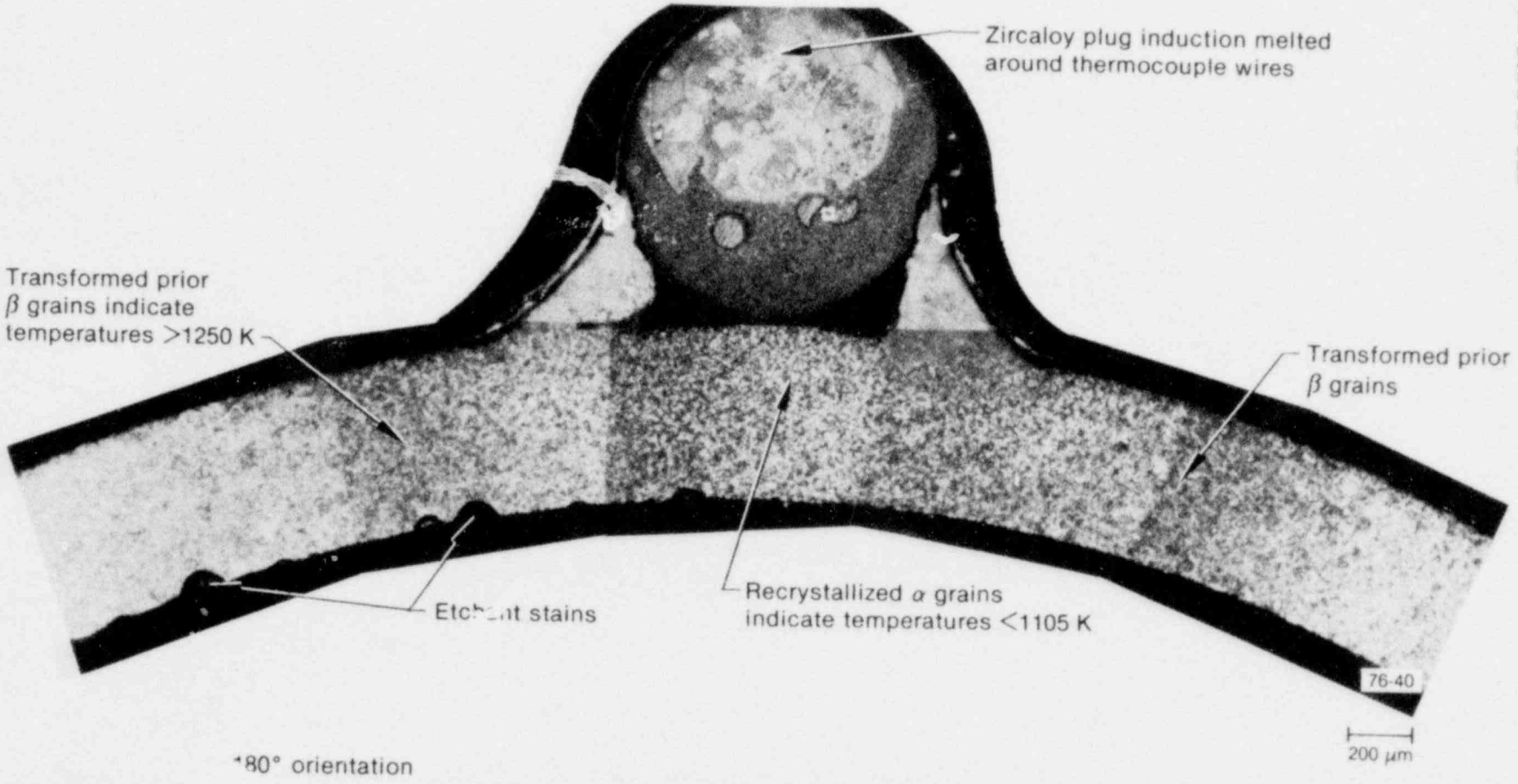

Figure 36. Transverse section of Test CHF Scoping fuel rod showing the microstructure near the 180-degree thermocouple on a plane located 0.525 m from the bottom of the fuel stack.

Table 12. Cladding embrittlement evaluation, Test CHF Scoping fuel rod

Maximum Cladding Temperature and Location[a]	Time in Film Boiling[b] (s)	Pawel's Criteria[c]		Scatena's Remaining Beta Phase Criterion[d]		Scatena's ECR Criterion[e]	
		Critical Oxidation Time (corrected) (s)	Failure Predicted	F_w	Failure Predicted	Equivalent Cladding Reacted (mole %)	Failure Predicted
1410 K—0.567 m	39	480	No	0.93	No	2	No

a. Temperatures determined from isothermal correlations based on reaction layer thicknesses (Reference 12); locations are distance from bottom of fuel stack.

b. Film boiling time is at maximum cladding temperature location as determined in Reference 12.

c. Cladding failure predicted when time in film boiling exceeds critical oxidation time. Correction factor applied to critical oxidation times to account for difference in cladding wall thickness of PBF test rods compared with out-of-pile tubes.

d. Cladding failure predicted when fractional thickness of remaining beta-phase zircaloy (F_w) is <0.5.

e. Cladding failure predicted when equivalent cladding reacted exceeds 17 mole %.

5. RESULTS AND ANALYSES - TEST PCM 8-1 RF

The primary objective of Test 8-1 RF was to investigate the behavior of a single fuel rod after DNB had been achieved by a coolant flow reduction while operating at a constant fuel rod power. Specific areas of interest were

1. The thermal and mechanical response of the test fuel rod following DNB
2. The coolant flow rate at which DNB occurred on the test fuel rod at constant power
3. The response and behavior of the measuring instruments.

The following sections present and evaluate the results of Test 8-1 RF in accordance with these objectives.

5.1 Summary of Results

This section provides a brief overview of the Test 8-1 RF results and an evaluation of the fuel rod behavior during post-DNB operation. Detailed results are presented in subsequent sections.

During Cycles 3 through 6, DNB occurred once at coolant mass flow rates in the range of 510 to 610 kg/s·m^2 and rod peak powers in the range of 59.4 to 61.0 kW/m. Departure from nucleate boiling occurred at 480 kg/s·m^2 and 56.7 kW/m during Cycle 2 and did not occur during Cycle 1. Fuel rod aging performed before the performance of the DNB cycles effectively solved the problem of premature DNB occurrence observed in Tests 8-1 RS and CHF Scoping. Sustained film boiling occurred only during Cycle 6. The only cladding surface thermocouple to indicate DNB and film boiling was located at 0.737 m above the bottom of the fuel stack; therefore, no information on film boiling propagation was obtained. Film boiling occurred for approximately 65 s during the test (total cumulative time that the cladding surface thermocouple indicated temperatures in excess of the rewet temperature of 670 K[9]).

Postirradiation examination of the fuel rod showed damage in the form of cladding collapse, waisting (cladding collapse at pellet interfaces), localized cladding collapse into chipped fuel pellet voids, permanent elongation, and minor oxidation. The cladding remained intact during and following the test. Cladding temperature estimates based on the measured extent of oxidation indicated that the cladding peak temperature was about 1590 K, which was 600 K greater than determined from cladding surface thermocouple measurements. Evaluation of the extent of cladding embrittlement in accordance with several documented methods indicated that insufficient embrittlement occurred to result in failure. Only minor fuel restructuring occurred during the test. The UO_2 grain size measurements indicated little, if any, grain growth.

5.2 Film Boiling

Departure from nucleate boiling did not occur during Cycle 1, but did occur during Cycles 2 through 6. Film boiling was allowed to develop only during Cycle 6. This section discusses the onset of DNB, film boiling propagation, and film boiling termination.

5.2.1 Onset of DNB. As discussed in Subsection 2.2.3.4, the DNB cycles were initiated by incremental decreases in the coolant mass flow while maintaining the fuel rod power, inlet temperature, and pressure constant (see Table 8). The occurrence of DNB was detected by monitoring changes in cladding surface temperatures and fuel centerline temperature. The device to measure cladding elongation failed during the power calibration and was not operational for any of the DNB cycles. Figures 37 through 42 show rod peak power, fuel centerline temperature, cladding surface temperature, and inlet coolant flow during each of the six DNB cycles. Table 13 summarizes the measured coolant mass flow and other pertinent data at the onset of DNB for each of the six cycles.

As shown in Table 13, DNB occurred during Cycles 3 through 6 at a coolant mass flow in the range of 510 to 610 kg/s·m^2, and rod peak powers in the range of 59.4 to 61.0 kW/m. No premature indications of DNB were detected during this test, indicating that aging of the cladding surface to remove adsorbed gases was effective.

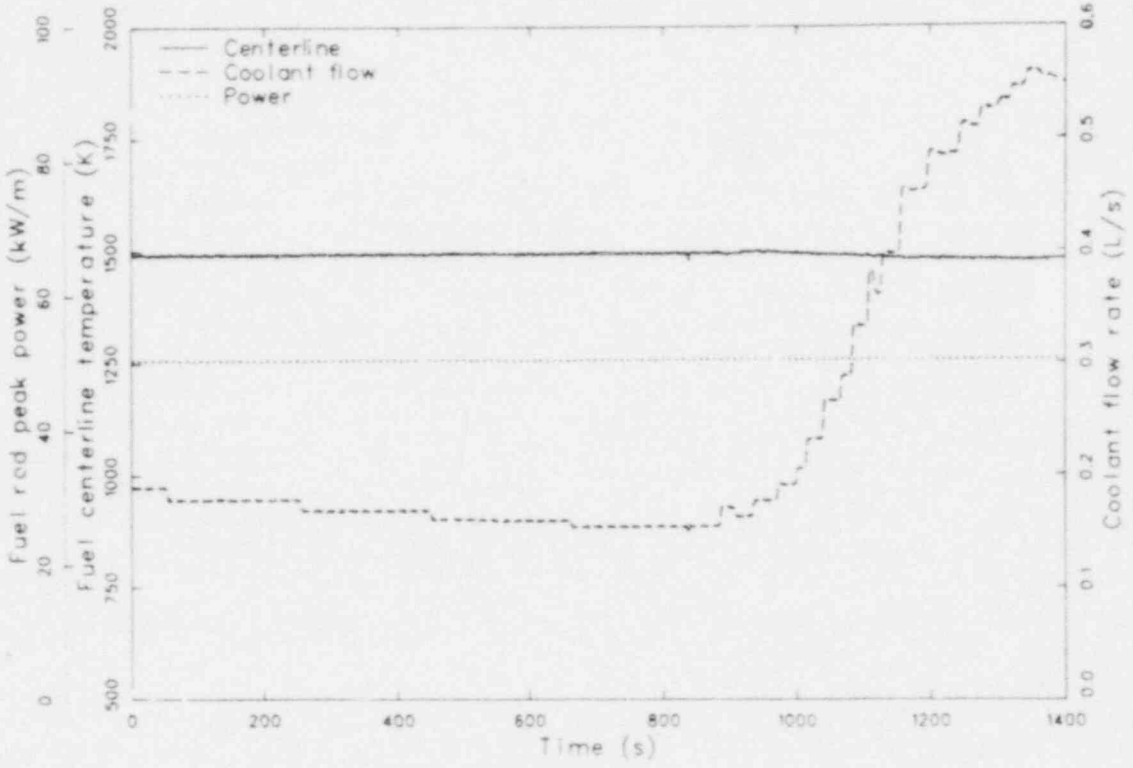

Figure 37. Fuel rod peak power, fuel centerline temperature, and coolant flow rate versus time during Test 8-1 RF (DNB Cycle 1).

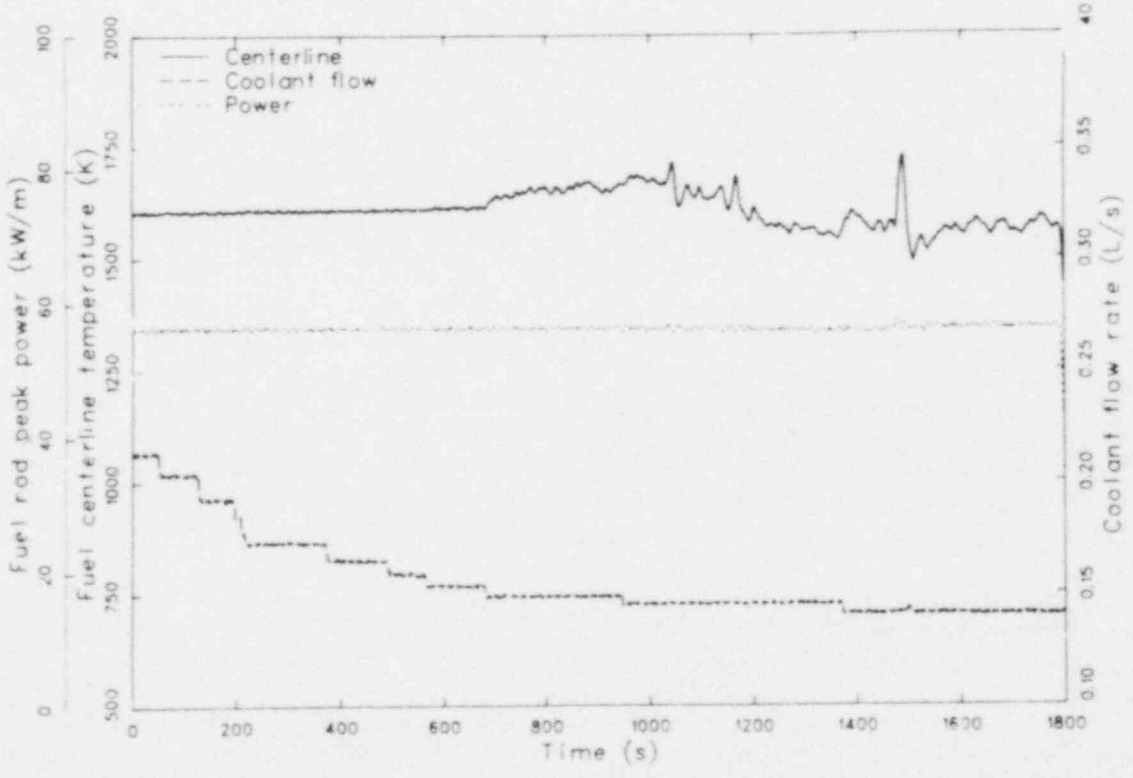

Figure 38. Fuel rod peak power, fuel centerline temperature, and coolant flow rate versus time during Test 8-1 RF (DNB Cycle 2).

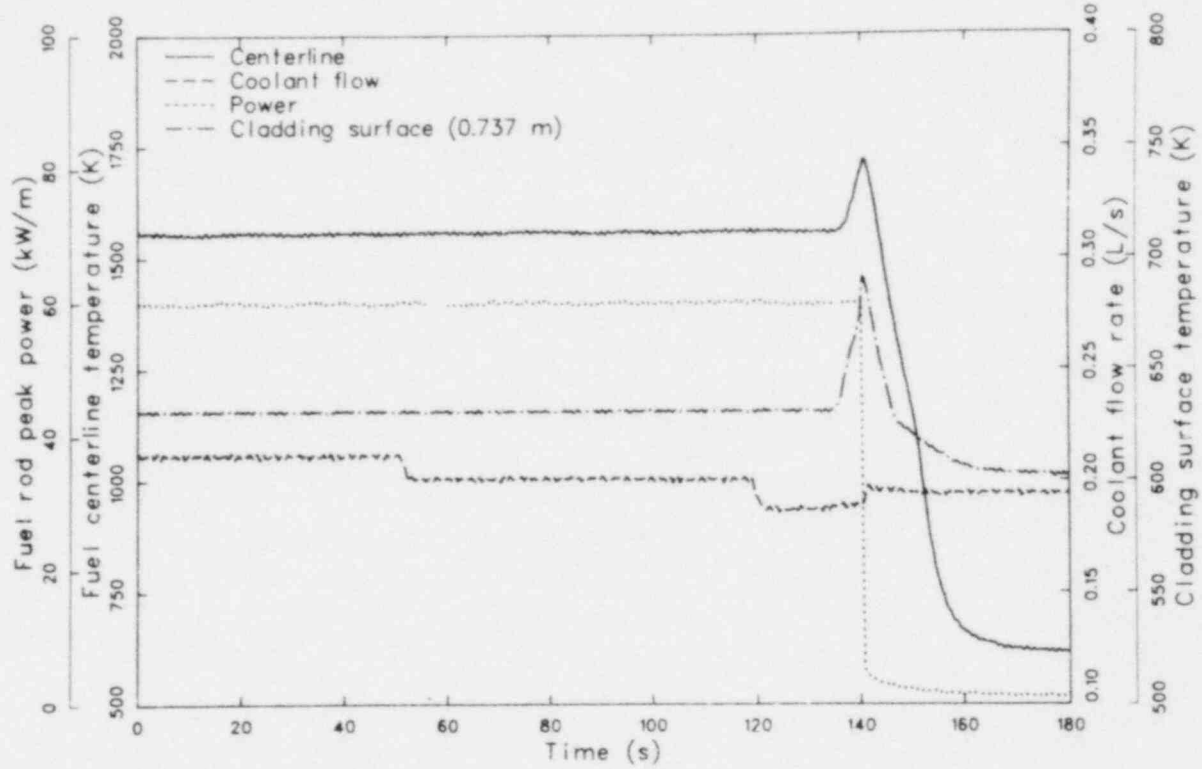

Figure 39. Fuel rod peak power, fuel centerline temperature, coolant flow rate, and cladding surface temperature versus time during Test 8-1 RF (DNB Cycle 3).

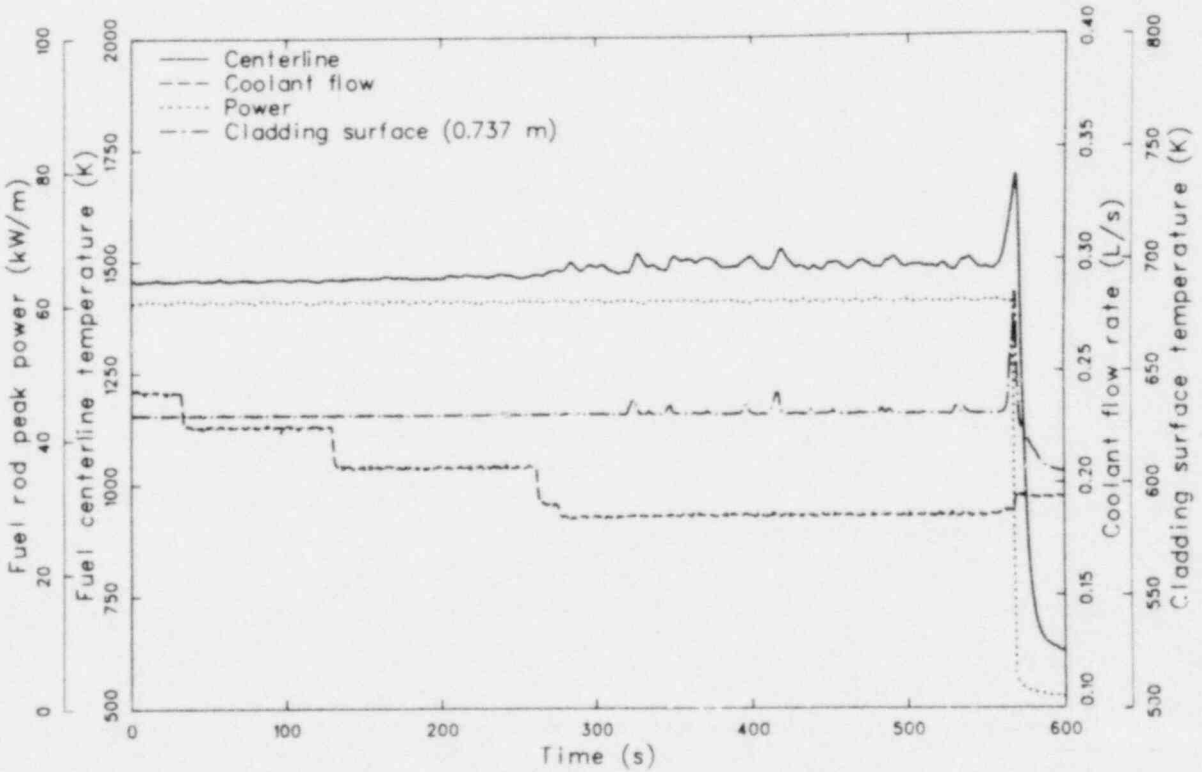

Figure 40. Fuel rod peak power, fuel centerline temperature, coolant flow rate, and cladding surface temperature versus time during Test 8-1 RF (DNB Cycle 4).

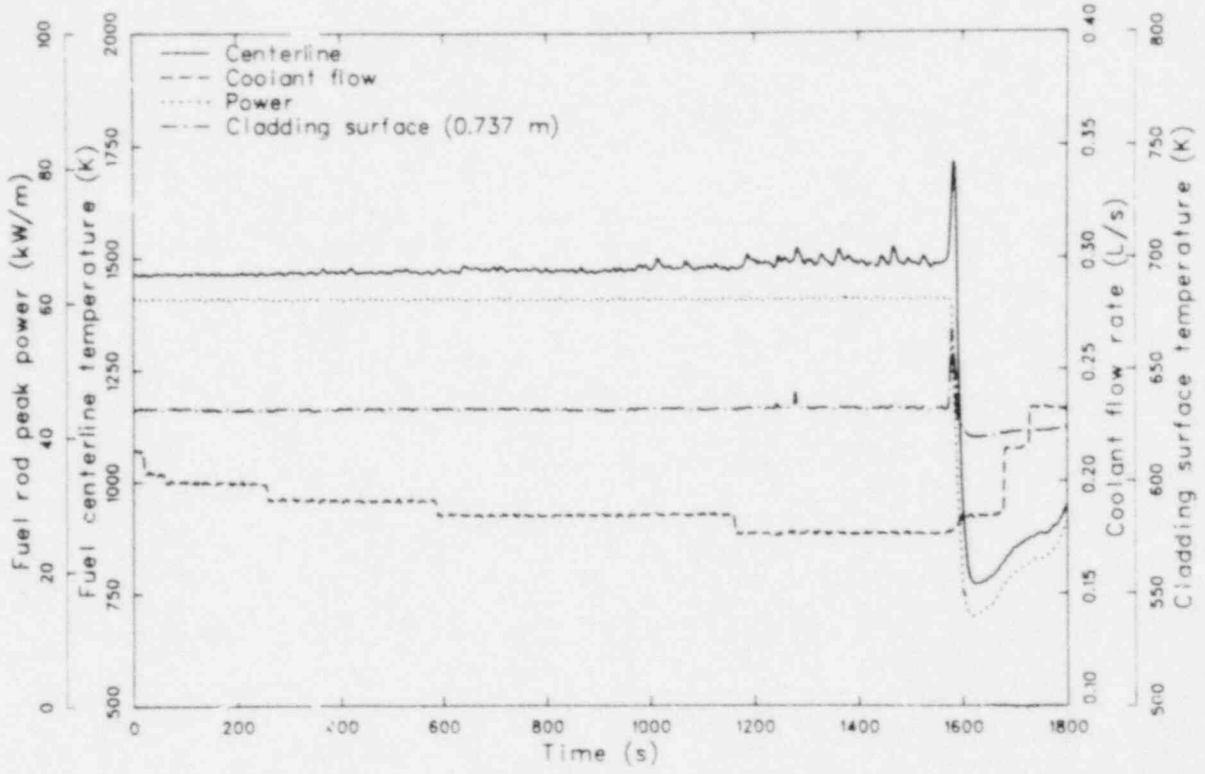

Figure 41. Fuel rod peak power, fuel centerline temperature, coolant flow rate, and cladding surface temperature versus time during Test 8-1 RF (DNB Cycle 5).

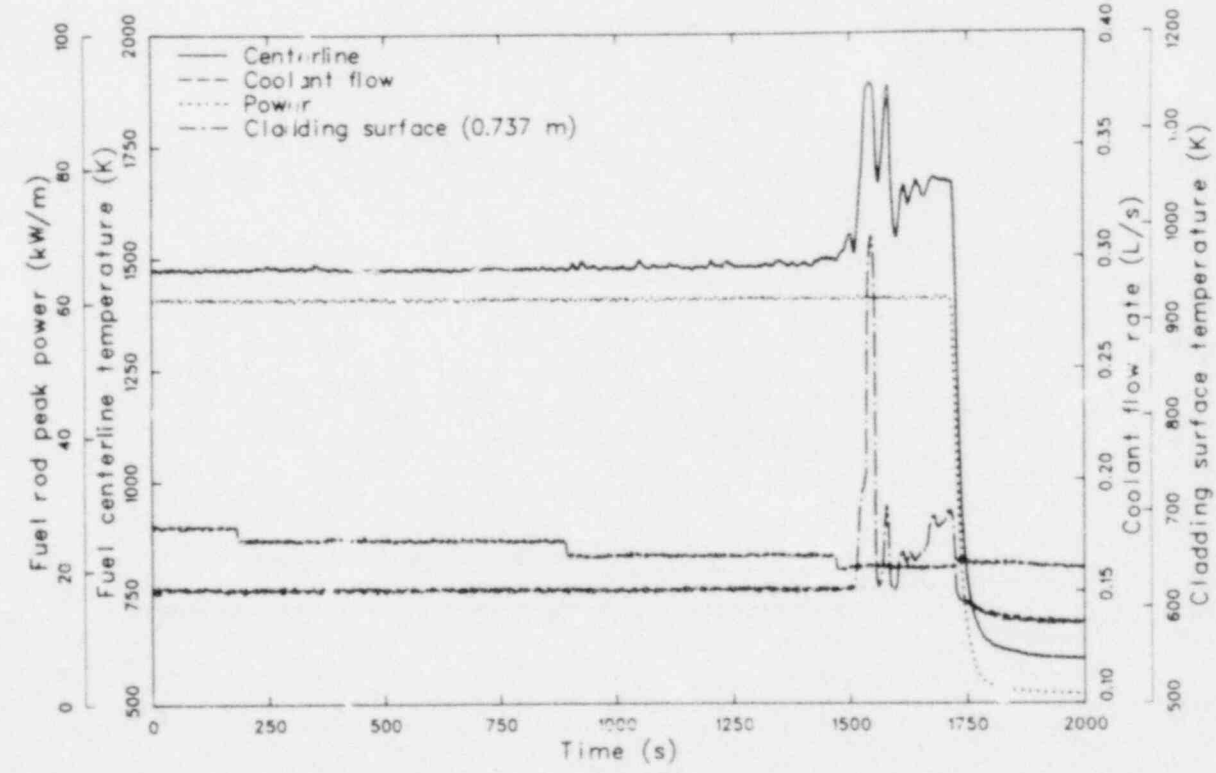

Figure 42. Fuel rod peak power, fuel centerline temperature, coolant flow rate, and cladding surface temperature versus time during Test 8-1 RF (DNB Cycle 6).

Table 13. Onset of DNB—Test 8-1 RF

DNB Cycle	Coolant Mass Flow at DNB ($kg/s \cdot m^2$)[a]	Rod Peak Power (kW/m)	Inlet Temperature (K)	Coolant Pressure (MPa)
1	[b]	50.8	600	15.2
2	480	56.7	602	15.2
3	610	59.4	599	15.2
4	600	60.7	600	15.2
5	570	61.0	600	15.2
6	510	60.7	600	15.2

a. Multiply coolant flow rate (L/s) in Figures 37 through 42 by 3237 to get mass flow in $kg/s \cdot m^2$.

b. DNB was not detected at 500 $kg/s \cdot m^2$.

Calculations were performed to predict the coolant mass flow at the onset of DNB for three of the cycles using the W-3[10] correlation. The calculated and measured values are compared in Table 14.

The calculated coolant mass flows for the onset of DNB are somewhat greater than those measured for Cycles 2 and 6. This discrepancy may be due, in part, to the use of the W-3 correlation at lower flow rates than were used to develop the correlation. The W-3 correlation was developed for coolant mass fluxes in the range of 1360 to 6800 $kg/s \cdot m^2$, whereas the measured values were nominally 500 $kg/s \cdot m^2$.

5.2.2 Propagation of Film Boiling. The thermocouple located at 0.737 m above the bottom of the fuel stack was the only cladding surface thermocouple to indicate DNB or film boiling during the test. Since the other cladding thermocouples, located at 0.533, 0.635, and 0.635 m did not indicate any occurrence of film boiling during the test, no information on film boiling propagation was obtained.

5.2.3 Termination of Film Boiling. All DNB cycles during Test 8-1 RF were terminated by manually decreasing the reactor power. Sustained film boiling occurred only during Cycle 6. Following termination of Cycle 6 by decreasing the reactor power, the 0.737-m thermocouple indicated rewet within a few seconds.

5.3 Posttest Condition of Fuel Rod

The posttest condition of the Test 8-1 RF fuel rod is shown in Figures 43 and 44. The fuel rod cladding remained intact, with no indication of failure as a result of the test and stresses induced during quenching and posttest handling. The primary effects of film boiling were discernible in the form of cladding collapse and waisting. Localized cladding collapse also occurred where chipped fuel pellet voids existed in the film boiling zone. The cladding surface exhibited a relatively continuous black oxide layer over the entire length of the fuel stack. The absence of a dull white zirconium oxide layer in the film boiling zone indicated that extensive metal-water reaction did not occur. The rod did not exhibit any permanent bow, which may have been the result of restraining screws incorporated in the flow shroud to prevent lateral movement of the fuel rod during testing. A permanent increase in fuel rod length of 1.6 mm was measured.

5.4 Cladding Behavior

Cladding temperatures achieved during Test 8-1 RF were sufficient to cause permanent cladding damage. This section presents estimates of the maximum cladding temperatures attained and discusses cladding deformation, microstructure, and embittlement.

Table 14. Comparison of measured and calculated coolant mass flow at onset of DNB during Test 8-1 RF

DNB Cycle	Rod Peak Power (kW/m)	Coolant Mass Flow at Onset of DNB ($kg/s \cdot m^2$)	
		Measured	Calculated
1	50.8	a	476
2	56.7	480	639
6	60.7	510	677

a. DNB was not detected at 500 $kg/s \cdot m^2$.

5.4.1 Cladding Temperature Estimates. As discussed in Subsection 3.4.1, cladding surface temperature measurements made with thermocouples are known to be atypically low because of fin-cooling effects. The cladding surface thermocouple assemblies for Test 8-1 RF were flattened to reduce protrusion into the coolant channel, thus reducing the fin-cooling effect. The flattened thermocouples protruded only 0.71 mm into the coolant channel, compared with 1.2 mm for the Tests 8-1 RS and CHF Scoping thermocouples.

Three postirradiation analysis methods were used to estimate maximum cladding surface temperatures attained during the test: (a) metallographic examination of cladding microstructures (see Subsection 5.4.3), (b) isothermal reaction rate correlations, and (c) BUILD5 computer code calculations. Descriptions of each technique and detailed results are presented in Reference 12.

The isothermal reaction rate correlation and the BUILD5 code were used to estimate the cladding temperature at the 0.768-m elevation. Results of the analysis were temperatures of 1450 K from the isothermal reaction rate correlation and 1590 K from the BUILD5 code. The BUILD5-calculated temperature is the best estimate of the cladding peak temperature attained during the test. The maximum temperature indicated by the 0.737-m thermocouple during the test was 990 K, about 600 K less than that determined by the BUILD5 code. These results indicate little improvement in the fin-cooling effect as a result of using flattened thermocouples.

5.4.2 Cladding Deformation. Radial cladding collapse and waisting result from high cladding temperatures combined with high differential pressure across the cladding (system pressure greater than fuel rod internal pressure). Cladding collapse likely occurred within a few seconds after the beginning of film boiling. The extent of cladding collapse is illustrated in Figure 45, which shows postirradiation outside diameter measurements versus axial position. Cladding collapse occurred over the range of 0.673 to 0.868 m above the bottom of the fuel stack, which is considered to be the film boiling zone. The maximum diametral reduction was 0.10 mm, extending from 0.699 to 0.787 m above the bottom of the fuel stack. This diametral reduction corresponds to a 57% closure of the fuel-cladding cold gap.

Localized cladding collapse into the voids of chipped pellets occurred. Figures 46, 47, and 48 show macrographs of transverse sections at various elevations. Cladding collapse into chipped pellet voids is clearly illustrated in these figures. Figure 48 shows that a protruding corner of the fuel was chipped, indicating mechanical interaction between the fuel and cladding. The cladding collapse into voids [illegible] in these figures suggests that this may be an effective mechanism for locking the fuel and cladding together.

Posttest measurement of the fuel rod length indicated an increase of 1.6 mm compared with the pretest measurement. Most of this increase in length probably occurred within the film boiling zone.

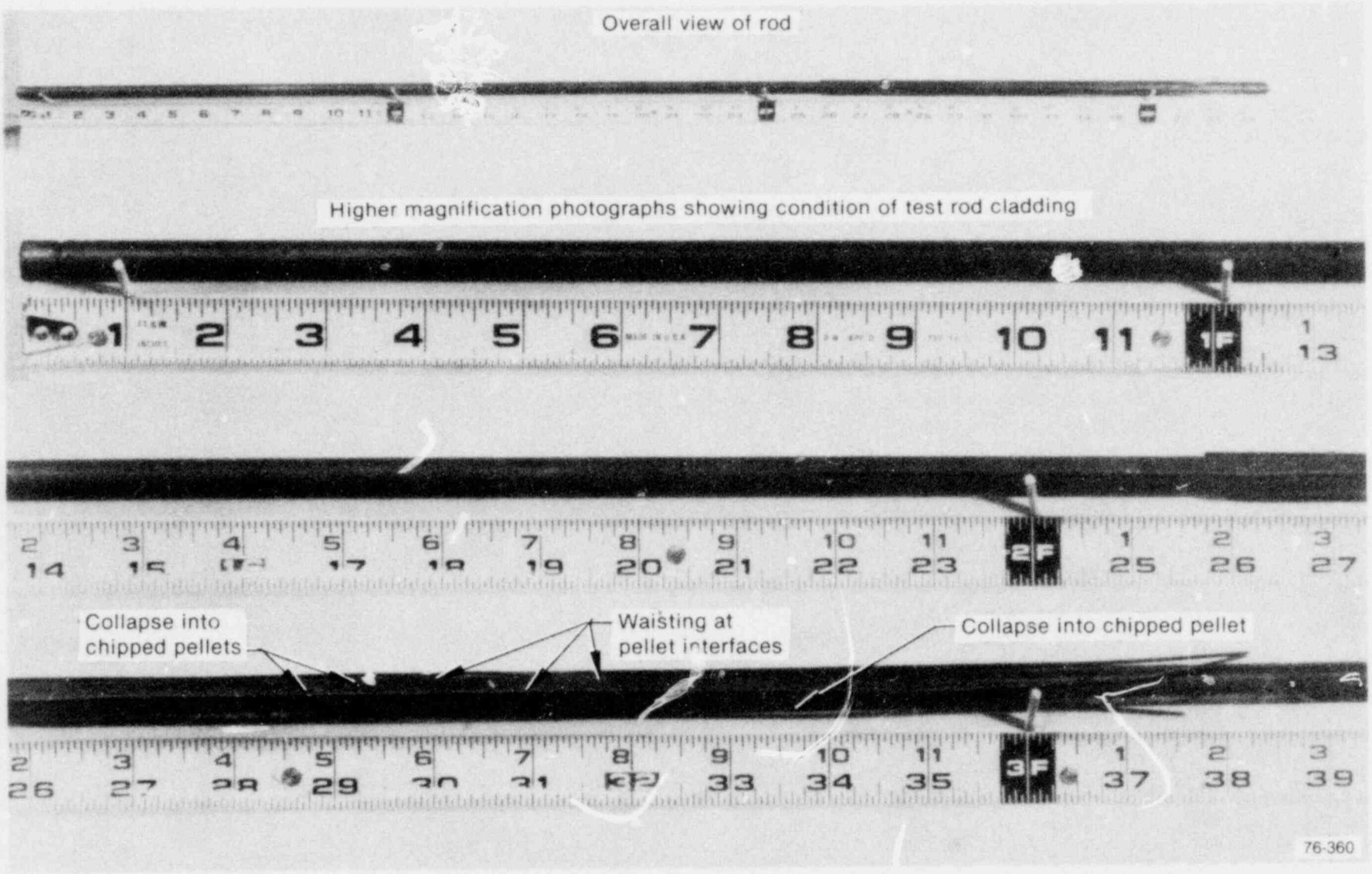

Figure 43. Posttest photograph of Test 8-1 RF fuel rod (0-degree orientation).

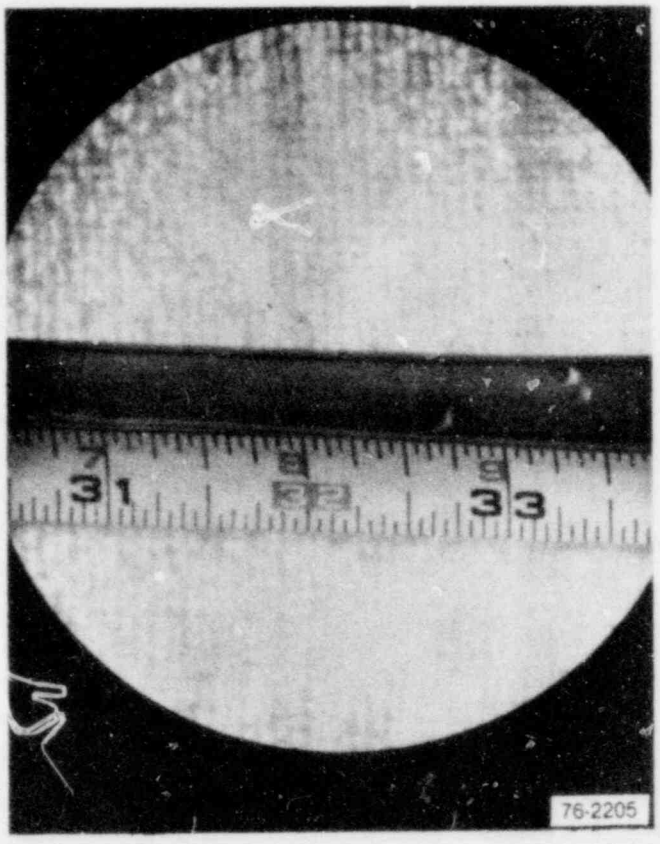

Figure 44. Cladding collapsed into interfaces and chipped regions at ends of Test 8-1 RF fuel pellets. The scale represents the distance from the bottom of the Test 8-1 RF fuel rod.

5.4.3 Cladding Microstructure. Cladding microstructure changes were induced by the high temperature operation during film boiling. These microstructure changes provide an indication of the maximum temperatures attained during the test. Examination of cladding samples showed the following microstructures (film boiling zone was 0.673 to 0.868 m above the bottom of the fuel stack):

1. Samples at 0.533 and 0.634 m contained stress-relieved zircaloy, which occurs for temperatures less than 920 K

2. A sample at 0.677 m contained stress-relieved alpha and alpha plus beta two phase zircaloy, which occur for temperatures in the range of 920 to 1250 K

3. A sample at 0.779 m contained recrystallized alpha and prior beta zircaloy, which occur for temperatures in the range of 920 to above 1250 K

4. Samples at 0.733 and 0.823 m contained recrystallized alpha zircaloy, which occurs for temperatures in the range of 920 to 1105 K.

Figure 49 shows a transverse section of the cladding at the 0.779-m elevation, which was determined from surface oxidation measurements to be in the approximate location of maximum cladding temperature (1590 K from BUILD5 analysis). As shown in the figure, the cladding microstructures indicate lower temperatures than determined from the BUILD5 calculations.

5.4.4 Cladding Embrittlement. The failure potential for the Test 8-1 RF rod was evaluated by the same three methods as used for the Tests 8-1 RS and CHF Scoping rods: (a) criteria based on oxygen concentration in the beta phase,[13] (b) the fractional thickness of remaining beta phase criterion,[14] and (c) the equivalent cladding reacted method.[14] The results of these calculations are summarized in Table 15.

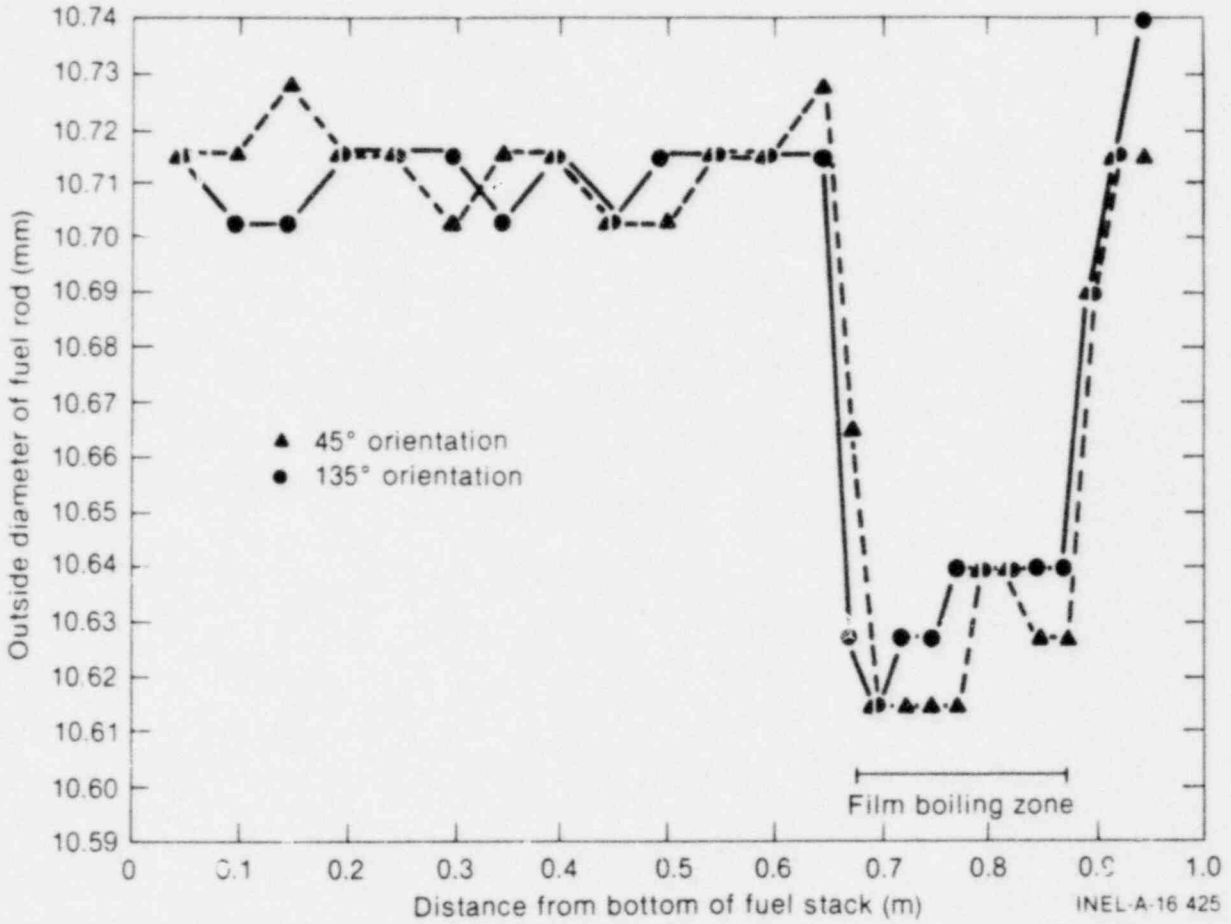

Figure 45. Postirradiation diametral measurements of Test 8-1 RF fuel rod.

As shown in Table 15, none of the three criteria predicts sufficient embrittlement to cause fuel rod failure, which is in agreement with the experimental findings, since the fuel rod remained intact during and after the test.

5.5 Fuel Behavior

Test 8-1 RF resulted in a minor amount of fuel restructuring. Postirradiation measured grain sizes were 2 to 3 μm at various axial locations near the edge and center of the fuel column; these sizes correspond to the approximate pretest grain size. No evidence of fuel melting, porosity migration, or fuel shattering in the form of intergrannular fracturing was detected.

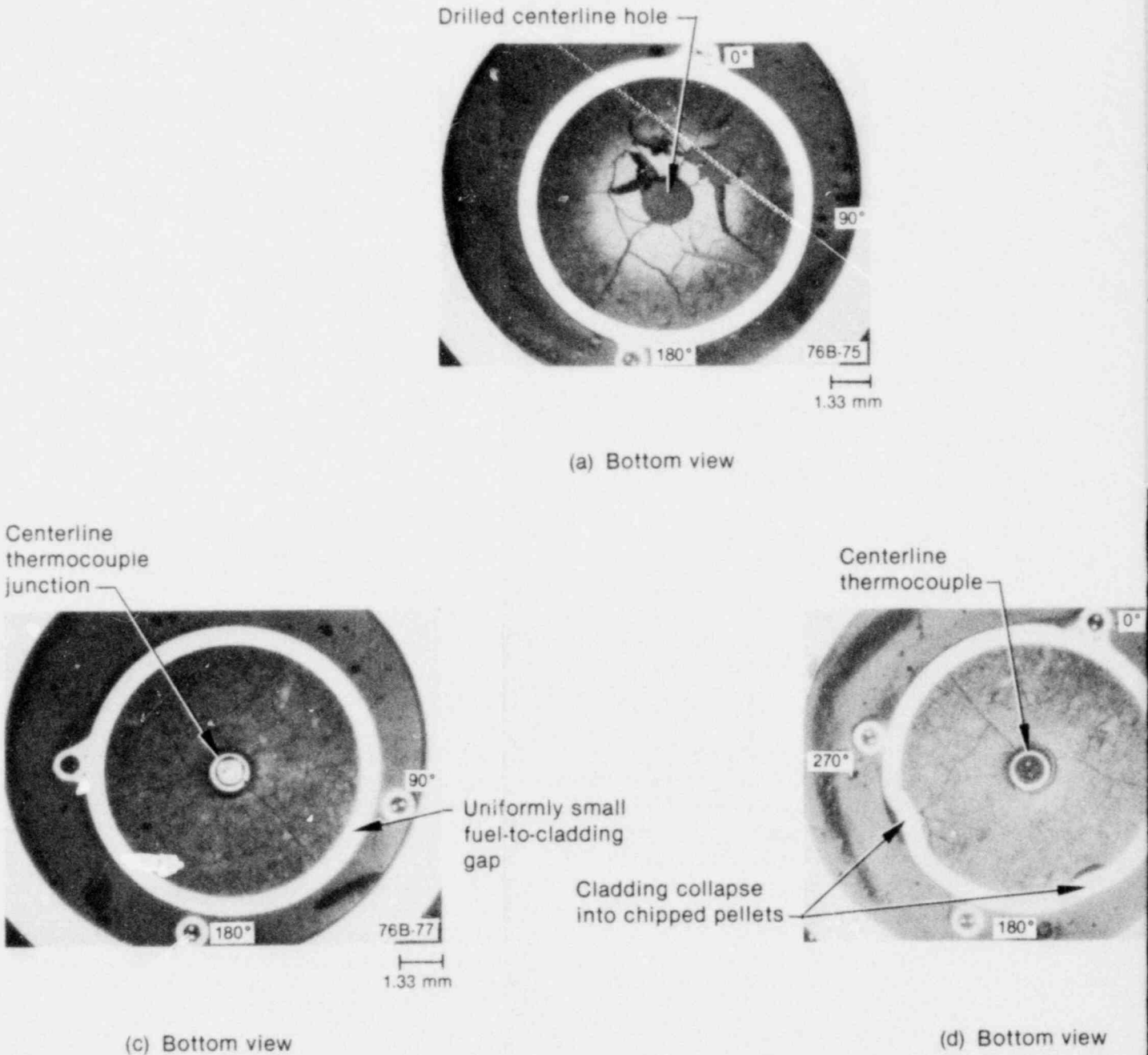

Figure 46. Transverse sections o' Test 8-1 RF fuel rod located (a) 0.6 bottom of fuel stack.

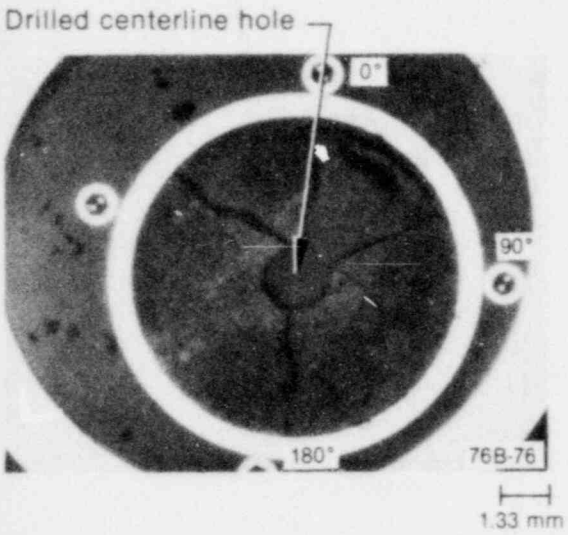

(b) Bottom view

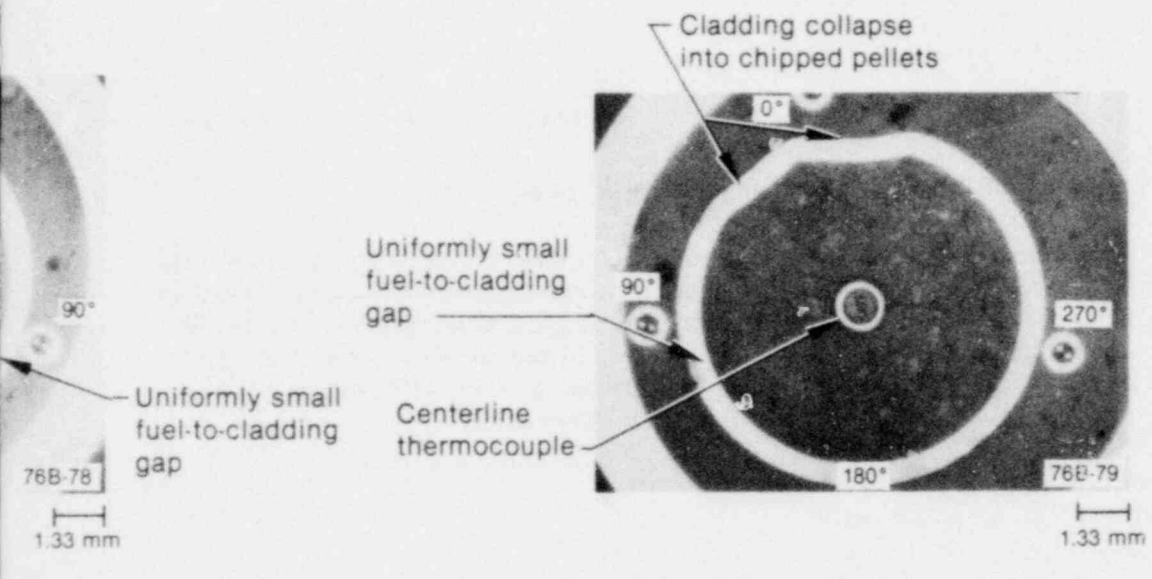

(e) Top view

34, (b) 0.733, (c) 0.779, and (d) 0.823 m above

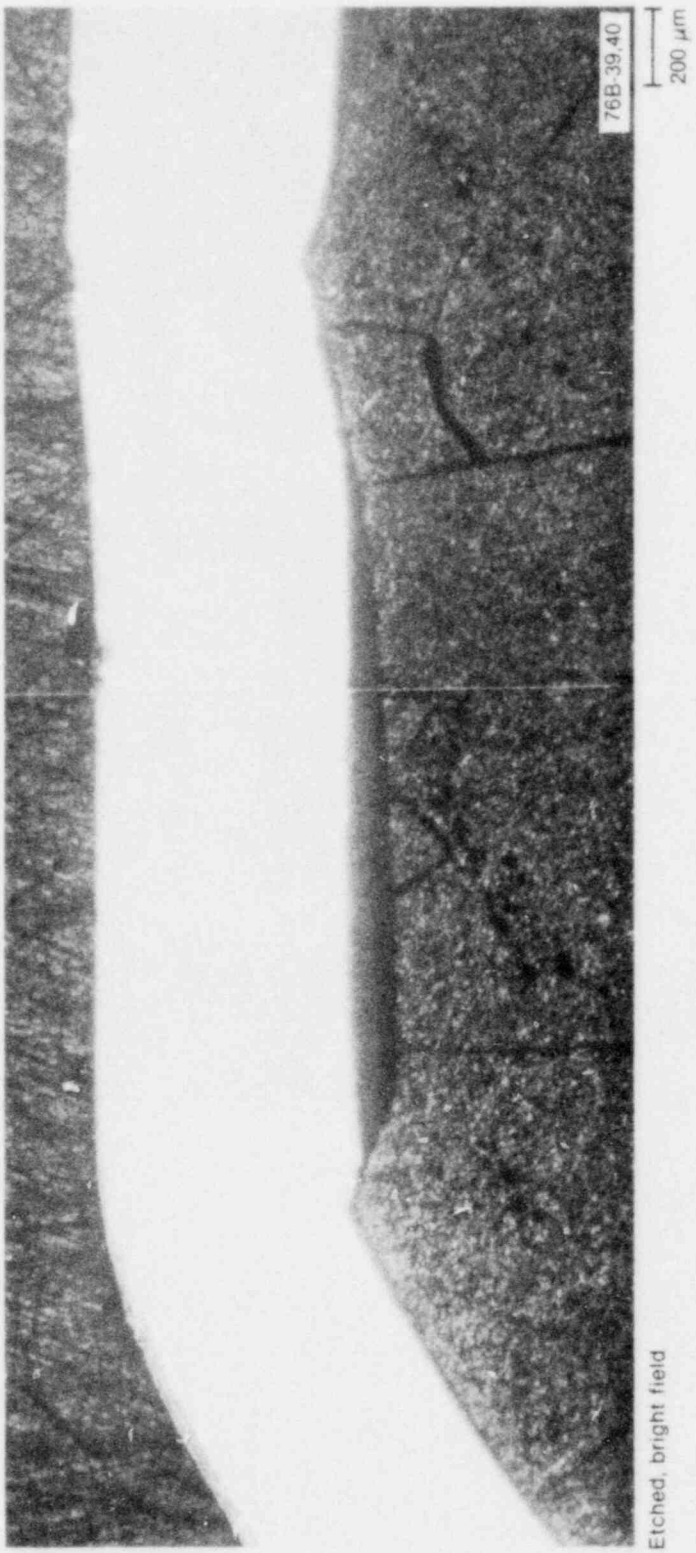

Figure 47. Transverse section of Test 8-1 RF fuel rod showing cladding collapsed into voids of a chipped fuel pellet located 0.779 m above the bottom of the fuel stack [see Figure 46(c)].

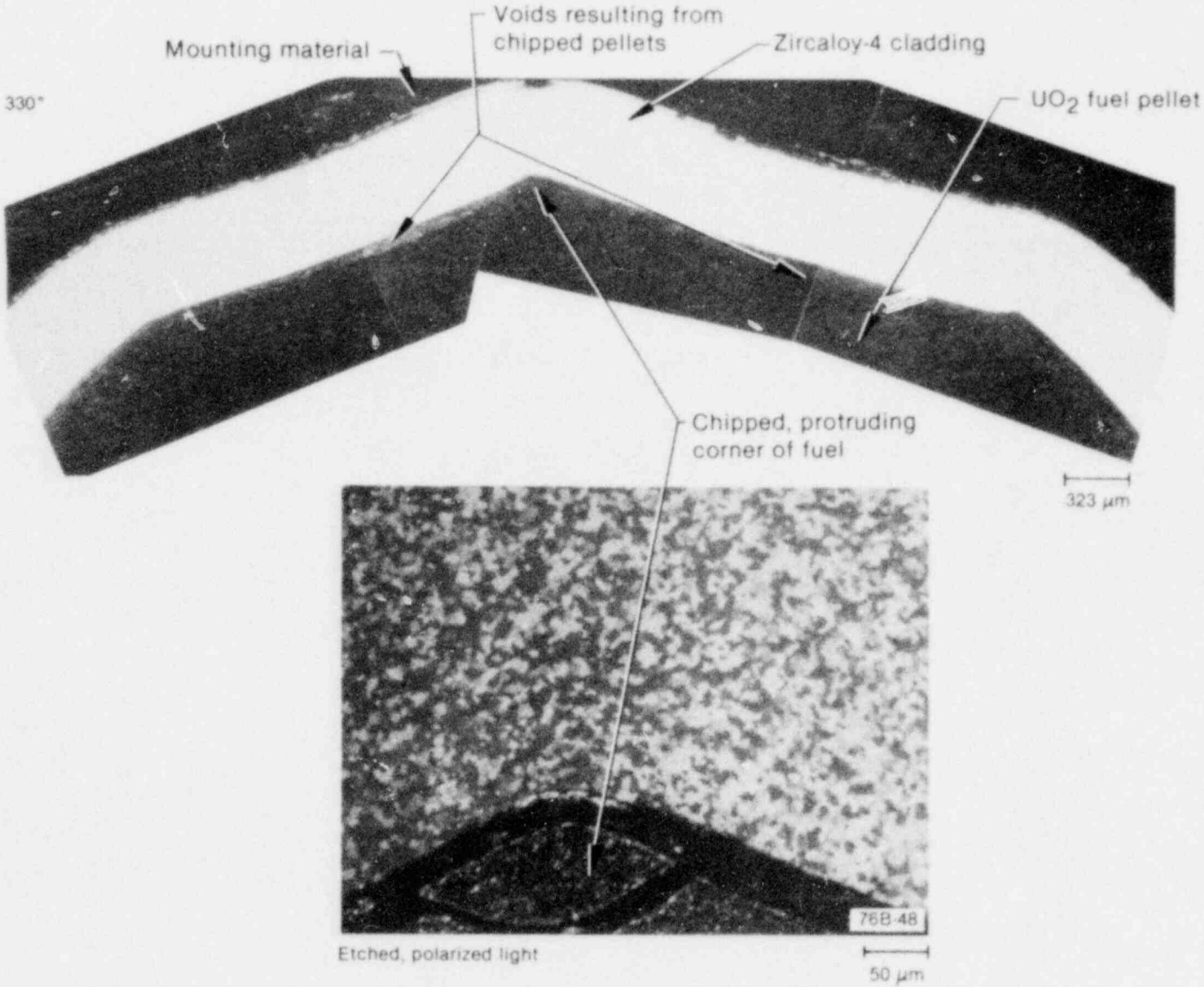

Figure 48. Transverse section of Test 8-1 RF fuel rod showing cladding collapsed into voids of a chipped pellet located 0.823 m above the bottom of the fuel stack [see Figure 46(d)].

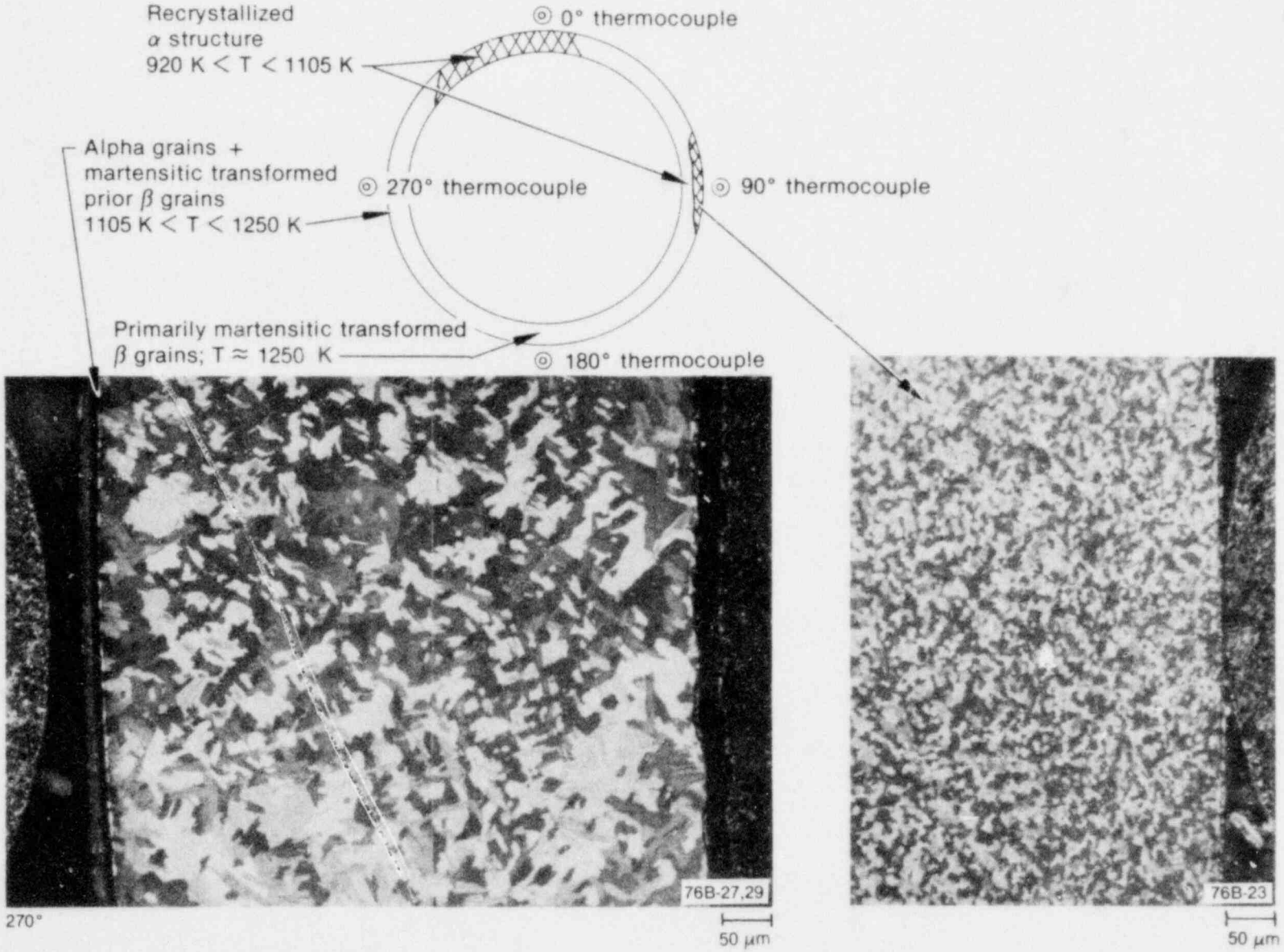

Figure 49. Transverse section of Test 8-1 RF fuel rod showing cladding microstructures observed 0.779 m above the bottom of the fuel stack.

Table 15. Cladding embrittlement evaluation, Test 8-1 RF fuel rod

Maximum Cladding Temperature and Location[a]	Time in Film Boiling[b] (s)	Pawel's Criteria[c]		Scatena's Remaining Beta Phase Criterion[d]		Scatena's ECR Criterion[e]	
		Critical Oxidation Time (corrected) (s)	Failure Predicted	F_w	Failure Predicted	Equivalent Cladding Reacted (mole %)	Failure Predicted
1450 K—0.779 m	78	380	No	0.79	No	2	No

a. Temperatures determined from isothermal correlations based on reaction layer thicknesses (Reference 12); locations are distance from bottom of fuel stack.

b. Film boiling time is at maximum cladding temperature location as determined in Reference 12.

c. Cladding failure predicted when time in film boiling exceeds critical oxidation time. Correction factor applied to critical oxidation times to account for difference in cladding wall thickness of PBF test rods compared with out-of-pile tubes.

d. Cladding failure predicted when fractional thickness of remaining beta-phase zircaloy (F_w) is <0.5.

e. Cladding failure predicted when equivalent cladding reacted exceeds 17 mole %.

6. DISCUSSION OF RESULTS

The primary experimental results of Tests 8-1 RS, CHF Scoping, and 8-1 RF are discussed and compared in this section. These three tests were the first PCM tests performed in the Power Burst Facility to evaluate the behavior of single, unirradiated, PWR-type fuel rods subjected to overpower or undercooling conditions sufficient to result in DNB and subsequent film boiling. Common, specific objectives of the tests included determination of (a) the fuel-rod-power/coolant-flow conditions required for the onset of DNB, (b) the thermal and mechanical response of the test rod to high temperature film boiling operation (c) the permanent damage to the fuel rod resulting from film boiling operation and stresses induced during quenching and posttest handling, and (d) the response and behavior of fuel rod and coolant instrumentation. The test results also provided data useful in evaluating and improving (a) analytical models used to predict the behavior of fuel rods under PCM conditions, (b) experimental methods used to conduct PCM tests, and (c) postirradiation examination methods and analyses. Thus, test results from these scoping tests provided a foundation for the planning, performance, and analysis of subsequent PCM tests designed to obtain a more detailed understanding of fuel rod behavior under power-cooling-mismatch conditions.

6.1 Conduct of Experiments

Each of the tests was initiated by performance of a thermal heat balance power calibration. The results of these calibrations agreed, within experimental uncertainties, with independent calibrations based on the posttest radiochemical analysis of fuel pellets from each of the test rods. Following the power calibration phase, DNB testing was begun in Tests 8-1 RS and CHF Scoping. Before DNB testing in Test 8-1 RF, however, a preconditioning phase to crack and restructure the fuel, and an aging phase to remove adsorbed gas from the cladding surface were performed. The cladding aging phase eliminated the premature occurrence of DNB during the first cycle of Test 8-1 RF, a phenomenon that occurred in both Tests 8-1 RS and CHF Scoping.

The DNB cycles for Tests 8-1 RS and CHF Scoping were performed by incrementally increasing the test rod power level while maintaining coolant mass flow, temperature, and pressure constant. The DNB cycles for Test 8-1 RF were performed by incrementally reducing the coolant mass flow while maintaining the test rod power and other coolant conditions constant. Both experimental methods provide acceptable means to achieve DNB and subsequent film boiling.

6.2 Onset of DNB and Film Boiling

During Tests 8-1 RS and CHF Scoping, DNB first occurred at lower than expected fuel rod peak powers; this premature occurrence of DNB was attributed to adsorbed gases on the cladding surface. Performance of a cladding aging phase (1 h at 53 kW/m rod peak power) before the performance of the DNB cycles for Test 8-1 RF effectively elimininated the occurrence of premature DNB. Numerous self-terminating occurrences of DNB were detected during Test 8-1 RS. These occurrences may have been caused by inlet coolant flow variations, the control of which was improved for Tests CHF Scoping and 8-1 RF. During Tests 8-1 RS and CHF Scoping, the rod peak power at the onset of DNB varied from cycle to cycle. No consistent pattern was obvious; however, with the exception of the premature DNB occurrences, the variations did not exceed about 10% when considered in terms of the differences in coolant mass flow rates. Similarly, the measured coolant mass flow rate at the onset of DNB during Test 8-1 RF varied from cycle to cycle, but, again, not more than about 10% when considered in terms of the differences in fuel rod peak powers. Figure 50 shows the fuel rod peak power versus coolant mass flux at the onset of DNB for the three tests (the premature DNB occurrences during Tests 8-1 RS and CHF Scoping are not included). Calculated values of the fuel rod peak power or coolant mass flow required to cause DNB using the W-3[10] and B&W-2[11] correlations varied in terms of agreement with measured values. The W-3 correlation more closely predicted the experimental measurements; the calculated fuel rod peak powers at the onset of DNB were within 10% of measurements during Tests 8-1 RS and CHF Scoping, and the calculated coolant mass flow rates at the onset of DNB were within 40% for Test 8-1 RF.

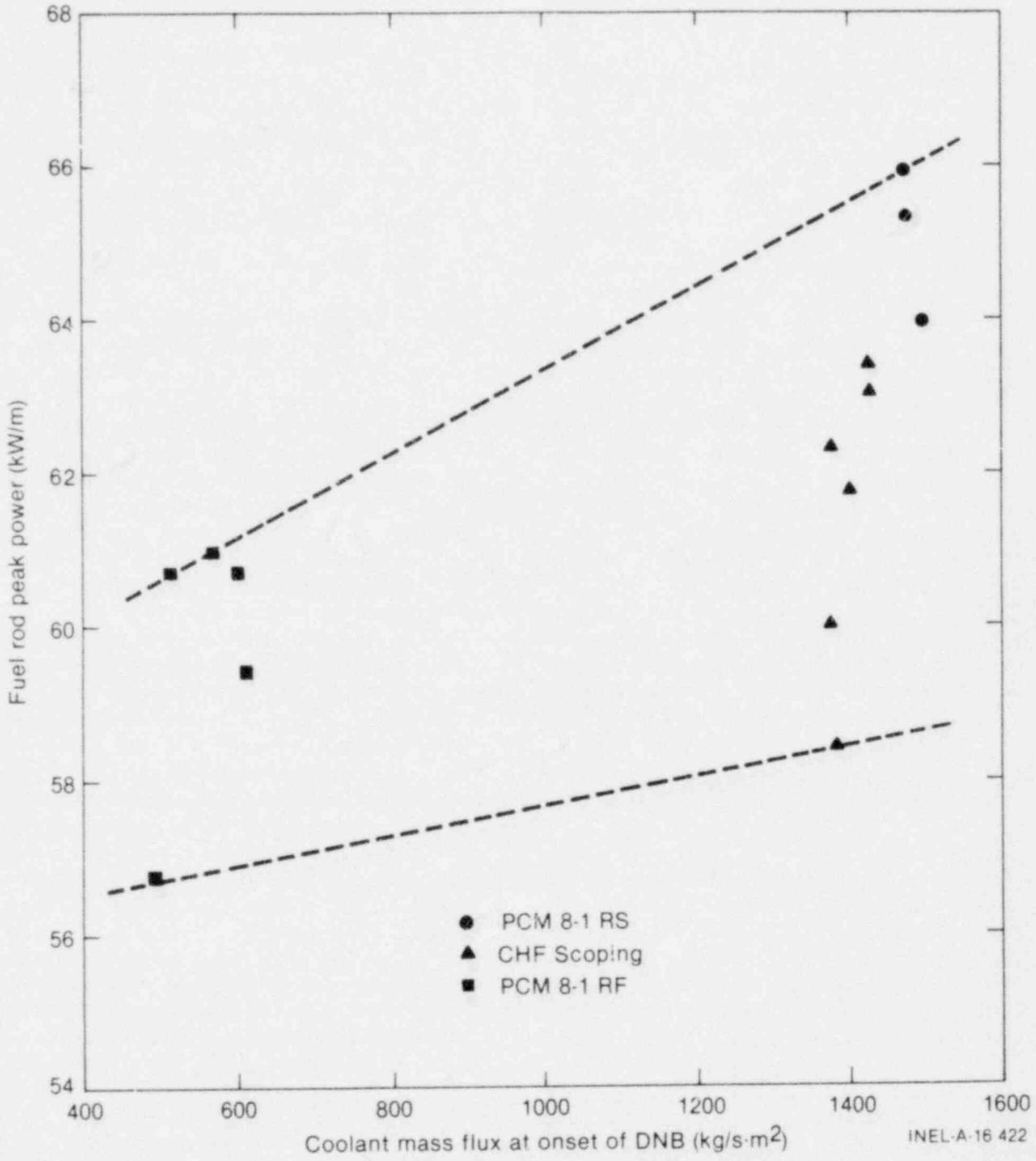

Figure 53. Power/flow at onset of DNB for Tests PCM 8-1 RS, CHF Scoping, and PCM 8-1 RF.

Significant differences in the duration of film boiling occurred for the three tests. During Test 8-1 RS, film boiling occurred for a total of about 660 s, whereas the film boiling time for Test CHF Scoping was about 40 s and for Test 8-1 RF was about 65 s. These film boiling times are the cumulative times that the cladding surface thermocouples indicated temperatures in excess of 670 K. The value of 670 K is the maximum rewet temperature for water/zirconium oxide,[9] above which liquid is repelled from the hot surface and rewetting cannot occur. Thus, the stated film boiling times should be considered minimums; actual total film boiling times for each of the tests may have been longer.

Posttest cladding collapse measurements indicated the axial extent of film boiling over the active fuel column length was about 42% for Test 8-1 RS, 45% for Test CHF Scoping, and 16% for Test 8-1 RF. Little quantitative information on the axial propagation of film boiling was obtained from the results of the three tests. Cladding surface thermocouple data during Test CHF Scoping, however, indicated that film boiling was initiated in the upper region of the rod and propagated axially downward, which agrees with expectations. Film boiling during all three tests was terminated by decreasing the power, either manually or by reactor scram. In all instances, cladding surface thermocouples indicated that rewet occurred within a few seconds after the power was decreased.

6.3 Overall Fuel Rod Effects

Cladding damage, primarily in the form of collapse, waisting, and oxidation, occurred within the film boiling region of each test rod. The Test 8-1 RS fuel rod exhibited significantly more damage than the other two test rods. Loss of cladding integrity, probably in the form of a cladding crack, first occurred on the Test 8-1 RS rod about 60 s after reactor shutdown. Complete fracture of the rod in two places occurred during posttest handling because of the highly embrittled condition of the cladding, resulting from extensive oxidation. Neither the Test CHF Scoping nor the Test 8-1 RF rods failed during or following testing. The Test CHF Scoping rod exhibited a permanent bend with a deflection of about 0.025 m, and the Test 8-1 RF rod showed evidence of localized cladding collapse into chipped pellet voids.

6.4 Cladding Behavior

Cladding surface temperatures measured by the thermocouples during film boiling were atypically low becaue of fin-cooling effects. Postirradiation analysis of the cladding based on the measured extent of oxidation and use of the BUILD5 computer code indicated that cladding surface peak temperatures reached 2020 K during Test 8-1 RS, 1610 K during Test CHF Scoping, and 1590 K during Test 8-1 RF. These peak temperatures were 550 to 850 K greater than measured during the tests. An attempt to reduce the fin-cooling effect by flattening the thermocouples for Test 8-1 RF had no detectable effect. The results of the postirradiation temperature estimates, generally confirmed by cladding microstructure changes, indicate that the cladding of all three test rods exceeded the zircaloy beta transformation temperature of 1250 K.

The likelihood of cladding failure from embrittlement was evaluated using three methods for each of the three test rods. The evaluations all indicated that sufficient embrittlement of the Test 8-1 RS fuel rod cladding occurred to expect failure, which agrees with the experimental findings. None of the three methods predicted sufficient embrittlement to cause cladding failure for the Tests CHF Scoping and 8-1 RF fuel rods, which is also in agreement with the experimental findings.

6.5 Fuel Behavior

Thermal restructuring of the UO_2 fuel resulting from high temperatures during film boiling occurred in the Tests 8-1 RS and CHF Scoping fuel rods. Pretest UO_2 grain sizes for the test rods were in the range of 2 to 4 μm. Postirradiation examination of the Test 8-1 RS fuel showed grain sizes near the center of the fuel column generally in the range of 8 to 40 μm, with one sample showing grains as large as 155 μm. Fuel shattering in the form of localized grain fracturing was observed in the Test 8-1 RS rod. The Test CHF Scoping fuel rod showed UO_2 grain sizes near the center of the fuel column in the range of 5 to 23 μm. Essentially no UO_2 grain growth was detected in samples from the Test 8-1 RF fuel rod. Examinations of the Test 8-1 RS fuel to determine if fuel melting occurred were inconclusive. Fuel temperature calculations based on UO_2 grain sizes

for the Test CHF Scoping rod indicated maximum temperatures slightly below the UO_2 melting temperature. Maximum temperatures measured by fuel thermocouples during the tests were 2550 K for Test 8-1 RS and 2430 K for Test CHF Scoping.

6.6 Instrument Performance

An important purpose of the initial three PCM scoping tests was to obtain information on the response, behavior, and reliability of the test instrumentation. Of the instruments mounted on or in the fuel rods, the major problems involved reliability and the effects of perturbations induced by the sensors. Cladding surface thermocouples were reliable and provided accurate indications of the onset of DNB; however, the fin-cooling effects of the sheathed sensors were significant. Measured cladding surface peak temperatures were as much as 850 K less than those determined by postirradiation examination methods. The reliability of the fuel centerline temperature thermocouples and internal fuel rod pressure transducers was questionable; the perturbation effect of fuel centerline temperature measuring devices was uncertain. The linear variable differential transformers used to measure axial fuel rod elongation were generally reliable and provided accurate data, although the device failed before performance of the DNB cycles for Test 8-1 RF.

The instruments used to measure coolant temperature, flow, and pressure conditions were generally reliable and provided adequately accurate data. The type of tests performed impose less stringent response requirements on coolant instruments.

7. CONCLUSIONS

The following conclusions have been derived from the results of Power-Cooling-Mismatch Tests 8-1 RS, CHF Scoping, and 8-1 RF.

1. Departure from nucleate boiling and subsequent film boiling can be induced by either increasing the fuel rod peak power or by reducing the coolant mass flow rate while maintaining other parameters constant; either method provides an acceptable means for investigating fuel rod behavior under PCM conditions.

2. The occurrence of premature DNB, observed in two tests, can be effectively prevented by operation in nucleate boiling for approximately 1 h (termed cladding aging) before inducing DNB. Premature DNB is believed to be caused by adsorbed gases on the cladding surface; cladding aging apparently outgasses the cladding.

3. Within nominal variations, and excluding premature DNB occurrences, the power/flow conditions required to induce DNB are generally similar and repeatable for fuel rods.

4. The extent of cladding damage resulting from film boiling depends on both the cladding temperatures attained and the total time in film boiling. Although significant damage in the form of cladding collapse and oxidation-induced cladding embrittlement can be sustained without rod failure, test results show that film boiling at high cladding temperatures eventually leads to sufficient oxidation of the cladding to result in loss of structural integrity.

5. Both the failure and nonfailure of the test rods were predicted based on the extent of oxidation-induced embrittlement of the cladding.

6. Fuel temperatures sufficient to result in fuel restructuring characterized by equiaxed UO_2 grain growth and granular fracturing near the center of the fuel column may result from film boiling operation with cladding temperatures greater than 1250 K.

7. Improved methods are needed to measure cladding surface temperatures, fuel centerline temperatures, and fuel rod internal pressure. Fin-cooling effects are significant for cladding surface thermocouples. Fuel centerline temperature thermocouples and internal pressure transducers provide unreliable results.

8. REFERENCES

1. United States Nuclear Regulatory Commission, Reactor Safety Research Program, *A Description of Current and Planned Reactor Safety Research Sponsored by the Nuclear Regulatory Commission's Division of Reactor Safety Research*, NUREG-75/058, June 1975.

2. D. T. Sparks and C. J. Stanley, *Power-Cooling-Mismatch Test Series, Test PCM-1 Fuel Rod Behavior Report*, NUREG/CR-0907, TREE-1374, August 1979.

3. G. W. Cawood et al., *Power-Cooling-Mismatch Test Series, Test PCM-2A Test Results Report*, ANCR-NUREG-1347, September 1976.

4. A. S. Mehner and K. Vinjamuri, *Fuel Rod Behavior During Test PCM-2*, NUREG/CR-0647, TREE-1332, April 1979.

5. D. E. Owen and K. Vinjamuri, *Power-Cooling-Mismatch Test Series, Test PCM-3 Test Results Report*, NUREG/CR-0902, TREE-1335, August 1979.

6. R. L. Johnson et al., *Fuel Rod Behavior During Test PCM-4*, NUREG/CR-0903, TREE-1336, August 1979.

7. F. S. Gunnerson and D. T. Sparks, *Behavior of Nine-Rod Fuel Assembly During Power-Cooling-Mismatch Conditions - Results of Test PCM-5*, NUREG/CR-1103, EGG-2002, November 1979.

8. R. B. Roemer, "The Effect of Power Transients on the Peak Heat Flux," *International Journal of Heat and Mass Transfer, 12*, 1969, pp. 953-964.

9. F. S. Gunnerson and P. S. Dunphy, *A Study of Film Boiling, Quench, and Rewet Phenomena During High Pressure Power-Cooling-Mismatch Testing*, NUREG/CR-1623, EGG-2052, October 1980.

10. L. S. Tong, *Boiling Crisis and Critical Heat Flux*, USAEC Report TID-25887, Westinghouse Eiectric Corporation, NTIS, 1972.

11. J. S. Gellerstedt et al., "Correlation of Critical Heat Flux in a Bundle Cooled by Pressurized Water," *Two Phase Flow and Heat Transfer in Rod Bundles Symposium, Winter Annual Meeting of the American Society of Mechanical Engineers, Los Angeles, California, November 18, 1969.*

12. S. L. Seiffert and R. R. Hobbins, *Oxidation and Embrittlement of Zircaloy-4 Cladding from High Temperature Film Boiling Operation*, NUREG/CR-0517, TREE-1327, April 1979.

13. R. E. Pawel, "Oxidation Diffusion in Beta Zircaloy During Steam Oxidation," *Journal of Nuclear Materials, 50*, 1974, pp. 247-258.

14. C. J. Scatena, *Fuel Cladding Embrittlement During a Loss-of-Coolant Accident*, General Electric Company, NEDO-10674, October 1972.

ATTACHMENT NOT FILMED

ANO. 8012110558

NO. OF PAGES 2 fiche

☐ DUPLICATE: ALREADY ENTERED INTO SYSTEM
UNDER ANO. _____

☒ ILLEGIBLE: HARD COPY AT:

☒ PDR

☐ CF

☐ OTHER _____